The Coevolution of Galaxies and Supermassive Black Holes: Insights from Surveys of the Contemporary Universe

Timothy M. Heckman[1] and Philip N. Best[2]

[1]Center for Astrophysical Sciences, Department of Physics & Astronomy, The Johns Hopkins University, Baltimore, Maryland 21218; email: heckman@pha.jhu.edu

[2]Institute for Astronomy, Royal Observatory Edinburgh, Blackford Hill, Edinburgh EH9 3HJ, United Kingdom; email: pnb@roe.ac.uk

Keywords

active galactic nuclei, Seyfert galaxies, quasi-stellar objects, QSOs, radio galaxies

Abstract

We summarize what large surveys of the contemporary Universe have taught us about the physics and phenomenology of the processes that link the formation and evolution of galaxies with their central supermassive black holes. We present a picture in which the population of active galactic nuclei (AGNs) can be divided into two distinct populations. The radiative-mode AGNs are associated with black holes (BHs) that produce radiant energy powered by accretion at rates in excess of ~1% of the Eddington limit. They are primarily associated with less massive BHs growing in high-density pseudobulges at a rate sufficient to produce the total mass budget in these BHs in ~10 Gyr. The circumnuclear environment contains high-density cold gas and associated star formation. Major mergers are not the primary mechanism for transporting this gas inward; secular processes appear dominant. Stellar feedback is generic in these objects, and strong AGN feedback is seen only in the most powerful AGNs. In jet-mode AGNs the bulk of energetic output takes the form of collimated outflows (jets). These AGNs are associated with the more massive BHs in more massive (classical) bulges and elliptical galaxies. Neither the accretion onto these BHs nor star formation in their host bulge is significant today. These AGNs are probably fueled by the accretion of slowly cooling hot gas that is limited by the feedback/heating provided by AGN radio sources. Surveys of the high-redshift Universe paint a similar picture. Noting that the volume-averaged ratio of star formation to BH growth has remained broadly constant over the past 10 Gyrs, we argue that the processes that linked the cosmic evolution of galaxies and BHs are still at play today.

1. INTRODUCTION

1.1. A Brief History

It has been nearly a century since Hubble (1925) decisively demonstrated that the Andromeda nebula is a vast island universe of stars similar to our own Milky Way galaxy. His discovery soon thereafter of an expanding cosmos filled with galaxies opened up a vista of an immense and seemingly serene Universe. However, this picture of serenity was deceptive. As we write this review, it is the 50-year anniversary of Maarten Schmidt's (1963) realization that the radio source 3C273 was associated with an optically unresolved object with the (then) enormous redshift of 0.158. Subsequent identifications of a whole population of quasi-stellar radio sources at even higher redshifts were soon followed by the discovery of a more numerous population of otherwise-similar but radio-quiet quasi-stellar galaxies (Sandage 1965). [It is fascinating in hindsight that the discovery of the cosmic X-ray background (Giacconi et al. 1962) and of the Kerr metric (Kerr 1963) occurred at the same time.] The concept of the Violent Universe was born.

It is beyond the scope of this review to examine the twists and turns that finally led to the consensus that all these quasi-stellar objects (QSOs) were the extremely luminous active nuclei of distant galaxies. Qualitatively similar objects had been found much earlier in the nuclei of some relatively nearby galaxies by Seyfert (1943). It is sobering that the significance of this discovery was long unrecognized: The first investigation into the nature of Seyfert galaxies was published 16 years later by Burbidge et al. (1959), who concluded that NGC 1068 was explosively ejecting ionized gas from its nucleus. Likewise, although other radio sources had been identified with distant galaxies before the discovery of QSOs—e.g., Cygnus A by Baade & Minkowski (1954)—there was great confusion as to the origin of this very large-scale radio emission, which had no obvious connection to the galaxy nucleus.

For most of the past five decades the communities that studied galaxies and active galactic nuclei (AGNs) remained largely disconnected. AGNs were studied primarily as laboratories in which to probe exotic high-energy processes. There was some effort to understand the role that the environment might play in triggering or fueling the AGN—for example, see the ancient review in this journal by Balick & Heckman (1982)—but there was virtually no concept that AGNs played any significant role in the evolution of typical galaxies. Of course, things could hardly be more different today. The notion of the coevolution of galaxies and AGNs has become inextricably ingrained in our current cosmogony. Indeed, this review represents the third article in this journal in consecutive years that deals with some aspect of this coevolution (Fabian 2012, Kormendy & Ho 2013).

The reasons for this change are easy to recognize. First came the realization that powerful AGNs (as represented by QSOs) were only the tip of the iceberg. Extensive surveys in the radio, optical, and X-ray domains revealed local populations of Seyfert and radio galaxies and established that signs of lower-level activity were commonplace in the nuclei of early-type galaxies. This strongly suggested that the AGN phenomenon—rather than being simply a rare spectacle—is a part of the lifecycle of typical galaxies. The demography and physical properties of these low-power AGNs have been comprehensively reviewed in this journal by Ho (2008).

A second reason followed from the documentation of the overall buildup over most of cosmic time of the populations of galaxies (as traced via star formation) and of supermassive black holes (SMBHs, whose growth is traced by AGNs). The evolution of the two populations is strikingly similar: a steep rise in both the star-formation rate (SFR) and SMBH growth rate by about a factor of 10 from redshift $z = 0$ to 1, a broad maximum in both rates at $z \sim 2$ to 3, and then a relatively steep decline at higher redshifts (see **Figure 1**) (Shankar et al. 2009 and references
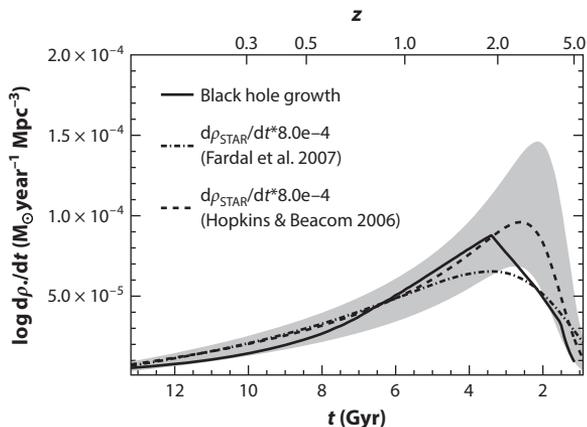
Figure 1

The cosmic history of black hole growth and stellar mass growth. The average black hole accretion rate is compared to the star-formation rate as a function of redshift, where the latter is given by Hopkins & Beacom (2006) and Fardal et al. (2007), scaled by the factor 0.8×10^{-3}. The shaded gray area shows the 3σ uncertainty region from Hopkins & Beacom (2006). Reprinted from Shankar et al. (2009) with permission.

therein). For at least the last ∼11 Gyr of cosmic history the ratio of these two growth rates has remained roughly constant with a value of order 10^3. Thus, at least in a volume-averaged sense, the growth of galaxies and SMBHs has been synchronized somehow.

Finally, and even more remarkably, observations over the past decade have not only established that SMBHs exist in the nuclei of (probably) all galactic bulges, they have shown that the properties of these present-day SMBHs and the galaxies in which they live are linked on a galaxy-by-galaxy basis. This impressive fossil record of coevolution has been exhaustively reviewed by Kormendy & Ho (2013). In addition to the accumulating observational evidence for the coevolution of galaxies and SMBHs, a considerable theoretical motivation to invoke this linkage has developed as well. Without some form of feedback from AGNs, neither current semianalytic models nor numerical simulations can successfully reproduce the properties of massive galaxies. This fascinating subject has been reviewed in this journal by Fabian (2012).

In conclusion, though the evidence to date remains indirect, it is hard not to infer that the cosmic evolution of galaxies and that of SMBHs have seemingly been driven by a suite of interlinked physical processes.

1.2. Our Perspective: Large Surveys of the Contemporary Universe

Our goal here is to review the evidence for the coevolution of galaxies and SMBHs as derived from large surveys of the contemporary (low-redshift) Universe. The majority of the growth of SMBHs and of the stellar components in galaxies occurred between redshifts of roughly 0.5 and 2, and the present-day growth rates of both populations are over an order of magnitude smaller than during the peak epoch. A reasonable question is then whether one can learn anything very useful by studying the contemporary Universe. We hope that by the end of the review the reader will agree with us that one can actually learn a great deal.

We believe that there are a number of reasons why this is the case. The contemporary Universe contains a rich fossil record that (once successfully decoded) reveals the processes that produced this record. Moreover, the basic physical processes that operated during the peak epoch

of SMBH/galaxy growth are still in place and can be studied in greater detail due to their relative proximity. However, the primary reason to study the contemporary Universe is that it is the only place where it has been possible to carry out the surveys of galaxies and SMBHs that are of sufficiently large size and whose data are of sufficiently high quality to have finally allowed us to be able to fully explore the complex inter-relationship between these two populations in a statistically robust way. This has led to a much clearer picture of both the fossil record of galaxy/SMBH coevolution and the processes by which the coevolution continues to play out.

The particular importance of high-quality optical spectroscopy cannot be overstated: These data form the interpretational backbone of the whole structure defined by extensive multiband imaging and photometric surveys. Of most relevance to the specific topic of our review, studies of the lower-luminosity objects that dominate the AGN population in the local Universe benefitted immensely from galaxy spectra obtained as part of the main galaxy sample of the Sloan Digital Sky Survey (SDSS; Strauss et al. 2002). The high quality of the spectra enabled them to be used to characterize both the AGNs and the stellar populations in the host galaxies. Finally, the uniformity and completeness of the SDSS main galaxy sample rendered it ideal for statistical studies of the multiparameter characteristics of the galaxy population in the contemporary Universe, including their AGN properties.

The uniformity and wide sky coverage of the 2dF Galaxy Redshift Survey (2dFGRS; Colless et al. 2001) and SDSS galaxy redshift survey make them an ideal starting point for studies of AGNs and their host galaxies in regions of the electromagnetic spectrum other than the optical. This encompasses the study of radio-selected AGNs using surveys such as the 1.4-GHz National Radio Astronomy Observatory (NRAO) VLA Sky Survey (NVSS; Condon et al. 1998) by Sadler et al. (2002) and Mauch & Sadler (2007) and the Faint Images of the Radio Sky at Twenty centimeters (FIRST; Becker et al. 1995) survey by Best et al. (2005a) and Best & Heckman (2012). Recently, samples of tens of thousands of nearby mid-IR-detected AGNs covering large areas of the sky have been constructed by cross-correlating sources detected by the *Wide-Field Infrared Survey Explorer* (WISE; Wright et al. 2010) with the SDSS (Donoso et al. 2012, Shao et al. 2013). X-ray data having the depth and wide-field sky coverage to fully exploit the SDSS galaxy sample do not exist. However, to date the *Swift/Burst Alert Telescope* (BAT) survey has detected over 700 (mostly local) AGNs at energies above 15 keV (Baumgartner et al. 2013). Near-IR data from WISE and vacuum-UV data from the *Galaxy Evolution Explorer* (GALEX; Martin et al. 2005) provide important additional information about AGN host galaxies. In subsequent sections, we summarize the new scientific insights that resulted from all these large surveys.

1.3. The Landscape of the Galaxy Population and How It Got That Way

To help frame the main issues addressed in this review it is helpful to briefly summarize the basic properties of the population of galaxies in the contemporary Universe and the current thinking about how these galaxies were built. The reader is referred to the review by Madau & Dickinson (2014) in this volume for all the details.

Results from the SDSS have shown that the galaxy population in the contemporary Universe occupies a very small part of the parameter space defined by the structure, stellar content, and chemical composition of a galaxy. In particular, the existence of clear bimodality in the galaxy population was revealed (Kauffmann et al. 2003b, Blanton et al. 2003, Baldry et al. 2004). One population (blue, for short) consists of galaxies with significant ongoing star formation, small stellar masses (M_*), low stellar surface mass densities ($\mu_* = 0.5\,M_*/(\pi R_{50}^2)$, where R_{50} is the radius containing 50% of the light; see Section 2.4), and small concentrations ($C = R_{90}/R_{50}$) of their light (late Hubble type). The other (red) consists of galaxies with little ongoing star
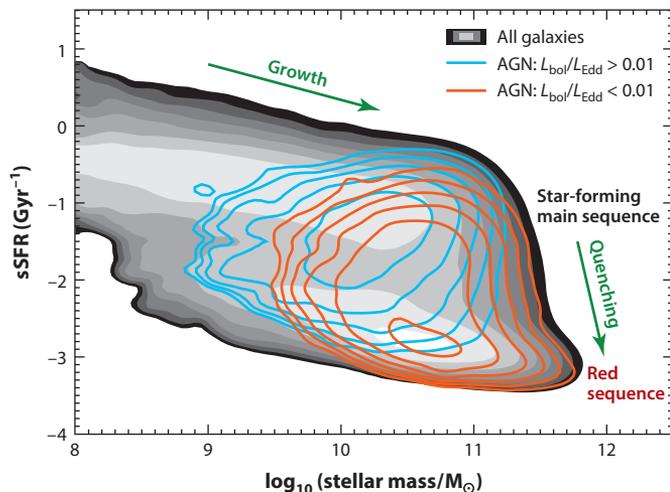
Figure 2

The distribution of galaxies in the SDSS main galaxy sample on the plane of stellar mass versus specific star-formation rate (sSFR = SFR/M_*). The grayscale indicates the volume-weighted distribution of all galaxies, with each lighter color band indicating a factor of two increase. Galaxies predominantly fall within two regions: a main sequence of star-forming galaxies and a red sequence of quenched galaxies. The blue and red contours show the volume-weighted distributions of high (>1%; mostly radiative-mode) and low (<1%; mostly jet-mode) Eddington-fraction AGNs, with contours spaced by a factor of two.

formation, large M_*, high μ_*, and large C (early Hubble type). The characteristic parameter values that mark the transition between populations are $M_* \sim 10^{10.5}\,M_\odot$, $\mu_* \sim 10^{8.5}\,M_\odot\,\text{kpc}^{-2}$, and $C \sim 2.6$. Subsequent work showed that the blue population is characterized by a tight, almost linear relationship between the SFR and M_* (Brinchmann et al. 2004, Schiminovich et al. 2007). This has come to be called the star-forming main sequence. **Figure 2** shows the relationship between M_* and the sSFR (sSFR = SFR/M_*) in the contemporary Universe.

Over the past few years, deep surveys have established that the qualitative distribution shown in **Figure 2** is characteristic of the galaxy population out to at least a redshift of 2 (e.g., Whitaker et al. 2012). The most significant difference is that the actual values of the sSFR on the star-forming main sequence evolve extremely rapidly with time: Elbaz et al. (2011) find as the age of the Universe (t_{cos}) increased from 2.2 to 13.6 Gyr ($z = 3$ to 0), the characteristic value of the sSFR declined with time as $t_{cos}^{-2.2}$.

The simplest picture for the evolution of a typical galaxy (e.g., Lilly et al. 2013) is that it evolves along the (strongly evolving) blue star-forming main sequence, increasing in mass through the accretion of cold gas from the cosmic web and (secondarily) through mergers with other galaxies. As it approaches a critical mass, its supply of cold gas is shut off, the star formation is quenched, and the galaxy then evolves into the red population. It can continue to increase in mass through subsequent mergers with other galaxies. It is presently not clear whether the mass scale at which quenching occurs pertains to the stellar mass or the dark matter halo mass.

The physical process(es) that quench the galaxy are unclear. In part, quenching may be due to a change in the nature of accretion: rapid accretion of cold streams of infalling gas at low mass transitioning to slow accretion of hot gas in hydrostatic equilibrium at high mass (e.g., Dekel et al. 2009). In principle these processes are included in numerical and semianalytic models of galaxy evolution. Nevertheless, these models require some additional process to be at play in order to reproduce the observed properties of massive galaxies. Heating and/or the ejection of surrounding

gas by an AGN-driven outflow to suppress the cold accretion is a popular idea. In addition the models also require AGN feedback to keep galaxies that arrive in the red/dead population from forming too many stars from the slow accretion of their hot halo gas. Thus, in the current paradigm, AGNs play a crucial role in the evolution of massive galaxies.

2. BASIC METHODOLOGY

2.1. Overview of the Local AGN Population

The fundamental property that we consider to define an AGN is that its power source involves extracting energy from the relativistically-deep potential well of an SMBH at or near the center of a galaxy.

In this review we present strong empirical evidence that the low-redshift population of AGNs can be divided into two main categories [we refer the reader to Antonucci (2012) for a complementary review]. The first category consists of objects whose dominant energetic output is in the form of electromagnetic radiation produced by the efficient conversion of the potential energy of the gas accreted by the SMBH. Historically, these objects have been called either Seyfert galaxies or QSOs depending upon rather vague and arbitrary criteria involving luminosity and/or redshift. In the rest of this review we refer to these as radiative-mode AGNs. The second category consists of objects that produce relatively little radiation and whose primary energetic output takes the form of the bulk kinetic energy transported in two-sided collimated outflows (jets). These jets may be ultimately powered by the accretion of gas or by tapping the spin energy of the SMBH. Historically, this AGN population has been called (low-excitation) radio galaxies. In this review we refer to them as jet-mode AGNs. As we show in this review, these two populations are virtually disjoint in terms of the basic properties of their SMBHs and host galaxies.

Let us then begin by describing the basic building blocks for these two types of AGNs (see **Figure 3** for schematic diagrams). We refer readers to the texts of Krolik (1999), Netzer (2013), Osterbrock & Ferland (2005), Peterson (1997), and the review by Yuan & Narayan (2014) in this volume for the gory details. In the first category (radiative-mode AGNs), the SMBH is surrounded by a geometrically thin, optically thick accretion disk through which an inflow occurs. The accretion disk has a radial temperature gradient, and the resulting total thermal continuum emission emerges from the extreme UV through to the visible portion of the electromagnetic spectrum. The accretion disk is surrounded by a hot corona that Compton-up-scatters the soft seed photons from the disk into the X-ray regime. As the X-rays impact the accretion disk their spectral energy distribution is modified through fluorescence and reflection off the accretion disk. The ionizing radiation from the disk and corona heats and photoionizes a population of dense gas clouds located on scales of light-days to light-years from the SMBH leading to the production of UV-, optical-, and near-IR-permitted emission lines. The velocity dispersion of the population of clouds is typically several thousand kilometers per second, leading to its designation as the broad-line region on the basis of the resulting emission-line spectrum.

On larger scales, the SMBH and accretion disk are surrounded by a region of dusty molecular gas (which we refer to as the obscuring structure). Its inner radius is set by the sublimation temperature of the most refractory dust grains and is hence larger in more luminous AGNs. In this region some of the incident UV/visible photons from the accretion disk and the soft X-rays from the corona are absorbed by the dust, and this absorbed energy emerges as thermal IR emission. The total column density of the obscuring structure spans a range in inferred column densities from roughly 10^{23} to 10^{25} cm^{-2}. The highest column densities are sufficient to absorb even hard X-rays (these cases are Compton-thick). As ionizing radiation escapes along the polar
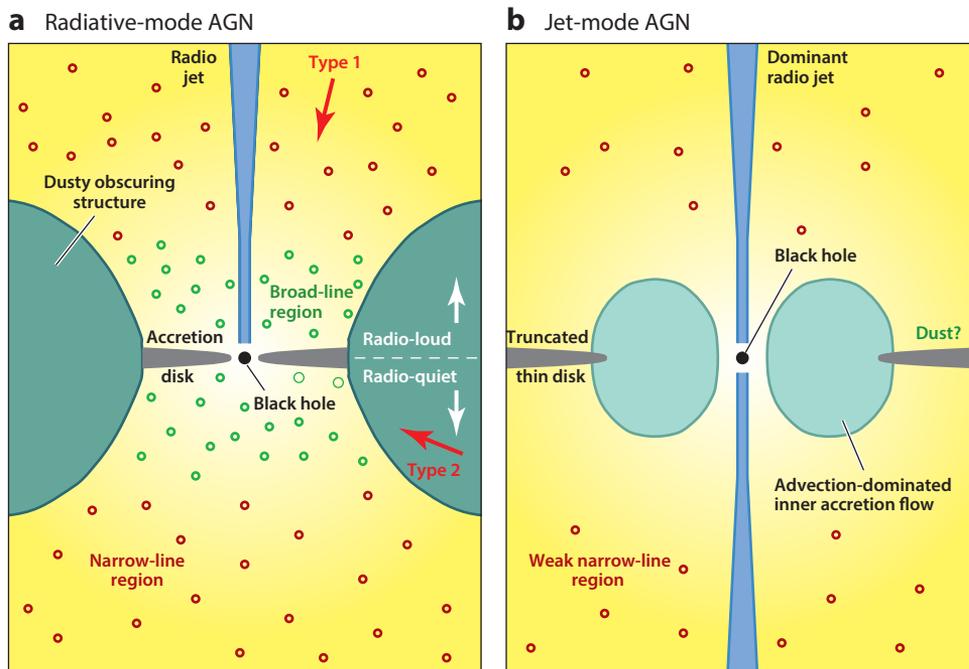
a Radiative-mode AGN

- Radio jet
- Type 1
- Dusty obscuring structure
- Broad-line region
- Accretion disk
- Radio-loud
- Radio-quiet
- Black hole
- Type 2
- Narrow-line region

b Jet-mode AGN

- Dominant radio jet
- Black hole
- Truncated thin disk
- Dust?
- Advection-dominated inner accretion flow
- Weak narrow-line region

Figure 3

Schematic drawings of the central engines of radiative-mode and jet-mode AGNs (not to scale).
(*a*) Radiative-mode AGNs possess a geometrically thin, optically thick accretion disk, reaching into the
radius of the innermost stable orbit around the central supermassive black hole. Luminous UV radiation
from this accretion disk illuminates the broad-line and narrow-line emission regions. An obscuring structure
of dusty molecular gas prohibits direct view of the accretion disk and broad-line regions from certain lines of
sight (Type 2 AGN), whereas they are visible from others (Type 1 AGN). In a small proportion of sources
(predominantly toward the high end of the range of black hole masses), powerful radio jets can also be
produced. (*b*) In jet-mode AGNs the thin accretion disk is replaced in the inner regions by a geometrically
thick advection-dominated accretion flow. At larger radii (beyond a few tens of Schwarzschild radii, the
precise value depending upon properties of the accretion flow, such as the Eddington-scaled accretion rate),
there may be a transition to an outer (truncated) thin disk. The majority of the energetic output of these
sources is released in bulk kinetic form through radio jets. Radiative emission is less powerful, but can ionize
weak, low-ionization narrow-line regions, especially where the truncation radius of the thin disk is relatively
low.

axis of the obscuring structure, it photoionizes gas on circumnuclear scales (a few hundred to a few
thousand parsecs). This more quiescent and lower-density population of clouds produces UV-,
optical-, and IR-forbidden and -permitted emission lines, Doppler-broadened by several hundred
kilometers per second, and is hence called the narrow-line region (NLR).

Observing an AGN from a sight line nearer the polar axis of the obscuring structure yields a
clear direct view of the SMBH, the disk/corona, and broad-line region (BLR). These are called
Type 1 (or unobscured) AGNs. When observing an AGN from a sight line nearer the equatorial
plane of the obscuring structure, this central region is hidden and these are called Type 2 (or
obscured) AGNs. This is the basis for the standard unified model for radiative-mode AGNs (e.g.,
Antonucci 1993), which asserts that the Type 1 and 2 populations differ only in the viewing angle
from which the AGN is observed. The presence of AGNs can still be inferred in the Type 2
objects from the thermal IR emission from the obscuring structure, from hard X-rays transmitted

through the structure (when it is Compton-thin), and from the emission lines with tell-tale line ratios from the NLR.

In some cases, the obscuring material can be the larger-scale dusty ISM of the host galaxy. This is particularly relevant when the host galaxy's disk is viewed at a large inclination or the galaxy is in the throes of an ongoing major merger with a strong central concentration of dusty gas. This material is sometimes sufficient to obscure the optical, UV, and soft X-ray emission from the AGN accretion disk and BLR, but insufficient to attenuate the hard X-rays (e.g., Gelbord 2003). The effect of this is nicely demonstrated by Lagos et al. (2011), who use SDSS data to show that the host galaxies of optically obscured AGNs are skewed toward edge-on orientations, whereas those optically classified as Type 1 have a much higher probability of having a face-on orientation.

In the second category (jet-mode AGNs), a distinct mode of accretion onto the SMBH exists that is apparently associated with low accretion rates and is radiatively inefficient. The geometrically thin accretion disk is either absent or is truncated in the inner regions, and is replaced by a geometrically thick structure in which the inflow time is much shorter than the radiative cooling time (e.g., Narayan & Yi 1994, 1995; Quataert 2001; Narayan 2005; Ho 2008). These are called advection-dominated or radiatively inefficient accretion flows (ADAFs/RIAFs). A characteristic property of these flows is that they are capable of launching two-sided jets. Note that powerful jets are also launched by a small fraction of radiative-mode AGNs (e.g., radio-loud QSOs). The jets are (far and away) most easily detected via the synchrotron emission they produce at radio wavelengths. This can extend from optically thick (synchrotron self-absorbed) emission on parsec scales all the way out to regions far beyond the stellar body of the galaxy (reaching megaparsec scales in extreme cases). In typical local radio galaxies the jets travel at relativistic velocities (Lorentz gammas of several) when launched, but appear to rapidly decelerate and destabilize as they interact with the gaseous halo of the host galaxy and transition to subsonic turbulent plumes. At the highest radio luminosities (most commonly found in the radio-loud radiative-mode AGNs), the jets survive as highly collimated structures until they terminate as bright shocks (hot spots) at the interface with the circumgalactic or intergalactic medium. The survival or disruption of the jets leads to the Fanaroff & Riley (1974) morphological classification of radio galaxies (see Urry & Padovani 1995 for further discussion).

Missing from the above description are the objects that may trace the lowest-luminosity portion of the AGN population. This population has been reviewed in this journal by Ho (2008). Since his review, evidence has grown that at least some of the objects previously classified as the lowest-luminosity AGNs (the low-ionization nuclear emission-line regions, or LINERs, with the very weakest optical emission lines) are not bona fide AGNs (e.g., Cid Fernandes et al. 2011, Yan & Blanton 2012). However, the remaining more powerful LINERs are very likely to be members of the jet-mode AGN population (e.g., Nagar et al. 2005; Ho 2008; P.N. Best & T.M. Heckman, in preparation), albeit with rather modest radio luminosities.

Figure 4 summarizes this description of the local AGN population and how the common AGN classes fit within it. The blue text within that figure describes the properties of a typical example of each category of AGNs. As the review develops, we describe the evidence for this and discuss the range of properties seen for each AGN class.

2.2. Finding AGNs

This review is focused on insights into the coevolution of SMBHs and galaxies that have been derived from large surveys of the local Universe. For such investigations of the radiative-mode AGNs it is the obscured (Type 2) AGNs that are far and away the more valuable. In these objects the blinding glare of the UV and optical continuum emission from the central accretion disk has
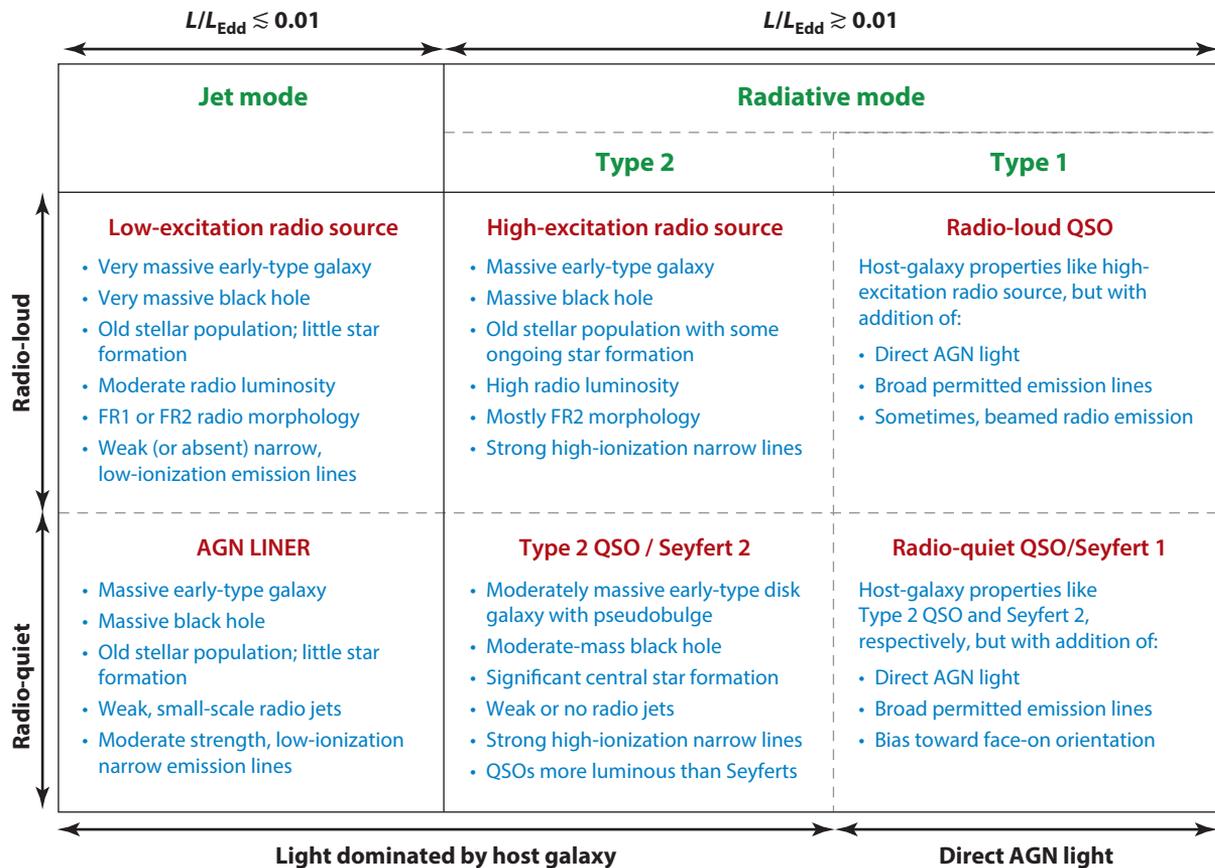
$L/L_{Edd} \lesssim 0.01$ | $L/L_{Edd} \gtrsim 0.01$

| **Jet mode** | **Radiative mode** | |
| | **Type 2** | **Type 1** |

Radio-loud

Low-excitation radio source
- Very massive early-type galaxy
- Very massive black hole
- Old stellar population; little star formation
- Moderate radio luminosity
- FR1 or FR2 radio morphology
- Weak (or absent) narrow, low-ionization emission lines

High-excitation radio source
- Massive early-type galaxy
- Massive black hole
- Old stellar population with some ongoing star formation
- High radio luminosity
- Mostly FR2 morphology
- Strong high-ionization narrow lines

Radio-loud QSO
Host-galaxy properties like high-excitation radio source, but with addition of:
- Direct AGN light
- Broad permitted emission lines
- Sometimes, beamed radio emission

Radio-quiet

AGN LINER
- Massive early-type galaxy
- Massive black hole
- Old stellar population; little star formation
- Weak, small-scale radio jets
- Moderate strength, low-ionization narrow emission lines

Type 2 QSO / Seyfert 2
- Moderately massive early-type disk galaxy with pseudobulge
- Moderate-mass black hole
- Significant central star formation
- Weak or no radio jets
- Strong high-ionization narrow lines
- QSOs more luminous than Seyferts

Radio-quiet QSO/Seyfert 1
Host-galaxy properties like Type 2 QSO and Seyfert 2, respectively, but with addition of:
- Direct AGN light
- Broad permitted emission lines
- Bias toward face-on orientation

Light dominated by host galaxy | **Direct AGN light**

Figure 4

The categorization of the local AGN population adopted throughout this review. The blue text describes typical properties of each AGN class. These, together with the spread of properties for each class, are justified throughout the review. Abbreviations: FR1/FR2, Faranoff & Riley (1974) Class 1/2; LINER, low-ionization nuclear emission-line region; QSO, quasi-stellar object.

been blocked by the natural coronagraph created by the dusty obscuring structure. The remaining UV and optical continuum is generally dominated by the galaxy's stellar component (Kauffmann et al. 2003a), which can then be readily characterized. In the sections to follow we therefore restrict our discussion of radiative-mode AGNs to techniques that can recognize Type 2 AGNs. For the jet-mode AGNs the intrinsic UV and optical emission from the AGN is generally weak or absent unless the observer is looking directly down the jet axis (e.g., Urry & Padovani 1995). Thus, the host-galaxy properties can be easily studied without contamination.

The relevant techniques that have been used for very large surveys of the local Universe are based on (*a*) optical spectroscopy to identify emission from the AGN-powered NLR, (*b*) mid-IR photometry to identify the warm dust emission from the obscuring structure, (*c*) hard X-ray imaging spectroscopy to detect emission from the accretion disk corona, and (*d*) nonthermal radio continuum emission to locate jets and jet-powered structures.

For the radiative-mode population, one important caveat to keep in mind is the degree to which Type 2 AGNs and their hosts are the same as those of Type 1. In the most simplistic version of the AGN unified model described above, this complete overlap would be the case. However, in reality

the fraction of the sky covered by obscuring material (as seen from the SMBH) varies significantly from AGN to AGN. In this case, the AGNs observed as Type 1 (2) will be systematically drawn from the portion of the AGN parent population with a smaller (larger) covering factor for the obscuring material. It would therefore not be surprising if the properties of Type 1 and Type 2 AGNs and their hosts differed in some systematic fashion.

2.2.1. Optical emission-line surveys. Large-scale spectroscopic surveys of the contemporary Universe (particularly 2dFGRS and SDSS) have revolutionized the study of emission-line AGNs, by providing high-quality spectra for over a million galaxies, with well-understood selection functions. The broad emission lines and strong nonstellar continuum emission in Type 1 radiative-mode AGNs offer easily detectable and unambiguous evidence of the presence of an AGN origin [detailed discussions of the identification of Type 1 AGNs and of the criteria used to discriminate between Type 1 and Type 2 AGNs in the SDSS are discussed by Richards et al. (2002) and Hao et al. (2005b)]. In contrast, the optical signature of Type 2 radiative-mode AGNs, and of jet-mode AGNs, is the presence of narrow emission lines. In general, such narrow emission lines can also be produced by ordinary populations of O stars associated with ongoing star formation. However, the relative intensities of the strong forbidden and permitted emission lines resulting from photoionization by the relatively hard continuum from an AGN differ systematically from those produced by the much softer continuum of O stars. This approach to recognizing AGNs was first systematized by Baldwin et al. (1981; BPT) and later refined by Veilleux & Osterbrock (1987). The diagnostic diagrams (commonly referred to as BPT diagrams) compare pairs of emission-line flux ratios. Primary among these is the flux ratio pair [OIII] 5007/Hβ versus [NII]6584/Hα, but the [OI] 6300/Hα and [SII] 6716,6731/Hα flux ratios provide diagnostics that are complementary to [NII]/Hα (e.g., Kewley et al. 2006; see **Figure 5**). The same diagnostic diagrams work for Type 1 AGNs provided that only the narrow components of the Balmer lines are considered (e.g., Stern & Laor 2012a).

We show a set of diagnostic diagrams for the SDSS main galaxy sample in **Figure 5** (taken from Kewley et al. 2006). The basic morphology of these diagrams reveals the presence of two
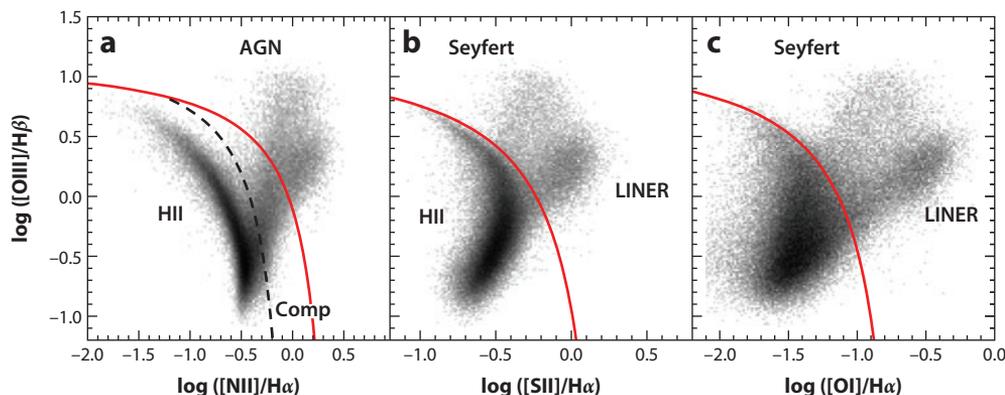

Figure 5

A set of diagnostic diagrams for the Sloan Digital Sky Survey main galaxy sample taken from Kewley et al. (2006). The red line is the maximal starburst line from Kewley et al. (2001), whereas the dashed line in panel *a* shows the more stringent dividing line between pure star-forming galaxies and AGNs adopted by Kauffmann et al. (2003a). The separation between star-forming galaxies and AGNs is most cleanly done using panel *a*, whereas panels *b* and *c* can be used to separate Seyferts from LINERs (low-ionization nuclear emission-line regions).

populations. The first is that of purely star-forming galaxies whose locus runs from the upper left to lower middle of the plots in a sequence of downwardly increasing metallicity (e.g., Pettini & Pagel 2004). The second is the AGN population, which is joined to the star-forming sequence at the high-metallicity end and then extends upward and to the right.

Physically, the observed difference in the emission from high-metallicity gas photoionized by an AGN reflects the increased rate of photoelectric heating by the hard AGN radiation field. This leads to a higher gas temperature and an increased strength of the collisionally excited forbidden lines relative to the recombination lines of hydrogen. Because real galaxies contain both AGNs and regions of star formation within the observed region, the extension of the AGN locus away from the star-forming sequence can be viewed as a mixing line along which the contribution to the total emission-line spectrum by the AGN increases relative to that from the star-forming regions as the points move further away from the star-forming locus. This inference is confirmed in a statistical sense by the result that the relative distribution of points along this sequence migrates downward toward the star-forming sequence as the redshift of the galaxy population at fixed stellar mass increases and the SDSS fiber encompasses a progressively larger region of the host galaxy (Kauffmann et al. 2003a, Kewley et al. 2006, LaMassa et al. 2013).

Kewley et al. (2001) used photoionization and stellar population synthesis models to define an upper boundary to the possible location of star-forming galaxies in the emission-line diagnostic diagrams, above which a clean sample of AGNs can be selected. Kauffmann et al. (2003a) used empirical methods, based on the tight locus of star-forming galaxies within the [NII]/Hα BPT diagram, to produce an alternative demarcation that should provide a more complete census of the AGN population that is less biased against AGNs in strongly star-forming galaxies. These demarcation lines are shown in **Figure 5**. Other authors have proposed further refinements of this division (e.g., Kewley et al. 2006, Stasinska et al. 2006, Cid Fernandes et al. 2011). This diagram has often been used to separate emission-line galaxies into three classes: star-formation-dominated (below and to the left of the Kauffmann et al. line), AGN-dominated (lying above and to the right of the Kewley line), and composite (between the Kewley and Kauffmann lines). In this review we do not distinguish between the composite and AGN-dominated objects (we regard them all as AGNs). It is important to emphasize here that though the optical emission lines used to classify AGNs and star-formation-dominated galaxies can be substantially affected by dust absorption, these optical classifications agree with mid-IR-based classifications in the great majority of cases (LaMassa et al. 2012).

In 1980 a separate class of optical emission-line AGNs was proposed, known as LINERs (Heckman 1980). LINERs are distinguished from Seyfert nuclei by the relative strength of their low-ionization emission lines; the original definition was based on the forbidden lines of oxygen, with LINERs having emission-line flux ratios [OII] 3727/[OIII] 5007 > 1 and [OI] 6300/[OIII] 5007 > 0.32. Subsequent classifications have built upon the diagnostic diagrams separating the AGN population into Seyferts and LINERs (see **Figure 5**). Although LINERs typically have lower nuclear luminosities than Seyferts, many of the fundamental characteristics of the objects close to the demarcation boundary are very similar to those of the low-luminosity end of the distribution of Seyferts (e.g., Kewley et al. 2006, Ho 2008, Netzer 2009).

Stasinska et al. (2008), Sarzi et al. (2010), Cid Fernandes et al. (2011), Capetti & Baldi (2011), and Yan & Blanton (2012) have all presented evidence that those LINERs with the weakest emission lines (which are located in galaxies with predominantly old stars) are not powered by an AGN. Instead, most of these papers argue that they are produced by photoionization of neutral atomic gas by a population of post-asymptotic giant branch (PAGB) stars. A problem with this idea is that *Hubble Space Telescope* (HST) UV images of the bulge of M31 (the site of a LINER) do not reveal the predicted population of these PAGB stars (Brown et al. 1998, 2008; Rosenfield et al.

2012). For these weak LINERs to be photoionized by old stars, a population that is less luminous and more numerous than the PAGB stars would be needed.

In this review we are conservative and consider the possibility that weak LINERs are not members of the AGN population. Here we consider weak LINERs to be objects with [OIII] 5007 equivalent widths smaller than ~1 Å (e.g., Capetti & Baldi 2011). It is important to note that although these objects constitute the majority of LINERs in the SDSS, they contribute a negligible amount to the overall AGN emissivity of the contemporary Universe. It is also important to note that objects classified as LINERs in the SDSS span over two orders of magnitude in [OIII] luminosity ($L_{[OIII]}$) and roughly three orders of magnitude in $L_{[OIII]}/M_{BH}$ [Kewley et al. 2006, Netzer 2009; where M_{BH} is the black hole (BH) mass in solar units]. Although a stellar origin for the LINER emission is likely at the lowest luminosities, the more powerful LINERs are most likely to be AGNs (P.N. Best & T.M. Heckman, in preparation).

2.2.2. X-ray and infrared surveys. X-ray surveys have played a critical role in defining the radiative-mode AGN population and delineating its evolution over cosmic time [see Brandt & Hasinger (2005) for a thorough review]. In our review we are most interested in the population of Type 2 obscured AGNs in the contemporary Universe. The *Rosat* all-sky survey (Voges et al. 1999) has the requisite wide-field coverage, but the survey is very shallow compared with the SDSS in terms of finding AGNs, and its 0.1–2.4-keV band is too soft to recover the bulk of the obscured AGN population (e.g., Anderson et al. 2003, Shen et al. 2006). Hard X-ray observations are much more useful, and the current state of the art is represented by the survey undertaken with the BAT onboard the *Swift* gamma-ray burst observatory. As of late 2012, BAT observations have yielded a catalog of 1,171 X-ray sources detected in the 14–195-keV band, drawn from a survey with nearly uniform sensitivity over the entire sky on the basis of 70 months of observations (Baumgartner et al. 2013). Of these, over 700 are AGNs. At these high X-ray energies only Compton-thick obscured AGNs are under-represented, and indeed the 70-month catalog contains roughly equal numbers of Type 1 and Type 2 Seyfert galaxies.

The signature of an obscured AGN in the IR is unusually strong mid-IR (~3- to 30-μm) emission produced by the dusty obscuring structure. The *Infrared Astronomical Satellite* (IRAS) pioneered the detection and characterization of the local AGN populations in the mid- and far-IR (e.g., Miley et al. 1985, Spinoglio & Malkan 1989). Unfortunately, the sensitivity of IRAS was not well matched to the bulk of the optically selected local AGNs in the SDSS (e.g., Pasquali et al. 2005). The *Spitzer Space Telescope* was considerably more sensitive than IRAS, but it did not undertake wide-field surveys optimized to the local AGN population. Nonetheless, a number of different techniques based on near- and mid-IR color selection were developed to find AGNs using *Spitzer* data (e.g., Lacy et al. 2004, Stern et al. 2005, Richards et al. 2006, Donley et al. 2008). The situation has been revolutionized with the completion of the mission of NASA's WISE, which has detected near- and mid-IR emission from roughly 30,000 optically classified AGNs in the SDSS main galaxy sample (Donoso et al. 2012, Shao et al. 2013) and many other AGNs as well (e.g., Stern et al. 2012, Rosario et al. 2013). It is important to note here that though samples of AGNs selected by their optical emission lines, their mid-IR emission, or their hard X-ray emission are roughly similar to one another in terms of both the properties of the AGNs and the host galaxies (e.g., Kauffmann et al. 2003a, LaMassa et al. 2010, Winter et al. 2010, Shao et al. 2013), they may not be identical (e.g., Hickox et al. 2009, Koss et al. 2011, Juneau et al. 2013).

2.2.3. Radio continuum surveys. Radio continuum surveys offer an important means to find AGNs, particularly the jet-mode AGNs for which jets represent the bulk of the AGN's energetic output. For radiative-mode AGNs, the dusty obscuring structure is optically thin to radio

continuum emission, so the detection of radio-emitting Type 2 AGNs is also reasonably straight-forward. Deep radio sky surveys such as NVSS, FIRST, the Westerbork Northern Sky Survey (WENSS; Rengelink et al. 1997), and the Sydney University Molonglo Sky Survey (SUMSS; Bock et al. 1999) cover large sky areas with sufficient sensitivity to probe the majority of the radio-AGNs in the contemporary Universe, reaching down to at least $P_{1.4\,\mathrm{GHz}} \sim 10^{23}$ W Hz^{-1} out to $z \sim 0.1$. More problematic issues than simple detection, however, are the accurate association of observed radio sources with their optical host galaxies and the confirmation that the observed radio emission arises from AGN activity rather than being associated with star formation within the host galaxy.

The NVSS was the first large-area radio survey of sufficiently high angular resolution (45 arcsec) to permit automated cross-correlation with optical surveys (cf. Machalski & Condon 1999). However, the positional accuracy of NVSS sources is only 1–2 arcsec at 10-mJy flux levels, increasing to 4–5 arcsec or more at the 2.5-mJy flux limit of the survey (Condon et al. 1998). This leads to significant uncertainties in cross-identifying the radio sources with their optical host galaxies, which are further exacerbated by the extended and multicomponent nature of some radio sources: Even though more than 95% of $z < 0.1$ radio sources are contained within a single NVSS component, the radio centroid of asymmetric extended sources may not match the host-galaxy position. This leads to a trade-off between the reliability and the completeness of the matched sample. For example, Sadler et al. (2002) cross-matched the NVSS with galaxies from the 2dFGRS, accepting matches within 10 arcsec of the optical galaxy; they calculated that the catalog would be 90% complete at this level, but that 5–10% of the matches were expected to be false identifications.

Higher reliability samples can be derived using radio surveys with better angular resolution, such as the 5-arcsec resolution of FIRST (cf. the the SDSS. cross-matching by Ivezić et al. 2002). However, these surveys can miss extended radio emission, leading to the radio luminosity of sources larger than a few arcseconds being systematically low (Becker et al. 1995) and also to a much larger fraction of extended radio sources being split into multiple components. These multicomponent sources can usually be associated with host galaxies by visual inspection, which is practical for moderate sample sizes (e.g., Mauch & Sadler 2007), but not for the very large samples produced from the SDSS. Automated cross-matching routines therefore need to be used, which take account of the possible multicomponent nature of radio sources. So-called collapsing algorithms aim to identify multicomponent radio sources by using the angular separations, flux densities and flux-density ratios of close source pairs to determine whether these are likely to be associated (e.g., Magliocchetti et al. 1998); for optical cross-matching, the relative separations and position angles from the host-galaxy position offer further information (e.g., McMahon et al. 2002, de Vries et al. 2006). Best et al. (2005a) developed a combined approach, using data from both NVSS (for reliable luminosities) and FIRST (for accurate cross-matching), along with all of the above information and incorporating visual analysis for the most extended radio sources. They were able to develop samples with ∼95% completeness and ∼99% reliability. Adaptations of this method have since been widely used (e.g., Sadler et al. 2007, Donoso et al. 2009, Lin et al. 2010, Best & Heckman 2012).

The derived radio source populations comprise a mixture of AGNs and star-forming galaxies. A variety of different methods have been adopted in the literature for separating radio-loud AGNs from star-forming galaxies. Perhaps the cleanest of these uses the ratio of far-IR to radio luminosity: Star-forming galaxies show a very tight correlation between these properties (see review by Condon 1992), whereas radio-loud AGNs are offset to brighter radio luminosities. This technique has been widely used at higher redshifts (e.g., Ibar et al. 2008, Sargent et al. 2010, Padovani et al. 2011, Simpson et al. 2012), but the shallow depth of wide-area far-IR surveys has limited its use locally (cf. Sadler et al. 2002). For local galaxies, the information provided by the large spectroscopic surveys can be used instead. The standard emission-line ratio diagnostic diagrams offer an approach consistent with that used to classify emission-line-selected AGNs, although a large fraction of the

radio population lack the required emission-line detections (Sadler et al. 1999, Best et al. 2005a). Radio-loud AGNs can also be identified as being offset from the tight correlation that star-forming galaxies display between Hα emission-line luminosity and radio luminosity (Kauffmann et al. 2008, Vitale et al. 2012). An alternative method developed by Best et al. (2005a) considers the 4,000-Å break strength (a measure of stellar population age; see Section 2.4.2) against the ratio of radio power per stellar mass on the basis that star-forming galaxies with a wide range of star-formation histories occupy a similar locus in this plane.

These different AGN/star-formation classification schemes agree on the classification of most sources, but also produce significant differences (see the comparison by Best & Heckman 2012). Primary among these differences is the way that radio-quiet AGNs are classified. These AGNs often display compact radio cores and weak jet-like structures, but those which lack these features lie on the same far-IR to radio correlation as star-forming galaxies (Roy et al. 1998). This suggests that the bulk of their radio emission is powered by star formation. The emission-line diagnostic diagrams classify these sources as AGNs, because the AGN drives the emission-line ratios away from the star-forming locus, but in contrast the sources are generally classified as star forming using the far-IR–to–radio or emission line–to–radio luminosity ratio diagnostics or the 4,000-Å break strength. Best & Heckman (2012) combined these different classification methods to provide a sample of 18,286 radio-loud AGNs from the SDSS, excluding radio-quiet AGNs (see **Figure 6**). This is the sample used to construct relevant plots throughout this review.

2.3. Determining AGN Physical Properties

2.3.1. Proxies for bolometric luminosity in radiative-mode AGNs. In this section we discuss how best to estimate the bolometric luminosity of radiative-mode AGNs. Type 2 AGNs are (by definition) obscured and this complicates the estimation of perhaps the most basic physical property of an AGN: its total (bolometric) luminosity. We cannot directly observe the great bulk of this radiant energy and must therefore rely on attempting to calibrate various proxies for the bolometric luminosity on the basis of the radiation that does escape. Let us then assess these various proxies and begin by briefly listing their pros and cons.

2.3.1.1. Proxy 1: The [OIII] 5007 emission line. The proxy that we primarily use later in this review is the luminosity of the [OIII] 5007 narrow emission line. The [OIII] line is produced in AGNs by ionizing radiation that escapes along the polar axis of the dusty obscuring structure where it photoionizes and heats ambient gas clouds on radial scales of order 0.1 to 1 kpc from the SMBH (in the NLR).

Pros: (1) This line is easily observed and can be measured (if present) in the existing SDSS spectra of a few million galaxies. (2) Because the NLR lies outside the very high column density in the obscuring structure, its emission suffers far less attenuation owing to dust near the AGN than the optical emission from the accretion disk. Modest amounts of dust extinction can be corrected using the ratio of the fluxes of the narrow Hα and Hβ emission lines (the Balmer decrement). Typical implied corrections are 1 to 2 mag (e.g., Kewley et al. 2006).

Cons: (1) Significant amounts of more widespread dust extinction due to the galaxy ISM may be present, and it may not be possible to reliably correct for this extinction if it is too large. (2) The [OIII] line can be contaminated by a contribution owing to star formation (which will be significant in the composite objects shown in **Figure 5**). Examples of the empirical techniques for correcting for contamination by stellar ionization are described by Kauffmann & Heckman (2009) and Wild et al. (2010). (3) The luminosity of the line depends on the uncertain fraction of the AGN ionizing luminosity that is intercepted by clouds in the NLR.
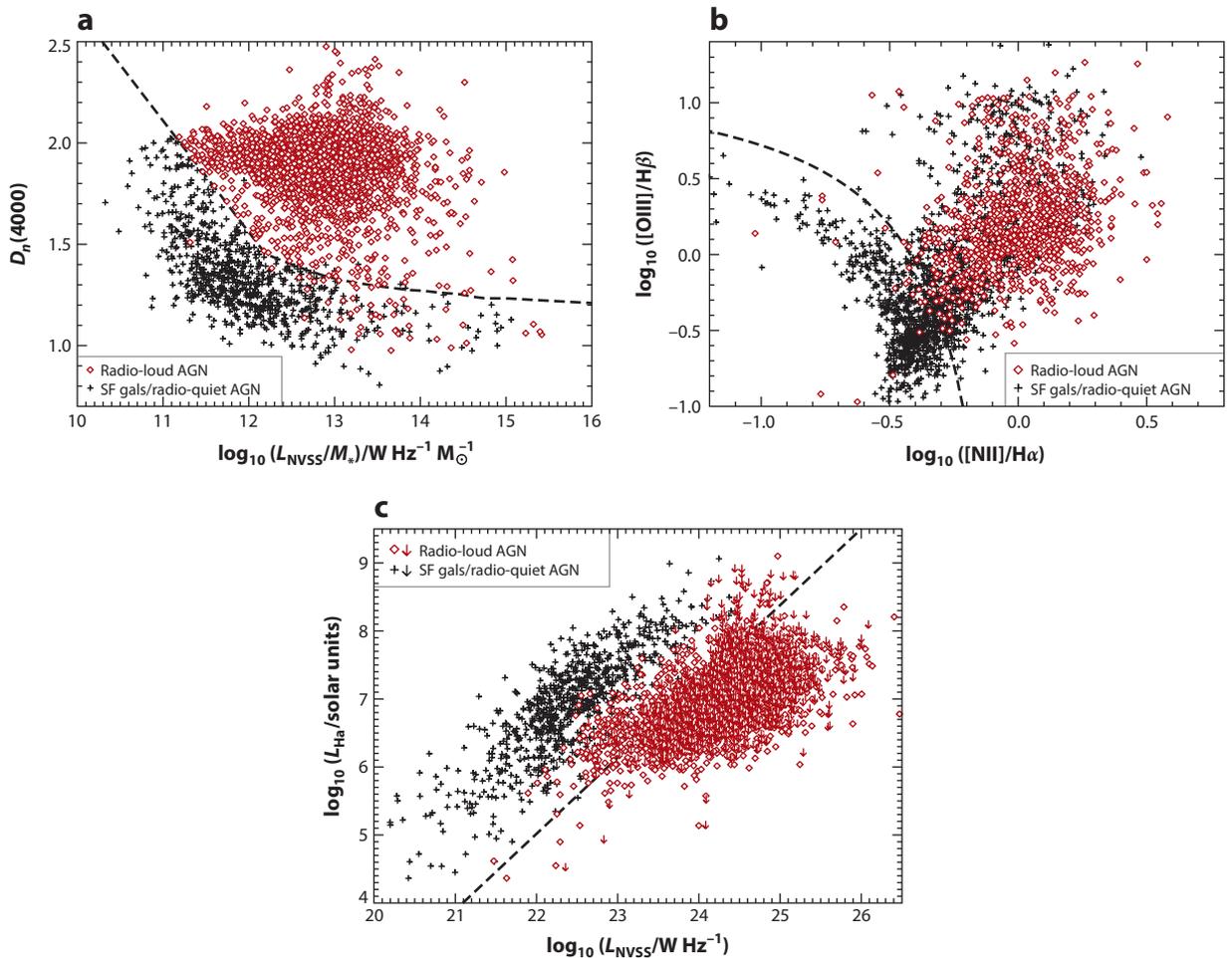
Figure 6

Diagnostic diagrams showing the galaxies within the Sloan Digital Sky Survey main galaxy sample that are detected in the radio waveband above $S_{1.4\,GHz} = 5$ mJy. These diagrams are used to separate genuine radio-loud AGNs from other radio-detected galaxies in which the radio emission is powered by star formation (this includes both radio-quiet AGNs and star-forming galaxies). (*a*) The "D(4000) versus $L_{1.4\,GHz}/M$" method, originally developed by Best et al. (2005a). (*b*) The widely used "BPT" (Baldwin-Phillips-Terlevich) emission-line ratio diagnostic. (*c*) The relationship between Hα and radio luminosity (*arrows* indicate upper limits to the Hα luminosity). In all plots, the dotted lines indicate the division used by Best & Heckman (2012) for that classification method. For the BPT diagnostic diagram, this division separates AGNs from star-forming galaxies in terms of what powers the emission lines, rather than what powers the radio emission. The division line in the $L_{H\alpha}$ versus $L_{1.4\,GHz}$ plot was defined to ensure a clean sample of genuine radio-loud AGNs below the division. Through combinations of the locations of galaxies in the three diagrams [see Best & Heckman (2012) for details], sources can be given an overall classification as radio-loud AGNs (*red diamonds*) or star-forming (SF) galaxies/radio-quiet AGNs (*black crosses*). Adapted from Best & Heckman (2012) with permission.

2.3.1.2. Proxy 2: The [OIV] 25.9-micron and [NeV] 14.3,24.3-micron emission lines. These proxies have the same physical origin as the [OIII] 5007 line, arising from photoionized gas in the NLR.

Pros: (1) They arise well outside the region of the heaviest obscuration. (2) As mid-IR lines they are much less affected by dust extinction than the [OIII] 5007 line. (3) They have ionization

potentials above the HeII edge at 54.4 eV (where a population of massive stars produces very little radiation). They therefore suffer much less contamination from stellar photoionization than [OIII]. This is especially true for [NeV]. This advantage relative to [OIII] has been exploited by Satyapal et al. (2008, 2009) and Goulding & Alexander (2009) to identify examples of low-luminosity AGNs in the nuclei of nearby late-type galaxies that were not recognized as AGNs based on optical spectra that were dominated by regions of star formation.

Cons: (1) They are expensive to observe (having been detected in hundreds of objects rather than hundreds of thousands). (2) The luminosity depends on the uncertain fraction of the AGN ionizing luminosity that is intercepted by clouds in the NLR.

2.3.1.3. Proxy 3: The mid-infrared continuum.

This is produced by warm dust in the obscuring structure and as such represents the reprocessing of the primary UV/visible emission from the accretion disk and the soft X-rays from its corona.

Pros: (1) Thanks to WISE, we now have measurements of the near- to mid-IR continuum in a very large sample of galaxies in the nearby Universe (comparable in size with the SDSS main galaxy sample). (2) It represents a substantial fraction of the bolometric luminosity (roughly 25% in Type 1 AGNs where we directly observe nearly all the emission).

Cons: (1) The mid-IR light from the obscuring structure may not be emitted in an isotropic way and correction for this effect is uncertain at the level of factors of several (Buchanan et al. 2006; but see Gandhi et al. 2009). This effect is largest at the shortest mid-IR wavelengths. (2) The net observed mid-IR emission is the sum of the emission from the AGN and dust heated by hot stars. A decomposition of these two emission processes is uncertain and model dependent. This effect is worse at longer IR wavelengths.

2.3.1.4. Proxy 4: The hard X-ray continuum.

In a Type 2 AGN the observed hard X-ray emission is a combination of whatever radiation succeeds in traversing the obscuring structure plus emission from the central AGN that has been scattered or reprocessed into our line of sight (e.g., Murphy & Yaqoob 2009).

Pros: (1) The hard X-ray emission probes regions very close to the SMBH (the accretion disk corona), but suffers far less obscuration than optical or UV observations of the accretion disk. (2) This hard X-ray emission is a rather unambiguous indicator of an AGN (rather than a starburst) at luminosities greater than about 10^{42} erg s^{-1}.

Cons: (1) Hard X-rays are poor probes of the AGN emission at the high column densities often inferred for the obscuring structure. This is true for column densities above 10^{24} cm^{-2} in the 2–10 keV band and above 10^{25} cm^{-2} even in the *Swift*/BAT band. These latter are the Compton-thick AGNs. (2) The *Swift*/BAT wide all-sky survey is quite shallow relative to the SDSS in its ability to detect AGNs.

2.3.1.5. Estimating the bolometric luminosity.

Having briefly described the various proxies, we now summarize the evidence as to how well they actually do in estimating the AGN bolometric luminosity. The problem with this is that we do not know the ground truth needed to make this evaluation. The best approach is to intercompare these different proxies among the Type 2 AGNs and also to evaluate their behavior relative to the Type 1 AGNs (where obscuration is minimized) (see **Figure 7**).

LaMassa et al. (2010) examined a wide range of proxies in two complete samples of Type 2 AGNs. One was selected on the basis of the flux of the [OIII] 5007 emission line from the SDSS and the other was selected on the basis of the mid-IR (12-μm) flux measured with IRAS
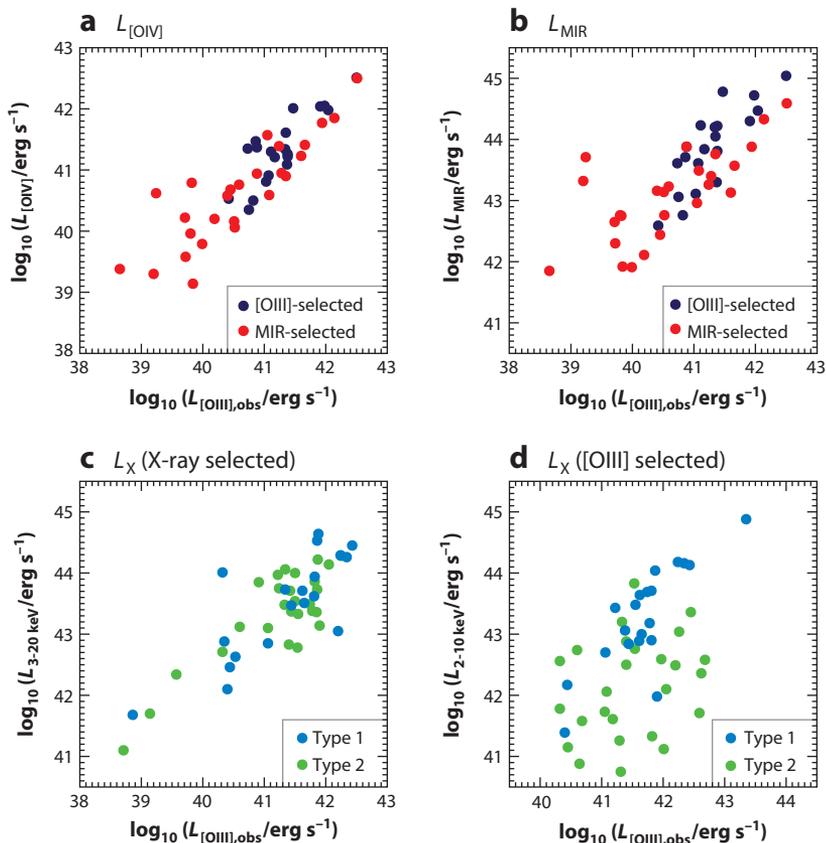
Figure 7

Relationships between different estimators of bolometric luminosity for radiative-mode AGNs. A comparison of the [OIII] emission-line luminosity with (*a*) the [OIV] line luminosity and (*b*) mid-IR (MIR) continuum luminosity, for samples of galaxies selected from their [OIII] emission line and their 12-μm mid-IR flux (data from LaMassa et al. 2010). The hard X-ray versus [OIII] luminosity for (*c*) X-ray-selected and (*d*) emission-line-selected samples of AGNs (data from Heckman et al. 2005). Type 2 AGNs in the emission-line-selected samples do not show a good correlation due to X-ray absorption.

(hereafter the SDSS-OIII and IRAS-MIR samples). The proxies they considered for the bolometric luminosity were the luminosities of the [OIII] 5007 line, the [OIV] 25.9-micron line, the mid-IR (12-μm) continuum, the hard X-ray *Swift*/BAT continuum, and the 8.4-GHz nuclear radio continuum. They examined the correlations between all possible pairs of the proxies and compared the distributions of the flux ratios of all proxy pairs with those of samples of unobscured Type 1 AGNs (cf. **Figure 7**). They concluded that the luminosity of the [OIV] line is the single best proxy and that the radio and hard X-ray luminosities are the worst. The problem with the hard X-ray luminosity is that many of the Type 2 AGNs in the SDSS-OIII and IRAS-MIR samples are Compton-thick and significantly obscured even in the *Swift*/BAT band (14–195 keV) (see also Heckman et al. 2005 and Winter et al. 2010). Similar conclusions were drawn by Rigby et al. (2009) on the basis of comparison of the flux ratio of the [OIV] 25.9-micron line and hard X-ray continuum (above 10 keV) in optically selected Type 1 and Type 2 AGNs drawn from the Revised Shapley-Ames Catalog (hereafter the RSA sample).

An analysis of multiple proxies in the RSA sample was undertaken by Diamond-Stanic et al. (2009). They found that the ratio of the flux of the 2–10-keV continuum and the [OIV] emission line was smaller on average in the Type 2 AGNs than in Type 1 AGNs and varied by about three orders of magnitude. This implies a wide range in the amount of attenuation of the 2–10-keV X-ray emission in these Type 2 AGNs (see **Figure 7**). They also found that the flux ratio of the [OIII] 5007/[OIV] 25.9-micron lines was systematically smaller in Type 2 than in Type 1 AGNs and showed more scatter in the RSA sample. They argued that this was a result of a greater amount of dust extinction in Type 2 AGNs (by typically 1 to 2 mag). LaMassa et al. (2010) found a much smaller offset in this ratio in the SDSS-OIII and IRAS-MIR samples (implying a mean excess extinction of [OIII] by only about 0.5 mag in the Type 2 AGNs). These results do underscore the importance of correcting the [OIII] flux for extinction (when possible).

Shao et al. (2013) have analyzed WISE observations of a sample of 30,000 Type 2 AGNs identified in SDSS spectra. They find an excellent overall correlation between the luminosities of the (extinction-corrected) [OIII] 5007 emission line and the (starlight-subtracted) 4.6-micron emission from hot AGN-heated dust (rms scatter of about 0.3 dex). Moreover, the partitioning of the AGN emission as a function of host-galaxy parameters is the same based on the [OIII] and 4.6-micron emission (once LINERs were excluded). Finally they show that the existing color-color techniques that have been used to identify AGNs from *Spitzer* and WISE data recover only the most luminous AGNs (objects in which the AGN significantly outshines its host galaxy in the near- and mid-IR). This misses most of the optically identified Type 2 AGNs in the SDSS, which have lower luminosities.

A simple summary of the above is that there is no single perfect proxy for the bolometric luminosity in obscured AGNs. Even relatively good proxies produce estimates of the bolometric luminosity of any individual obscured AGN that will be uncertain at the level of a factor of several (in a root-mean-square sense). Given the huge number of AGNs with measured [OIII] 5007 luminosities (e.g., Hao et al. 2005b, Kauffmann & Heckman 2009), we adopt this as our default proxy for the optically selected Type 2 AGNs. Based on an analysis of multiwaveband data for two samples of Type 1 AGNs, Heckman et al. (2004) calculated a mean bolometric correction to the [OIII] 5007 luminosity of a factor of 3,500. This refers to [OIII] luminosities derived from the raw [OIII] flux with no correction for dust extinction and assumes that Type 1 and Type 2 AGNs have the same bolometric correction. Kauffmann & Heckman (2009) adopted a mean bolometric correction of 600 for the extinction-corrected [OIII] 5007 luminosity. This was based on the multiwaveband data subsequently presented by LaMassa et al. (2010) and is consistent with the average value for the extinction of the [OIII] emission as measured in Type 2 Seyferts by Kewley et al. (2006). We adopt this factor 600 bolometric correction for calculations within this review.

Netzer (2009) finds similar mean bolometric corrections for the observed and extinction-corrected [OIII] 5007 luminosities. He argues, however, that the bolometric correction for a given AGN will depend on the ionization state of the gas in the NLR and that a combination of the luminosities of the [OIII] 5007 and [OI] 6300 lines is a more robust estimator of the bolometric luminosity. We agree with this point, but note that the [OI] 6300 line is significantly weaker than the [OIII] 5007 line (by a factor of typically 3 in LINERs and 10 in Seyfert nuclei). Requiring the [OI] line to be well detected diminishes the ability to probe AGNs at lower luminosities and/or over larger volumes in the SDSS main galaxy sample. The difference between Netzer's method and ours is most significant in the case of LINERs. As we have discussed above, a number of recent papers have concluded that the majority of LINERs in the SDSS (those with the weakest emission lines) are not bona fide AGNs. However, for the minority population of LINERs that are clearly AGNs we agree that Netzer's methodology is better.

Finally, it is important to note that these bolometric corrections can be luminosity dependent. This dependence is well established in the hard X-ray regime where the bolometric correction increases systematically with luminosity (e.g., Marconi et al. 2004). There have been claims and counter claims about a luminosity dependence for the bolometric correction to the [OIII] luminosity. Most recently, Stern & Laor (2012b) have analyzed SDSS spectra of a large sample of Type 1 AGNs and find that in log-log plots the [OIII] luminosity has a sublinear dependence on the UV continuum luminosity and on the broad Hα luminosity, but a linear dependence on the hard X-ray luminosity. They derive a bolometric correction to the [OIII] luminosity that increases by an order of magnitude over the range between $L_{[OIII]} \sim 10^{6.5}$ and $10^9\,L_\odot$. However, Shao et al. (2013) find a linear dependence of the [OIII] luminosity on the mid-IR luminosity (from WISE) for Type 2 SDSS AGNs over the same range in [OIII] luminosity. LaMassa et al. (2010) found a superlinear dependence of $L_{[OIII]}$ on the mid-IR continuum luminosity for Type 2 AGNs. Hainline et al. (2013) confirm this relationship, extending it to the yet higher luminosities of Type 2 QSOs. The implied bolometric correction to $L_{[OIII]}$ decreases by about an order of magnitude between $L_{[OIII]} \sim 10^6$ and $10^{9.5}\,L_\odot$ (i.e., the opposite of the result Stern & Laor found for Type 1 AGNs). The reason for this disagreement is not clear. Hainline et al. also find a possible saturation in $L_{[OIII]}$ at MIR luminosities above about $10^{12}\,L_\odot$ and attribute this to a transition to matter-bounded conditions where the AGN is effectively photoionizing the entire galaxy ISM (see also Netzer et al. 2006). We emphasize in closing that most of the results reviewed below (and our own new analyses) have assumed a luminosity-independent bolometric correction for $L_{[OIII]}$ in Type 2 AGNs.

2.3.2. Mechanical energy outflow rates in radio jets. We now turn our attention to estimating the energy outflow rate in radio jets. In jet-mode AGNs, this can greatly exceed the radiative bolometric luminosity. It can also make a significant contribution to the total energetics in the small population of radio-loud radiative-mode AGNs.

The AGN jets are observable through their radio synchrotron emission. Monochromatic radio luminosity represents only a small fraction of the energy transport: The mechanical (kinetic) power of the jets is estimated to be about 2 orders of magnitude larger (Scheuer 1974). The jet mechanical power (P_{mech}) can be estimated from the synchrotron emission using the minimum energy condition to estimate the energy stored in the radio lobes. This assumes that the magnetic field has the strength that minimizes the combined energy content of particles and magnetic fields needed to produce the observed synchrotron emission (see Miley 1980). This is then combined with the age of the radio source (from synchrotron spectral aging techniques or radio source growth models; cf. Willott et al. 1999) and an efficiency factor that accounts for losses due to work done by the expanding radio source (Rawlings & Saunders 1991).

Our incomplete knowledge of the physics of radio sources leads to significant uncertainties in this estimation. Primary among these are the composition of the radio jet plasma and the low-energy cutoff of the electron energy distribution. The observed synchrotron emission traces only the highly relativistic electron population, and there are indications that the energy density in protons may be up to an order of magnitude higher (e.g., Bell 1978). Similarly, extrapolating the electron energy distribution down from the observed limit of $\gamma > 100$ to $\gamma \sim 1$ can increase the energy estimates by a factor of a few (depending upon the spectral index). Willott et al. (1999) combined all of the uncertainties into a single factor, f_W, that through observational constraints they determined to lie between $\sim$1 and 20. Subsequent work favored values toward the upper end of that range (e.g., Blundell & Rawlings 2000, Hardcastle et al. 2007). The mechanical jet power

derived by Willott et al., expressed in terms of the 1.4-GHz radio luminosity, corresponds to

$$P_{\text{mech,sync}} = 4 \times 10^{35}(f_W)^{3/2}(L_{1.4\,\text{GHz}}/10^{25}\,\text{W Hz}^{-1})^{0.86}\,\text{W}. \qquad (1)$$

Note that weak dependencies on other radio source properties such as environment and source size also exist (see also Shabala & Godfrey 2013), but can be ignored to first order. O'Dea et al. (2009) used deep multifrequency radio data for 31 powerful radio galaxies to observationally estimate the pressure, volume, and spectral age of the lobes, and hence to derive the jet power. Daly et al. (2012) combined these with the radio luminosities to derive a relation between P_{mech} and L_{radio} and found a slope of 0.84, almost exactly the same as the Willott et al. theoretical prediction. Their normalization is consistent with Equation 1 for $f_W \sim 5$.

The expanding radio sources inflate lobes of relativistic plasma, which in X-rays can be observed as bubbles, or cavities, in the surrounding hot gas (Böhringer et al. 1993). As X-ray facilities developed the sensitivity and angular resolution to accurately measure the extent of these cavities and the pressure of the surrounding intergalactic medium, an alternative method of estimating the radio jet power became available. Bîrzan et al. (2004) derived the pV energy associated with the cavities in a sample of groups and clusters and used the buoyancy timescale (e.g., Churazov et al. 2001) to estimate their ages. They combined these cavity powers with the monochromatic 1.4-GHz radio luminosities to show that the two were well correlated, with a scatter of $\sim$0.7 dex. Further cavity power measurements in systems ranging from giant elliptical galaxies to the most massive clusters have refined this correlation (e.g., Dunn et al. 2005, Rafferty et al. 2006, Bîrzan et al. 2008, Cavagnolo et al. 2010; see **Figure 8**). The largest uncertainty in this method is the determination of the cavity energy from the measured pressure and volume: $E_{\text{cav}} = f_{\text{cav}}\,pV$. The work done inflating the cavity implies $f_{\text{cav}} > 1$, whereas for the relativistic plasma of the radio lobes the enthalpy of the cavity is $4pV$. Additional heating arising directly from the radio jet shocks (e.g., Forman et al. 2007) could imply higher values of f_{cav}, with some authors arguing that f_{cav}
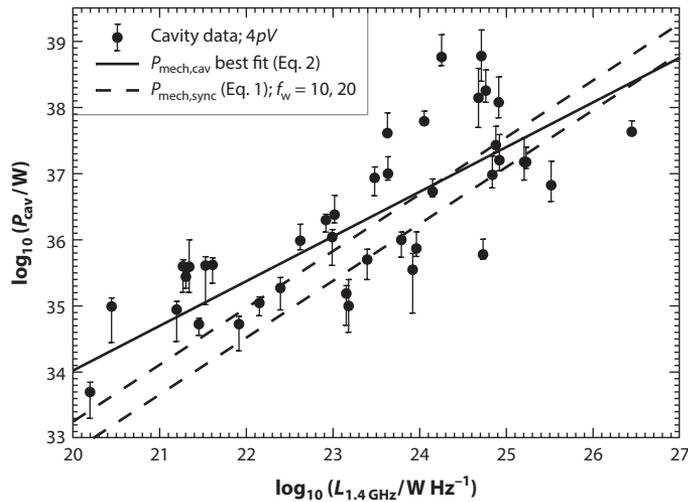

Figure 8

The jet mechanical energy of radio sources, estimated as $4pV$ from cavities and bubbles in the X-ray gas, versus the monochromatic 1.4-GHz radio luminosity. Data are primarily sourced from Cavagnolo et al. (2010), Bîrzan et al. (2008), and Rafferty et al. (2006). The solid line indicates the best-fit linear relation given in Equation 2 [$P_{\text{mech, cav}} = 7 \times 10^{36}\,f_{\text{cav}}(L_{1.4\,\text{GHz}}/10^{25}\,\text{W Hz}^{-1})^{0.68}\,\text{W}$]. For comparison, the dotted lines show the synchrotron estimate of Equation 1 [$P_{\text{mech,sync}} = 4 \times 10^{35}(f_W)^{3/2}(L_{1.4\,\text{GHz}}/10^{25}\,\text{W Hz}^{-1})^{0.86}\,\text{W}$] for values of $f_W = 10$ and 20.

can be as high as $\sim$10 (e.g., Nusser et al. 2006). The value of $f_{cav} = 4$ is the one usually adopted (e.g., Cavagnolo et al. 2010) and is consistent with a broad balance between AGN heating and radiative cooling in massive clusters (see Section 6).

Figure 8 shows a compilation of jet mechanical energy (assuming $4pV$) and radio luminosity measurements, primarily drawn from the analysis of Cavagnolo et al. (2010), recast into the same format as Equation 1. From this we derive a best-fit linear relation of

$$P_{mech, cav} = 7 \times 10^{36} f_{cav}(L_{1.4\,GHz}/10^{25}\,W\,Hz^{-1})^{0.68}\,W. \qquad (2)$$

Equations 1 and 2 show very similar slopes, and for factors of $f_{cav} = 4$ and $f_W = 15$, the normalizations also agree for typical sources of $L_{1.4\,GHz} \sim 10^{25}\,W\,Hz^{-1}$ (see **Figure 8**). Although discrepancies would exist for lower values of f_W (cf. Daly et al. 2012), the degree of agreement between these two independent estimators is encouraging. Hereafter in this review, Equation 2 with $f_{cav} = 4$ is adopted to calculate jet mechanical power from the radio luminosity.

2.3.3. Black hole masses, Eddington ratios, and accretion rates. The masses for SMBHs have been determined in two types of situations. In the case of Type 1 AGNs, the time-dependent response of the gas in the BLR to changes in the ionizing continuum flux can be used to infer a size for the BLR (from light-travel-time arguments). This size, together with the measured velocity dispersion in the BLR, can be used to estimate M_{BH} under the assumption that gas is acting solely under the dynamical influence of the SMBH. This technique is called reverberation mapping and has been recently reviewed by Peterson (2013). The subsample of SMBHs with masses determined by reverberation mapping can be used to calibrate a relation between M_{BH} and a combination of the widths of the broad emission lines and the optical continuum luminosity in Type 1 AGNs (e.g., Kaspi et al. 2000, Bentz et al. 2013).

In this review we are focused on Type 2 and jet-mode AGNs and their relationship to the more numerous population of inactive galaxies. In these cases, M_{BH} has been measured directly through the dynamical modeling of the spatially resolved kinematics of stars and/or gas. This subject has been recently reviewed by Kormendy & Ho (2013). There are still fewer than 100 galaxies in which M_{BH} has been determined directly. In order to estimate M_{BH} in large surveys like the SDSS, indirect (secondary) techniques must be used. The most widely used secondary technique is based on a fit to the relationship between M_{BH} and the stellar velocity dispersion (σ) of the surrounding galactic bulge (the M-σ relation—Ferrarese & Merritt 2000, Gebhardt et al. 2000; see **Figure 9**). This technique is particularly useful for the SDSS main galaxy sample. The SDSS fiber typically covers the region within a radius of a few kiloparsecs of the nucleus. The typical hosts for the SDSS AGNs are early-type galaxies (see Section 4 below), and thus the measured stellar velocity dispersion is representative of the bulge.

Most of the results in the literature that used the M-σ relation were based on the fit given by Tremaine et al. (2002): $\log(M_{BH}/M_\odot) = 8.13 + 4.02\log[\sigma/(200\,km\,s^{-1})]$. More recent work has found a steeper slope and a different normalization than the Tremaine et al. fit (see the Kormendy & Ho 2013 review). More specifically, the recent analyses by Graham & Scott (2013), McConnell & Ma (2013), and Woo et al. (2013) find respective slopes of 6.18, 5.64, and 5.48 and zero points of 8.15, 8.32, and 8.33. Woo et al. (2013) also conclude that the relationship between BH mass and σ is consistent between samples of AGNs and quiescent galaxies (see **Figure 9**), and this conclusion was reinforced by an investigation of powerful AGNs with more massive BHs by Grier et al. (2013). In terms of applicability to the SDSS, note that the SDSS spectra can only reliably measure stellar velocity dispersions above $\sigma \sim 70\,km\,s^{-1}$, corresponding to BH masses larger than of order $10^6\,M_\odot$ (depending on which version of M-σ is adopted). A complementary probe of lower-mass SMBHs in the SDSS is provided by using mass estimates based on the broad
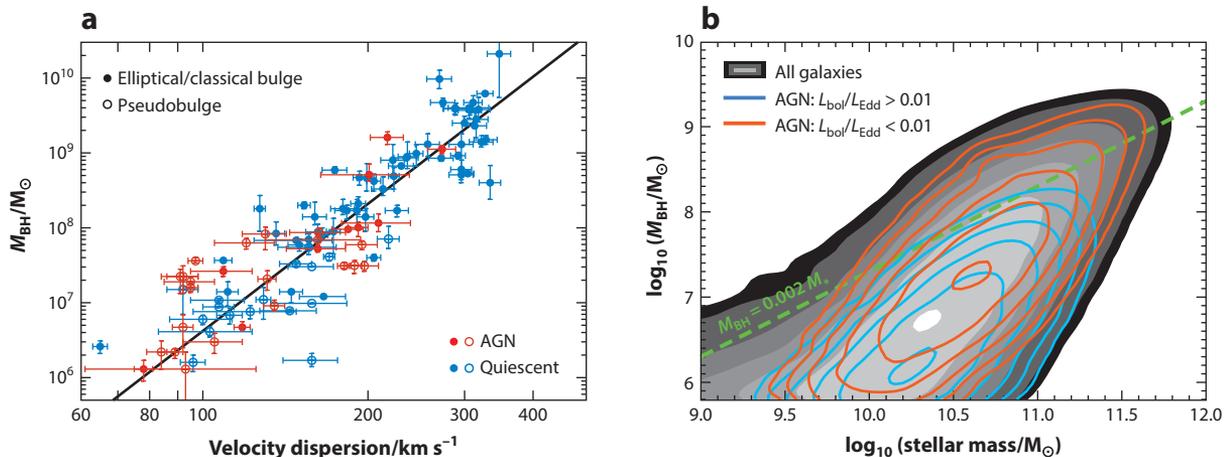
a

b

Figure 9

(*a*) The M_{BH}-σ relation of local galaxies with direct black hole mass measurements (data from Woo et al. 2013 and references therein). Both AGNs (the color-coding includes both radiative-mode and jet-mode AGNs) and quiescent galaxies are consistent with the McConnell & Ma (2013) relation, shown by the solid line. (*b*) The distribution of galaxies in the Sloan Digital Sky Survey main galaxy sample on the stellar mass versus black hole mass plane using black hole masses derived from the M_{BH}-σ relation. The grayscale indicates the volume-weighted distribution of all galaxies, with each lighter color band indicating a factor of two increase. The black hole mass is not a fixed fraction of the total stellar mass. This is also true for AGNs: The blue and red contours show the volume-weighted distributions of high (>1%; mostly radiative-mode) and low (<1%; mostly jet-mode) Eddington-fraction AGNs, with contours spaced by a factor of two.

emission-line width for Type 1 AGNs (Greene & Ho 2007b, Dong et al. 2012, Kormendy & Ho 2013).

Another secondary technique uses the correlation between M_{BH} and the stellar mass of the bulge (e.g., Marconi & Hunt 2003, Haring & Rix 2004). Although this is straightforward to apply to elliptical galaxies, the typical AGN host galaxies in the SDSS sample have significant bulge and disk components (Section 4). The SDSS images are shallow and do not well-resolve the bulge component in typical cases. This makes the task of robustly determining the bulge/disk mass ratio rather expensive in terms of computational time and the need for human intervention (e.g., Gadotti 2009, Lackner & Gunn 2012). Thus, this technique for estimating M_{BH} is less readily applicable to the SDSS AGN sample. Moreover, the new data compiled by Kormendy & Ho (2013) and the analysis by Graham & Scott (2013) both imply that the correlation of M_{BH} is significantly poorer with stellar bulge mass than with σ.

In this review we derive values for M_{BH} using the simple power-law M-σ relation used by McConnell & Ma (2013), specifically,

$$\log(M_{BH}/M_\odot) = 8.32 + 5.64 \log[\sigma/(200\,\mathrm{km\,s^{-1}})]. \tag{3}$$

It is important to emphasize here that it is not a reasonable approximation to assume that the BH mass is some fixed fraction of the total stellar mass. To illustrate this, we show in **Figure 9b** a plot of the total galaxy stellar mass versus the BH mass as estimated using our adopted M-σ relation for the SDSS main galaxy sample. The ratio of estimated BH–to–galaxy mass drops from an average of about $10^{-2.5}$ at $M_* \sim 10^{11.5}\,M_\odot$ to about 10^{-4} at $M_* \sim 10^{10}\,M_\odot$. As also shown in this figure, this is true for galaxies in general and for the hosts of both radiative-mode and jet-mode AGNs.

With an estimate of the AGN bolometric luminosity and SMBH mass in hand it is useful to then recast things in terms of the Eddington ratio for the AGN (L_{bol}/L_{Edd}). Here L_{Edd} is the

luminosity of the classical Eddington limit:

$$L_{\text{Edd}} = (4\pi G m_p c / \sigma_T) M_{\text{BH}} = 3.3 \times 10^4 M_{\text{BH}}, \qquad (4)$$

where for the numerical form of the relation the luminosity and mass are in solar units. More uncertain still is an estimate of the accretion rate onto the SMBH. This is typically computed assuming a fixed efficiency ϵ for the conversion of accreted mass into radiant energy:

$$L_{\text{bol}} = \epsilon \dot{M} c^2. \qquad (5)$$

It is typically assumed that $\epsilon \sim 0.1$. This relatively high efficiency is well motivated theoretically for a BH radiating at a significant fraction of the Eddington limit (i.e., the radiative-mode AGNs), but may substantially underestimate the accretion rate of AGNs with very small Eddington ratios (the jet-mode AGNs). We discuss this more quantitatively in Section 5 below.

2.4. Determining Basic Galaxy Parameters

2.4.1. From imaging and photometry. With the advent of digital surveys of large regions of the sky, astronomers were motivated to design automated algorithms for measuring the principle properties of galaxies (e.g., Lupton et al. 2002). The size of a galaxy is most often parameterized by the radius that encloses a fixed fraction (often 50%; written as R_{50}) of the total light. The shape of the radial surface-brightness profile provides a simple way to estimate the prominence of the bulge with respect to the disk: Galaxies with concentration index $C = R_{90}/R_{50} > 2.6$ are predominantly bulge-dominated systems, with Hubble classification of Type Sa or earlier, whereas galaxies with $C < 2.6$ are mostly disk-dominated systems (Shimasaku et al. 2001). Gadotti (2009) performed 2D bulge/bar/disk decompositions of a representative sample of galaxies from the SDSS and found that the concentration index correlated more tightly with the bulge-to-disk ratio than the Sérsic index n obtained from 1D profile fitting. Lackner & Gunn (2012) reached a similar conclusion from analysis of a larger SDSS sample. Recently, the power of citizen science has been exploited to create visual classifications of roughly 900,000 SDSS galaxies (Lintott et al. 2011). These classifications have been used to document the nature of the host galaxies of AGNs (e.g., Schawinski et al. 2010).

The stellar mass-to-light ratio (and hence the stellar mass) of a galaxy can be measured using multiband optical and near-IR photometry to an accuracy of ~10%. Although this spectral energy distribution is sensitive to both the (luminosity-weighted) age of the stellar population and the amount of dust reddening, these two effects operate in such a way that the relation between optical color and M/L is linear with little scatter if galaxies have undergone relatively smooth recent star-formation histories (Bell & De Jong 2001, Salim et al. 2005). These estimates assume a fixed stellar initial mass function. The effective surface mass density μ_* is then defined as $0.5 M_* / (\pi R_{50}^2)$.

The SFR of a galaxy can also be estimated from fits to the UV through near-IR multiband photometry (e.g., Salim et al. 2005). UV photometry from GALEX is particularly important as it probes the young stellar population in star-forming galaxies. We note, however, that in the absence of far-IR photometry, which allows the thermal emission from dust to be measured directly, SFRs estimated from UV/optical photometry can be significantly biased if the range of dust extinction values in the spectral energy distribution (SED) model library is incorrect (Saintonge et al. 2011, Wuyts et al. 2011a). Most of this dust emission powered by the reprocessing of UV light from massive stars emerges in the far-IR. Unfortunately, the depth of the all-sky IRAS survey is not well matched to the SDSS main galaxy sample, with only about 2% of these galaxies being reliably detected by IRAS at 60 and 100 μm (Pasquali et al. 2005). The situation has been improved in some respects by the WISE survey, which detects about 25% of the SDSS main galaxies in all

four WISE bands (3.4, 4.6, 12, and 22 μm). The disadvantage of the WISE data for estimating the SFR is that larger and more uncertain corrections need to be made to estimate the total IR luminosity than in the case of IRAS. In the case of AGNs, the WISE data suffer from the further problem of potential contamination by AGN-powered emission from warm dust in the obscuring structure, even at the longest-wavelength WISE band (22 μm).

Finally, radio continuum emission can also be used to estimate the SFR because it shows a strong correlation with the far-IR emission in star-forming galaxies (Condon 1992). Given the depth of the FIRST survey, the sensitivity of this technique over the SDSS volume is rather similar to that of the IRAS Faint Source Catalog, but—for our purposes—it has the disadvantage of being more susceptible to contamination by AGN emission than the far-IR.

2.4.2. From spectra. The spectra available for galaxies from the SDSS are taken through 3-arcsec diameter fibers. At the median redshift of the main galaxy sample ($z \sim 0.1$), only about 25–30% of the total light from the galaxy is sampled. As a result, estimates of the global SFRs of SDSS galaxies cannot be made using only the spectra (Brinchmann et al. 2004). The spectra do, however, provide a very useful probe of the central stellar populations of normal galaxies and AGN hosts.

The break occurring at 4,000 Å is the strongest discontinuity in the optical spectrum of a galaxy. The main contribution to the opacity comes from low-ionization metals. In hot stars, the elements are multiply ionized and the opacity decreases, so the 4,000-Å break will be small for young stellar populations and large for old, metal-rich galaxies. A break index, D(4000), was defined initially by Bruzual (1983). A definition using narrower and more closely spaced continuum bands was introduced by Balogh et al. (1999) and has the advantage of being considerably less sensitive to reddening effects.

Strong Balmer absorption lines arise in galaxies that experienced a burst of star formation that ended $\sim 10^8$ to 10^9 years ago, when A stars are the dominant contributors to the optical continuum (e.g., Dressler & Gunn 1983). Worthey & Ottaviani (1997) defined an $H\delta_A$ index using a central bandpass bracketed by two pseudocontinuum bandpasses. Kauffmann et al. (2003b) used stellar population models (Bruzual & Charlot 2003) to show that the locus of galaxies in the D(4000)-$H\delta_A$ plane is a powerful diagnostic of whether galaxies have been forming stars continuously or in bursts over the past 1–2 Gyr. In addition, these two stellar indices are largely insensitive to the dust attenuation effects that complicate the interpretation of broad-band colors. These indices are very useful diagnostics of the recent star-formation history of Type 2 and jet-mode AGNs.

Measurements of the $H\delta_A$ index that have a precision that is good enough to provide useful constraints require relatively high signal-to-noise data. However, the $H\delta$ line itself is only one of a handful of other high-order Balmer lines in the blue/near-UV portion of the spectrum. The situation can be significantly improved by utilizing the combined information in these lines. One technique for doing so uses principal component analysis. This approach has been successfully applied to SDSS spectra by Wild et al. (2007) and Chen et al. (2013b). More examples of the use of principal component analysis and other sophisticated techniques for extraction of information about the stellar content and star-formation history from the SDSS galaxy spectra are demonstrated by Panter et al. (2003, 2007), Cid Fernandes et al. (2005), and Yip et al. (2004).

3. BLACK HOLE MASS AND AGN LUMINOSITY FUNCTIONS

3.1. The Radiative-Mode Population

The luminosity functions for the radiative-mode AGNs (Seyferts and QSOs) can be constructed using a variety of different indicators. Some indicators, such as broad-band optical luminosities, are effective at probing unobscured BHs accreting near their Eddington limit at high redshifts.

However, when the accretion rate is low, these broad-band optical luminosities are dominated by stellar emission from the host galaxy. Moreover, the optical/UV continuum will not recover the obscured (Type 2) AGN population. Other indicators, such as high-ionization nebular emission-line luminosities, mid-IR continuum emission, and X-ray emission, have been used to probe lower accretion rate and obscured systems. Nice syntheses of these multiwaveband data have been undertaken by Hopkins et al. (2007b) and Shankar et al. (2009), who use them to produce bolometric luminosity functions for the radiative-mode AGNs that span the redshift range from ∼0 to 6.

At a given redshift, the AGN bolometric luminosity function can be approximated as a double power law:

$$d\Phi/d\log(L) = \phi_*/\left[(L/L_*)^{\gamma_1} + (L/L_*)^{\gamma_2}\right]. \tag{6}$$

This is characterized by a faint-end slope (γ_1), a bright end slope (γ_2), the characteristic luminosity of the break in the function (L_*), and the comoving space density of AGNs with that luminosity (ϕ_*). The evolution of the bright end of the luminosity function from redshifts ∼0 to 3 can be well described by a so-called pure luminosity evolution (PLE) model in which L_* evolves strongly with redshift while γ_2 and ϕ_* do not (Hopkins et al. 2007b). Fiore et al. (2012) show that this behavior of the bright AGN population may extend to even higher redshifts. The value for L_* (bolometric) increases from about $10^{11.5}$ L$_\odot$ at $z \sim 0$ to 10^{13} L$_\odot$ at $z \sim 2$ to 3, and then declines at higher redshift (e.g., Hopkins et al. 2007b, Shankar et al. 2009).

The first clear indications for a departure from the PLE model came from X-ray surveys of AGNs using the *Chandra X-Ray Observatory*, which generated complete samples of Type 1 AGNs down to significantly lower luminosities than was possible with optical surveys (see Brandt & Hasinger 2005). These surveys demonstrated that the space density of lower-luminosity AGNs peaks at lower redshift than that of higher-luminosity AGNs, a phenomenon that is often referred to as AGN downsizing. Similar results were later obtained by optical QSO surveys that pushed down to fainter flux levels. The QSO luminosity function of the completed 2dF-SDSS optically selected QSO survey (Croom et al. 2009) agrees extremely well in both amplitude and shape with the X-ray-selected QSO luminosity functions of Hasinger et al. (2005).

In terms of the luminosity function, this departure from a PLE model is primarily manifested as an evolution in the faint-end slope with γ_1 increasing from ∼0.3 at $z = 3$ to ∼0.9 at $z = 0$ (Hopkins et al. 2007b). The steep faint-end slope at low z is seen for both Type 1 and Type 2 AGNs and in both the [OIII] 5007 (Hao et al. 2005a,b) and hard X-ray (Ueda et al. 2011 and references therein) luminosity functions. Note that a faint-end slope of 1 corresponds to equal radiant output per bin in log L. This has an important implication: while at high redshifts the bulk of the radiant output occurs in AGNs near L_*, this is not the case in the contemporary Universe where it is spread rather evenly across a broad range in luminosity (and only about 20% is produced by AGNs with $L_{bol} > L_*$).

Heckman et al. (2004) used data from the SDSS to compute the integrated [OIII] luminosity emitted by (Type 2 and jet-mode) emission-line AGNs per unit BH mass for nearby BHs spanning the mass range $3 \times 10^6 - 10^9\,M_\odot$. They adopted a bolometric correction $L_{bol}/L_{[OIII]} = 3,500$ (see Section 2.3.1) and a mass-to-energy conversion efficiency of $\epsilon = 0.1$ to transform these ratios into estimates of the time taken for the entire population of BHs to have grown to their present-day mass, given their present-day volume-averaged accretion rate. They defined the mass-dependent volume-averaged growth time for the local population of BHs to be the total mass of the BH population per unit volume in a given BH mass bin divided by the total growth rate of the BH population per unit volume in the same BH mass bin. They then found that this volume-averaged growth time of the population was of order the Hubble time for BHs with masses less than
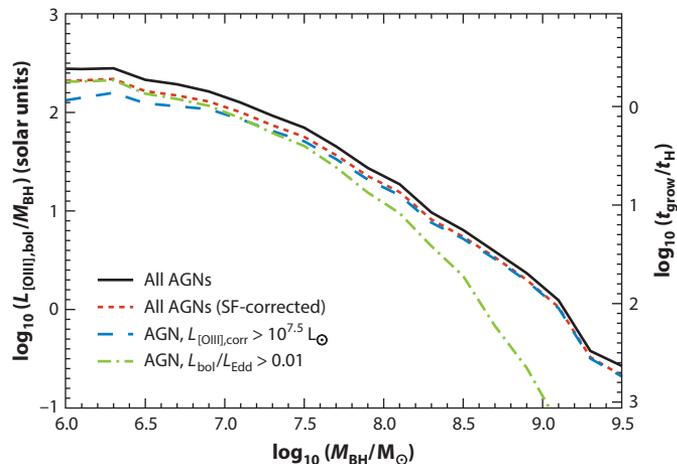
Figure 10

Logarithm of the ratio of the total bolometric radiated luminosity (as calculated from the [OIII] emission line; see Section 2.3.1) per unit volume due to emission-line AGNs of a given black hole mass to the total mass per unit volume in black holes at that black hole mass (both in solar units) in the contemporary Universe (see Heckman et al. 2004). The right axis shows the corresponding growth time (mass-doubling time) for the population of black holes in units of the Hubble time. The solid black line shows the result obtained by integrating over all AGNs in the sample. The dotted red line shows the effect of correcting the [OIII] luminosities for the contribution from star formation in composite galaxies. The dashed blue line shows the result obtained if only AGNs [reddening-corrected and star-formation (SF)-corrected] with [OIII] luminosities above $10^{7.5}$ L$_\odot$ are included. The dash-dot green line includes only AGNs with bolometric luminosities above 1% of the Eddington rate (this cut effectively reduces the sample to only radiative-mode AGNs).

$10^{7.5}$ M$_\odot$, but that this growth time increased sharply for higher mass BHs, implying that most of their mass was accreted at high redshifts (**Figure 10**). Greene and colleagues (Greene & Ho 2007a, Greene et al. 2009) reached similar conclusions for the local Type 1 AGN population in the SDSS.

Heckman et al. (2004) also studied the fraction of BHs of mass M_{BH} with accretion rates above a given value. They showed that these cumulative accretion rate functions cut off sharply at $\dot{M}_{BH}/\dot{M}_{Edd} \simeq 1$. Many more low-mass BHs than high-mass BHs had accretion rates near the Eddington limit (0.5% of 10^7 M$_\odot$ BHs are accreting above a tenth of the Eddington limit, as compared with 0.01% of BHs with masses 3×10^8 M$_\odot$). In a later paper, Kauffmann & Heckman (2009) analyzed Eddington ratio distribution functions in narrow bins of BH mass. They found that the distribution functions can be decomposed into a log-normal distribution of accretion rates, plus a power-law function that dominates at low Eddington ratio. We describe the dependence of this distribution function on the age of the central stellar population in Section 4.2 below.

3.2. The Jet-Mode AGNs

The broad nature of the radio luminosity function of local galaxies has been well-established for many years (e.g., Toffolatti et al. 1987, Condon 1989), but the large spectroscopic surveys have enabled both improved statistics and an accurate separation of the star-forming and radio-AGN populations. Radio luminosity functions derived from the Las Campanas redshift survey (Machalski & Godlowski 2000), the 2dFGRS (Sadler et al. 2002), the SDSS (Best et al. 2005a,

Best & Heckman 2012), and the 6-degree-field galaxy survey (6dFGS; Mauch & Sadler 2007) are all in excellent agreement and show that the local radio luminosity function of AGNs is well fitted by a double power-law model similar in form to Equation 6:

$$\rho = \rho_0 / \left[(P/P_0)^\alpha + (P/P_0)^\beta \right]. \tag{7}$$

At 1.4 GHz, the best-fitting values from combining all four spectroscopic surveys above give $\rho_0 = 10^{-(5.33\pm0.12)}$ Mpc^{-3} $\log_{10}(P)^{-1}$, $P_0 = 10^{24.95\pm0.14}$ W Hz^{-1}, $\alpha = 0.42 \pm 0.04$, and $\beta = 1.66 \pm 0.21$. Mauch & Sadler (2007) show that, at the faint end, the radio luminosity function of radio-loud AGNs continues with the same slope down to at least $P_{1.4\,GHz} \sim 10^{20}$ W Hz^{-1}. They argue that the luminosity function must begin to turn over at around $P_{1.4\,GHz} \sim 10^{19.5}$ W Hz^{-1}, or the total space density of radio sources would exceed the space density of galaxies brighter than L_*, which form the typical hosts. Cattaneo & Best (2009) similarly argue for a turnover no fainter than $P_{1.4\,GHz} \sim 10^{19.2}$ W Hz^{-1} by comparison with the local space density of SMBHs above $10^6\,M_\odot$. Thus, the observed radio luminosity functions now broadly constrain the entire distribution of AGN radio luminosities.

The AGN population as revealed by radio surveys is composed of two distinct categories of sources: a population with strong QSO/Seyfert-like emission lines (historically referred to as high-excitation sources) and a population with weak LINER-like emission lines (referred to as low-excitation sources; e.g., Hine & Longair 1979, Laing et al. 1994). In the language of the present review these are radiative-mode and jet-mode AGNs, where the high excitation sources form a small subpopulation of radiative-mode AGNs that produce powerful jets. Best & Heckman (2012) separated the radio luminosity function into these two radio source populations and showed that both are found over the full range of radio powers they observed (see **Figure 11**). The jet-mode sources constitute about 95% of the radio-AGN population at all radio luminosities below $P_{1.4\,GHz} = 10^{25}$ W Hz^{-1}, but the radiative-mode population becomes dominant above 10^{26} W Hz^{-1}. In the
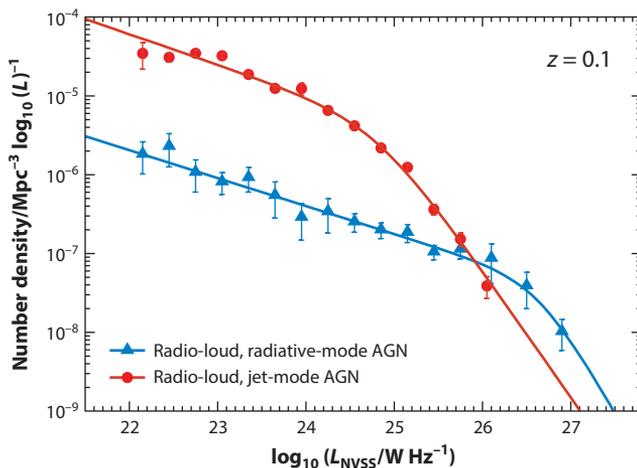

Figure 11

The local radio luminosity function of radio-loud AGNs split into radiative-mode and jet-mode sources. The data are largely drawn from the results of Best & Heckman (2012), who split these two populations and derived luminosity functions using radio-selected AGNs in the Sloan Digital Sky Survey main galaxy sample. However, as shown by Gendre et al. (2013), these results underestimate the luminosity function of the radiative-mode AGNs above 10^{26} W Hz^{-1}, where Type 1 AGNs dominate. Therefore the results of Gendre et al. are adopted for the three highest luminosity points of the radiative-mode population. The local radio luminosity functions are well fitted by broken power-law models.
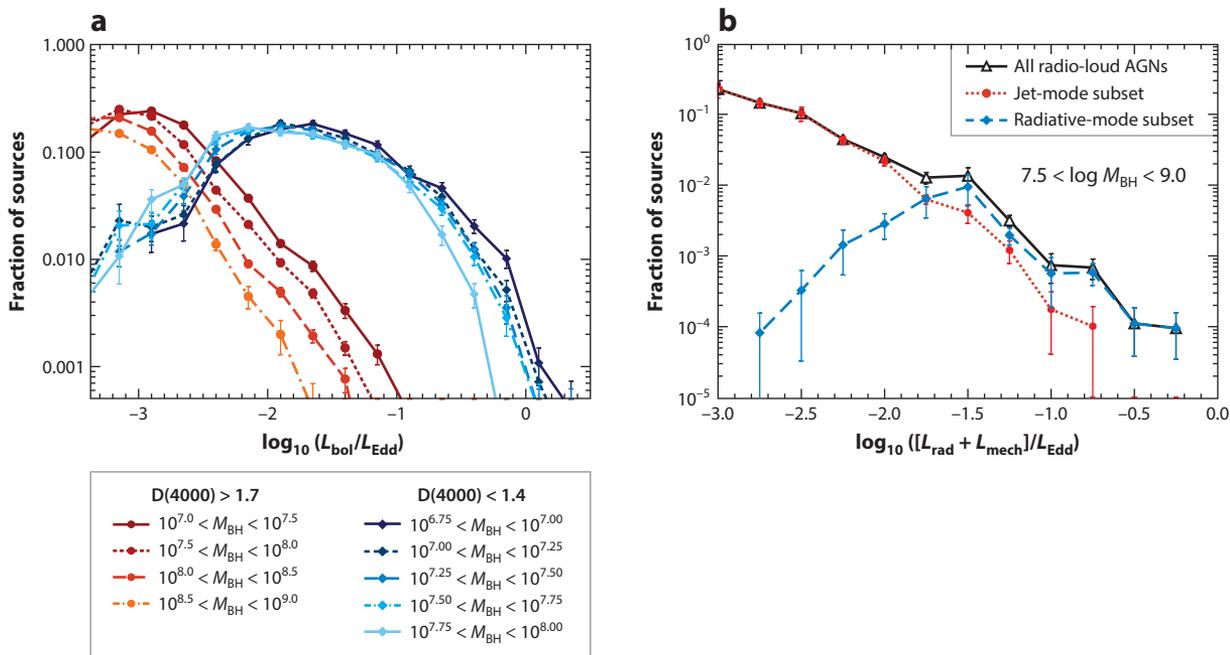
Figure 12

(*a*) The distribution of Eddington-scaled accretion ratios for emission-line-selected AGNs from the Sloan Digital Sky Survey (SDSS) main galaxy sample split by star-formation activity. Following Kauffmann & Heckman (2009), the distributions are shown separately for actively star-forming host galaxies [D(4000) < 1.4] and for passive host galaxies [D(4000) > 1.7], each for a range of black hole masses. Fractions plotted are within each 0.25-dex wide bin in the Eddington ratio. As found by Kauffmann & Heckman, the passive galaxies show a power-law distribution of Eddington fractions, the amplitude of which decreases with increasing black hole mass. In contrast, the Eddington ratios of the star-forming hosts show a log-normal distribution peaking at a few percent of Eddington. This distribution is largely independent of black hole mass (though this depends slightly upon the version of the M-σ relation adopted). (*b*) The Eddington-scaled accretion ratios of radio-loud AGNs from the SDSS split into jet-mode and radiative-mode sources; again, fractions plotted are within each 0.25-dex wide bin. Here the bolometric luminosity is calculated by summing the radiative and mechanical contributions. The two classes show distributions remarkably similar to the populations seen for emission-line AGNs in panel *a*.

radio samples derived from large spectroscopic surveys of the contemporary Universe, therefore, the radio-AGN population is predominantly composed of the jet-mode (low-excitation) sources.

The local radio-AGN population has historically been split by Fanaroff & Riley (FR; 1974) radio morphology, where FR2 sources are "edge-brightened" with jets that remain collimated until they end in bright hotspots, and FR1 sources are "edge-darkened" with jets that flare and gradually fade. The FR1 and FR2 populations are also found over a wide range of overlapping radio powers, with the switch in the dominant local population occurring at around $P_{1.4\,\mathrm{GHz}} \sim 10^{25}$ W Hz^{-1} (cf. Best 2009, Gendre et al. 2010). There is considerable overlap between the jet-mode AGN population and those radio sources morphologically classified as FR1s, and also between the radiative-mode AGNs with strong radio emission and the FR2s. However, the radio morphological split and the division in the nature of the accretion flow are not the same thing. The large overlap arises because the population switch occurs at similar radio powers, but there exists a large cross-population of jet-mode FR2s (e.g., Laing et al. 1994) and a smaller population of radiative-mode FR1s (e.g., Heywood et al. 2007), as quantified by Gendre et al. (2013).

Best et al. (2005b) considered the distribution of radio emission associated with AGN activity across galaxies of different BH masses. They showed that the prevalence of radio-AGN activity

is a very strong function of BH mass, rising as $f_{rad} \propto M_{BH}^{1.6}$. This offered a proper quantification of earlier widespread statements in the literature that radio-loud AGNs are found only in galaxies at the top end of the black hole mass function (BHMF). Best et al. (2005b) also considered the bivariate distribution of radio luminosity and BH mass. They found that the shape of the radio luminosity function showed only weak dependence on BH mass.

The Eddington ratio distribution function of radio-loud AGNs can be calculated by summing the jet mechanical luminosity and the bolometric radiative luminosity (cf. Section 2.3) to provide the total energetic output of the AGNs. Best & Heckman (2012) showed that the radiative-mode and jet-mode radio sources show distinct distributions of Eddington ratios, with the latter typically accreting below 1% of their Eddington rate, whereas the former have typical accretion rates between 1% and 10% of Eddington. Considering sources with BH masses between $10^{7.5}$ and $10^9 \, M_\odot$, **Figure 12***b* shows the distribution of Eddington ratios of radio-loud AGNs in the SDSS main galaxy sample, above 10^{-3} of the Eddington limit (incompleteness prohibits analysis below this level). The jet-mode sources dominate at low Eddington ratios and show a roughly power-law distribution with a slope of about -1.5. In contrast, the radiative-mode population shows a distribution peaked at a few percent of the Eddington limit.

3.3. The Black Hole Mass Function

The supermassive BHMF is defined as the comoving number density of BHs per bin in log mass at a given redshift. The techniques used to determine the BHMF have been reviewed recently by Kelly & Merloni (2012). Here we briefly summarize the properties and implications of the BHMF.

In the contemporary Universe the BHMF can be measured in an empirical model–independent fashion by adopting the measured scaling relation between BH mass and the bulge mass or velocity dispersion (described in Section 2.3.3). Combined with the measured volume density of bulges as a function of velocity dispersion or stellar mass from the SDSS, the BHMF can then be computed. Shankar et al. (2009) have compared the BHMF derived in this way by different groups (**Figure 13**).

The two main conclusions to be drawn from **Figure 13** are that the distribution of mass in BHs today peaks in BHs with masses of around $10^{8.5} \, M_\odot$ and that the mass distribution is actually quite narrow (half the total mass in BHs resides in the mass range from $\sim 10^{7.8}$ to $10^{8.8} \, M_\odot$). The integral of this distribution represents the total mass per unit volume in the contemporary Universe ($\rho \sim 10^{5.7} \, M_\odot \, \mathrm{Mpc}^{-3}$). This mass density is directly connected to the total energetic output of AGNs over the history of the Universe (Soltan 1982). Consistency with the cosmic evolution of the AGN bolometric luminosity function (summarized above) implies a mean accretion efficiency ($\epsilon = L_{bol}/\dot{M}c^2$) of order 10% (Yu & Tremaine 2002, Marconi et al. 2004, Hopkins et al. 2007b, Shankar et al. 2009).

At higher redshifts the BHMF has usually been computed in a model-dependent fashion. These computations take the present-day BHMF as a boundary condition and use a continuity equation to relate the evolution of the BHMF to the accretion history as inferred from the evolution of the AGN luminosity function. To compute BHMF(z), an assumption must be made about the mean AGN light curve [$L(M_{BH}, t)$] and the accretion efficiency (ϵ). Examples of this approach are shown by Marconi et al. (2004), Shankar et al. (2009, 2013) and Cao (2010). An alternative technique for measuring BHMF(z) uses the mass function of actively accreting BHs and the so-called black hole fundamental plane (Merloni & Heinz 2008).

All these analyses reach qualitatively similar conclusions: The BHMF grows antihierarchically, with the population of more massive BHs being produced at higher redshifts. The population of BHs with masses $>10^9 \, M_\odot$ was largely in place by $z \sim 2$. Since $z \sim 1$, only the population of
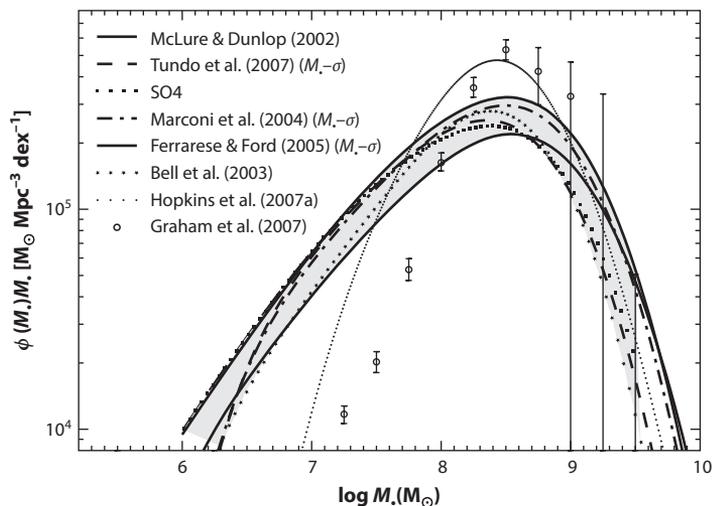
Figure 13

A collection of estimates of the distribution of mass across the local black hole population (i.e., the local black hole mass function scaled by black hole mass) taken from Shankar et al. (2009). The shaded gray area represents the range of estimates based on local scaling relations of M_{BH} with σ, M_{Bulge}, and L_{Bulge}. Readers are referred to Shankar et al. (2009) for details.

BHs with masses below about $10^8 \, M_\odot$ has been growing significantly. As we have summarized above, this inference is directly confirmed by measurements of the mass-dependent growth rates of SMBHs in the contemporary Universe (Heckman et al. 2004, Kauffmann & Heckman 2009).

4. HOST-GALAXY PROPERTIES

4.1. Overview

In the introduction to this review we summarized the overall landscape defined by the population of galaxies in the contemporary Universe and described the bimodal galaxy population [lower-mass, lower-density, star-forming (blue) versus higher-mass, higher-density, quiescent (red) galaxies]. Here we want to see where the population of growing BHs today lives within this landscape. Both the structural properties of the galaxies and their stellar populations turn out to be crucial in this regard. We begin with an overview of both the radiative-mode and jet-mode AGNs in this section, and then follow with detailed discussions of the two populations in the two sections to follow.

To fully appreciate the interplay between the structural properties and the stellar population in AGN host galaxies, it is worth taking a guided tour of the pair of multipanel plots shown in **Figures 14** and **15**, derived from the SDSS. **Figure 14** plots the volume-weighted values of various key parameters in the 2D space of stellar mass (M_*) and D(4000). The top four panels show the distributions of M_*, BH mass (M_{BH}), extinction-corrected [OIII] luminosity from AGNs ($L_{[OIII]}$; tracing bolometric radiative output), and the production of mechanical energy in radio jets (L_{mech}). The bottom four panels show the ratios of $L_{[OIII]}/M_*$, $L_{[OIII]}/M_{BH}$, L_{mech}/M_*, and L_{mech}/M_{BH}.

The plot weighted by M_* shows the basic layout of the bimodal galaxy population. The plot weighted by M_{BH} shows a shift toward higher values of M_* (consistent with the steep dependence of M_{BH} on M_* shown in **Figure 9**). The plot weighted by $L_{[OIII]}$ traces the growth of BHs through accretion (this is essentially tracing the radiative-mode population of AGNs). It is immediately
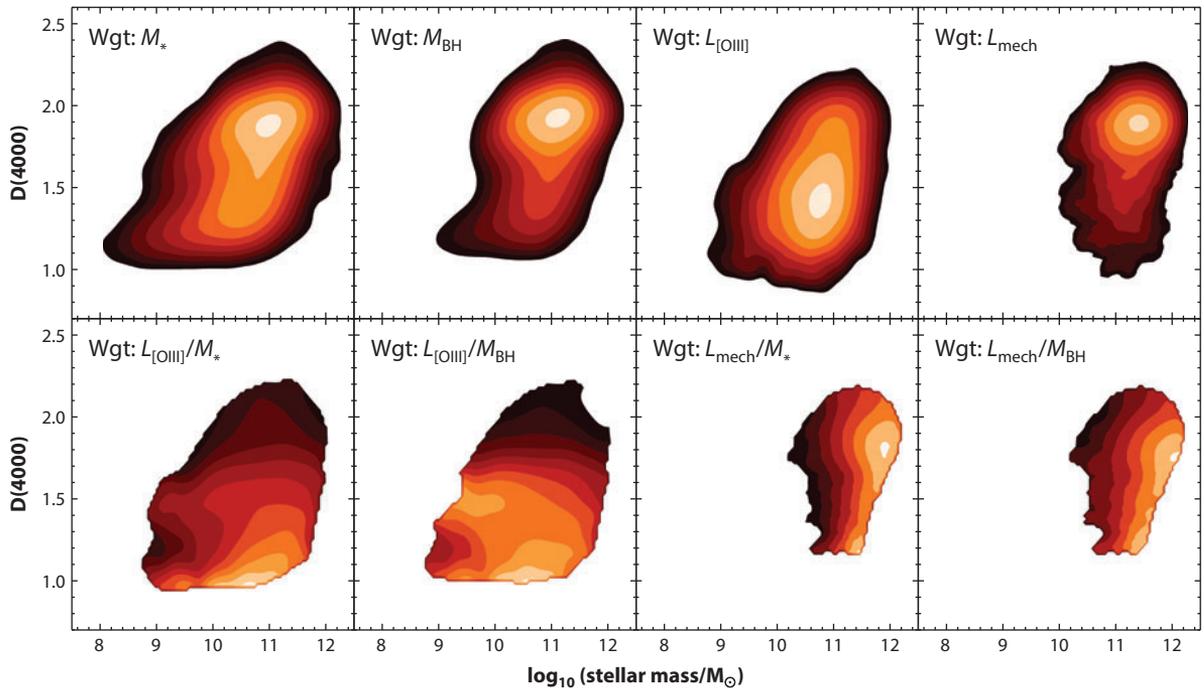
Figure 14

(*Top*) The distribution of galaxies from the Sloan Digital Sky Survey main galaxy sample in the plane of stellar mass versus 4,000-Å break strength, weighted according to (from *left* to *right*) stellar mass, black hole mass, reddening-corrected [OIII] line luminosity (i.e., bolometric radiative luminosity), and jet mechanical luminosity. Each color band corresponds to a factor of two difference, increasing from dark to light. (*Bottom*) Ratios of upper panels (same color coding) to illustrate the distributions of (from *left* to *right*) bolometric radiative luminosity per stellar mass, bolometric radiative luminosity per black hole mass, jet mechanical luminosity per stellar mass, and jet mechanical luminosity per black hole mass.

clear that BH growth is occurring primarily in moderately massive galaxies ($M_* \sim 10^{10}$ to a few times 10^{11} M$_\odot$) with a young central stellar population (see Kauffmann et al. 2003a; also see **Figure 2**). This is further quantified by the panels below. The plot of $L_{\rm [OIII]}/M_*$ shows a strong dependence on the age of the stellar population and only a weak dependence on M_* over the range from $M_* \sim 10^{10}$ to $10^{11.5}$ M$_\odot$. The plot of $L_{\rm [OIII]}/M_{\rm BH}$ (a proxy for the Eddington ratio) tells a similar story, but here the dependence is almost entirely in stellar age with essentially no dependence on stellar mass for a given value of D(4000).

A complementary set of plots is shown in **Figure 15**, which shows the same set of distributions in the 2D space of $M_{\rm BH}$ versus D(4000). These plots reinforce the conclusions above. The growth of BHs as traced by [OIII] emission primarily occurs in the lower mass BHs ($\sim 10^{6.5}$ to 10^8 M$_\odot$; Heckman et al. 2004), more specifically in the subset of those BHs that live in galaxies undergoing significant central star formation. The plots of $L_{\rm [OIII]}/M_*$ and $L_{\rm [OIII]}/M_{\rm BH}$ both illustrate the fact that the strong dependences of these ratios are primarily on the age of the central stellar population.

Turning our attention now to the panels involving $L_{\rm mech}$, we see that the jet-mode population of AGNs is almost disjoint from the radiative-mode AGNs in the properties of the host galaxies and their BHs (see also **Figure 2**). The bulk of the jet mechanical energy is produced by the most massive BHs ($M_{\rm BH} \sim 10^8$ to $10^{9.5}$ M$_\odot$) living in the most massive galaxies ($M_* \sim 10^{11}$ to 10^{12} M$_\odot$)
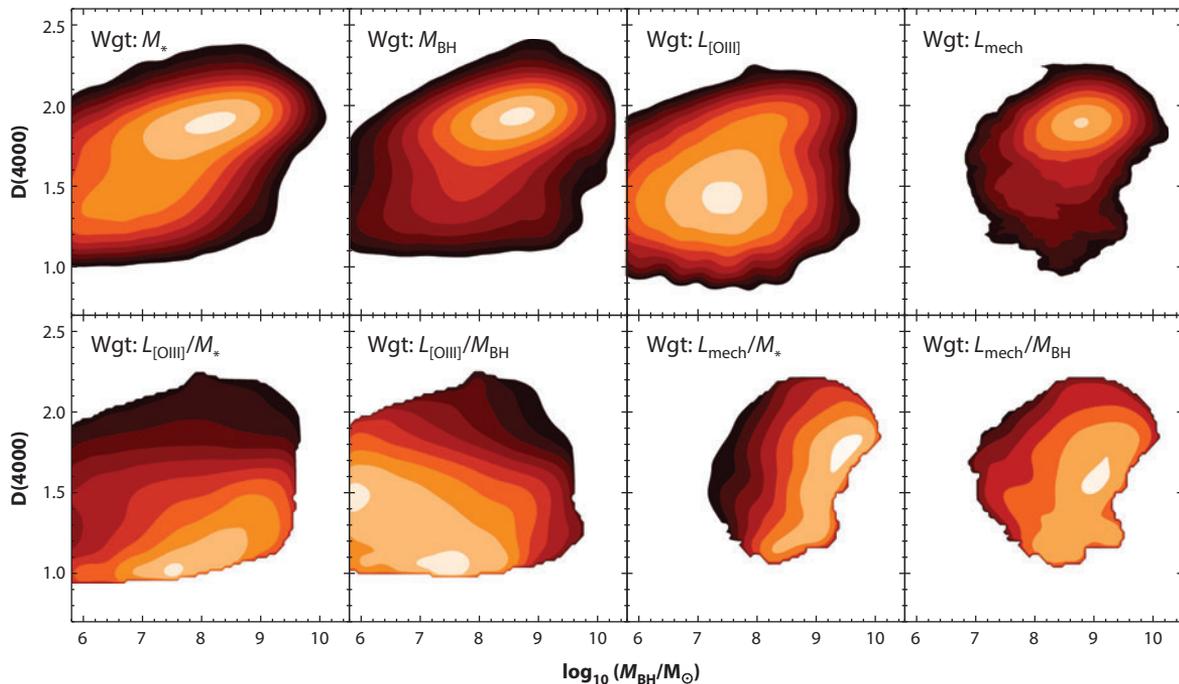
Figure 15

As **Figure 14**, but now showing the distributions in the black hole mass versus 4,000-Å break strength plane.

and generally having old stellar populations (although there is a minority population of massive galaxies with younger stellar populations). In direct contrast to the radiative-mode AGNs, the plots of L_{mech}/M_* and L_{mech}/M_{BH} show strong positive correlations with both M_* and M_{BH} (see Best et al. 2005b), but only weak dependences on the age of the stellar population.

The main dependences revealed in these 2D plots are summarized in a simpler form in **Figure 16** in which the mass-normalized AGN outputs are plotted as 1D functions of M_*, μ_*, and D(4000). Three key conclusions are evident.

First, there is only a slow rise of about 0.5 dex in L_{rad}/M_* on M_* over the range from 10^9 to $10^{10.7}$ $M_\odot$, but then there is a steeper drop at higher masses. This can be contrasted with the very steep increase in L_{mech}/M_* with M_*. This shows that the predominant form of energy produced by BHs switches from radiation to jet energy at the highest stellar masses ($>10^{11.5}$ $M_\odot$). The crossover corresponds to $M_{BH} > 10^9$ $M_\odot$. It is intriguing that the sum of the mass-normalized L_{rad} and L_{mech} remains relatively constant over the full stellar mass range plotted. Because the ratio of BH to galaxy stellar mass rises strongly with increasing mass (**Figure 9**), this near-constancy would not apply to AGN output normalized to BH mass (e.g., **Figure 10**).

Second, both modes of BH output plummet precipitously below the characteristic value $\mu_* \sim 10^{8.5}$ $M_\odot$ kpc^{-2} that divides the bimodal galaxy population described in Section 1.3. The effective growth of BHs evidently requires conditions of high central density.

Finally, the strong overall increase in L_{rad}/M_* moving from old [D(4000) > 2] to intermediate-age [D(4000) $\sim$ 1.5] stellar populations, followed by saturation at still younger ages, is very clear. This was shown most explicitly by Kauffmann & Heckman (2009) and is consistent with **Figure 12a**. In contrast, the jet output is only significant when compared with the radiative output in the galaxies having the oldest stellar populations (see Best et al. 2005b).
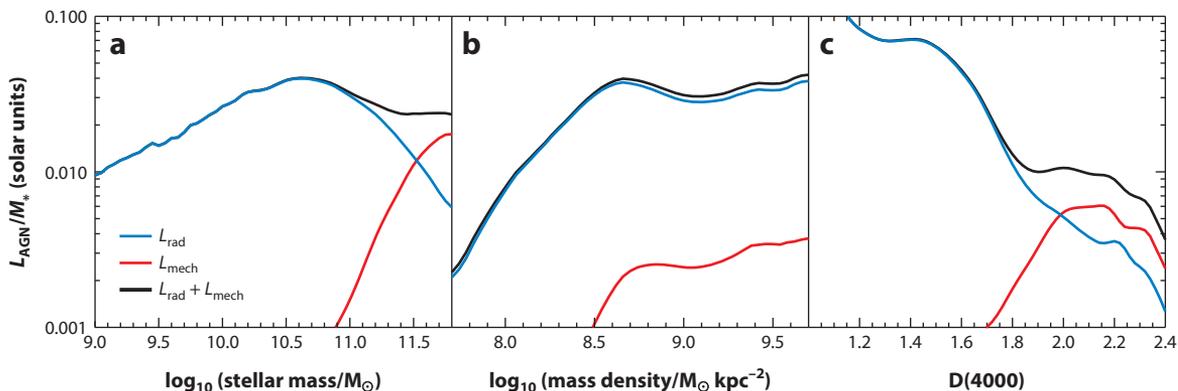
Figure 16

The distribution of AGN luminosity per unit stellar mass among galaxies from the Sloan Digital Sky Survey main galaxy sample as a function of (*a*) galaxy stellar mass, (*b*) stellar surface mass density, and (*c*) 4,000-Å break strength. In each plot the blue line indicates the radiative luminosity output (estimated from the [OIII] emission line), the red line shows the mechanical luminosity output in the radio jet, and the black line shows the sum of the two.

Taken together these figures clearly support the division of the AGN population into two separate modes, as we have stressed throughout our review. The broad conclusions on host-galaxy properties of the different AGN populations are summarized in **Figure 4**.

4.2. The Hosts of Radiative-Mode AGNs

The above plots for the radiative-mode AGNs lead to a simple and physically satisfying conclusion: The accretion-driven growth of BHs in the contemporary Universe primarily occurs in centers of galaxies where two criteria are met: (*a*) there is an abundant supply of cold gas (whose presence is implied by recent or ongoing star formation) and (*b*) the stellar surface mass density is high. Putting these two criteria together, it is natural to conclude that there is really one overarching requirement, namely an abundant central supply of cold and dense gas (e.g., Larson 2010). This is shown in an explicit and compact way in **Figure 17**. In this section, we expand on this by considering different aspects of the relationship between BH growth and star formation in some detail.

4.2.1. The relationship to the star-formation rate. So far we have discussed the relationship between AGNs and star formation only in a qualitative sense. Here we summarize what has been learned about the quantitative relationship. Let us consider the correlation between SFR and AGN luminosity. There are two complementary approaches to this. One is to select a sample of AGNs spanning a range of luminosity and then measure the SFRs for each. This is conceptually simple, but ignores the fact that many galaxies do not host detectable AGNs, and these galaxies are ignored in the above approach. Thus, the second approach is to examine the distribution of AGN luminosity as a function of SFR for a complete sample of galaxies selected without regard to the presence of an AGN.

As an example of the first approach, Kauffmann et al. (2003a) used the SDSS to measure the distribution of the strength of the 4,000-Å break for AGNs as a function of raw [OIII] luminosity. Based on subsequent calibration (by Brinchmann et al. 2004) of the 4,000-Å break as a function of sSFR (sSFR = SFR/M_*), there is a clear but shallow dependence: As the [OIII] luminosity increases from 10^6 to 10^9 L$_\odot$, the median sSFR only increases from $10^{-11.3}$ to 10^{-10} year^{-1}. This is consistent
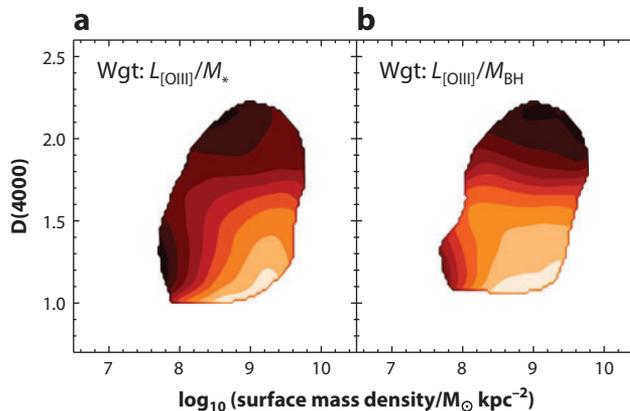
Figure 17

(*a*) The distributions of AGN bolometric radiative luminosity per unit galaxy stellar mass and (*b*) bolometric radiative luminosity per black hole mass in the stellar surface mass density versus 4,000-Å break strength plane. (Color banding as in **Figure 14**.) Radiative-mode AGN activity clearly requires both an abundant supply of cold gas (indicated by recent or ongoing star formation) and a high stellar surface mass density.

with the SDSS-based results of LaMassa et al. (2013), who find that the mean sSFR in Type 2 Seyferts (within a radius of about 2 kpc) only increases from $\sim 10^{-11}$ to 10^{-10} year^{-1} as the ratio of L/L_{Edd} increases from $\sim 10^{-3}$ to ~ 1. Similarly, they found that the SFR in this central region only increases from 0.1 to 1 $M_{\odot}$ year^{-1} as the extinction-corrected [OIII] luminosity increases from $10^{6.5}$ to 10^9 L$_{\odot}$ (i.e., SFR $\propto L_{AGN}^{0.4}$). Diamond-Stanic & Rieke (2012) and Netzer (2009) find steeper but still sublinear relations between SFR and AGN luminosity (SFR $\propto L_{AGN}^{0.6-0.8}$). Rosario et al. (2012) find no correlation (at $z \sim 0$) between the global (galaxy-wide) SFR and AGN luminosity for AGN bolometric luminosities below about 10^{44} erg s^{-1} and SFR $\propto L_{AGN}^{0.5}$ at higher luminosity.

The second approach was taken by Kauffmann & Heckman (2009). They looked at the distribution of the Eddington ratio (L_{bol}/L_{Edd}) as a function of the amplitude of the 4,000-Å break for a complete SDSS-based sample of galaxies (see **Figure 12a**). They found that for galaxies with predominantly old central stellar populations, the probability of finding an AGN decreases with increasing Eddington ratio as a power law. Using the calibration of Brinchmann et al. (2004), the results of Kauffmann & Heckman (2009) imply that the normalization of this power law increases roughly linearly with the central sSFR over the range in the latter from $\sim 10^{-12}$ to $10^{-10.5}$ year^{-1}. However, at higher values of central sSFR, the Eddington ratio distribution transitions to a log-normal distribution that peaks at an Eddington ratio of about 3%. In this regime, the Eddington ratio distribution is independent of the central sSFR. It is also largely independent of the mass of the BH (though the precise details depend upon the version of the M-σ relation adopted). Thus, Kauffmann & Heckman found no simple monotonic relation between central star formation and BH growth rates. Once the central region of the galaxy has a mass-doubling time (M_*/SFR) that is comparable with the current Hubble time, the SMBH growth rate saturates and is not boosted by additional star formation. We discuss some possible interpretations of this in Sections 5 and 6 below.

The combination of power-law plus narrow-peaked distribution for the Eddington ratio distribution found for emission-line AGNs bears close resemblance to the results of the radiative-mode versus jet-mode decomposition of Eddington ratio distributions for radio-AGNs (Section 3.2; **Figure 12b**). This fits with the picture discussed above, that radiative-mode AGNs are generally found in star-forming host galaxies, whereas jet-mode AGNs are mostly in passive galaxies. It also

indicates that the main properties of the Eddington ratio distribution are largely independent of whether or not an AGN is classified as radio-loud. This further justifies our approach throughout this review of considering just two fundamental AGN modes (cf. **Figure 4**).

4.2.2. The radial distribution of star formation and cold gas.

The physical connection between the fueling of the SMBH and star formation should be clearer on smaller scales near the SMBH. Kauffmann et al. (2007) compared this relationship determined on two scales. They found that the luminosity of the AGNs (relative to the Eddington limit) correlates much more tightly with the youth of the central stellar population of the galaxy as probed with the SDSS spectra than with its global stellar population as probed with SDSS and GALEX optical/UV imaging. They concluded that ongoing star formation in the global galaxy disk is a necessary but not sufficient condition for ongoing star formation in the center and the concurrent growth of the SMBH: young bulges and their growing SMBHs are only found in galaxies with star-forming disks, but many galaxies with star-forming disks have dead bulges and quiescent SMBHs.

A similar result was found by Diamond-Stanic & Rieke (2012) based on an analysis of *Spitzer* mid-IR imaging and spectroscopy of a sample of very nearby Seyfert galaxies. They found that the correlation between the SFR and the rate of SMBH growth (measured using the luminosity of the [OIV] 25.9-μm line) was significantly stronger for the SFR measured in the inner-most kiloparsec than for the entire galaxy. The radial distribution of the star formation as a function of the AGN luminosity was mapped in a statistical sense by LaMassa et al. (2013) for a sample of 28,000 Type 2 Seyfert galaxies drawn from the SDSS. They examined the SFR within the SDSS fiber for subsamples matched in both host-galaxy properties and AGN luminosity, but spanning a range in mean redshift from $z \sim 0.05$ to 0.15 (so that the fiber mapped the star formation over different radial scales in each subsample). They found that as the AGN luminosity increased, the total star formation increased and became more and more centrally concentrated (located within about 2 kpc of the nucleus).

On smaller radial scales, the stellar populations in nearby Type 2 Seyfert nuclei have been investigated by Cid Fernandes et al. (2001) using optical spectra that probe typical radial scales of only a few hundred parsecs. By computing L_{bol}/L_{Edd} for this sample, we find that a young stellar population can be directly detected surrounding about 75% of the Seyfert nuclei with luminosities exceeding 10% of the Eddington limit, but only in about 25% of those with lower luminosities. This investigation was extended to lower AGN luminosities and still smaller scales using ground-based and HST spectra by Cid Fernandes et al. (2004a,b) and González Delgado et al. (2004), respectively. They found that the nuclear stellar populations were usually old, except in cases whose optical emission-line properties were consistent with an ionizing contribution from both an AGN and young stars.

A complementary picture emerges from consideration of the radial distribution of the cold gas associated with star formation. By comparing the hosts of radio-quiet AGNs with control samples of non-AGNs matched in stellar mass, structural properties, and mean stellar age, Fabello et al. (2011) found that the global atomic gas (HI) content of a galaxy had no effect on the accretion rate on the central BH. This agrees with earlier studies of the HI content of smaller samples of Seyfert galaxies (Heckman et al. 1978, Mirabel & Wilson 1984, Ho et al. 2008), which did not show systematic differences in HI content in Seyferts compared with normal galaxies. Atomic gas in a galaxy is generally spread out in a large-scale disk, and the surface density of the HI exhibits a dip or even a hole in the center of the galaxy. If gas is present in the vicinity of the BH, it is likely to be at high enough densities that it would exist primarily in molecular form.

Surveys of the global molecular content of AGN hosts using the millimeter wave $J = 1$–0 CO emission line show only small (Heckman et al. 1989) or no (Maiolino et al. 1997, Saintonge

et al. 2012) differences in the molecular content of AGN hosts compared with normal galaxies (in terms of CO luminosity normalized by galaxy optical luminosity, H_I mass, or SFR). On smaller radial scales, thick, clumpy disks of molecular gas with radii $\sim$30 pc have been found at the centers of nearby Seyfert galaxies (e.g., Hickox et al. 2009). More recently, Hicks et al. (2013) examined molecular gas on 50-pc to 1-kpc scales in a matched sample of Seyfert and quiescent galaxies and showed that the Seyferts had more centrally concentrated H_2 surface-brightness profiles.

The presence of dust can serve as a proxy for cold gas. Kauffmann et al. (2007) showed that the central regions of the host galaxies of more rapidly growing BHs were more heavily dust-reddened than were the same regions in the hosts of low-power AGNs. Simoes Lopes et al. (2007) used HST imaging to show that all of the 65 AGN host galaxies they studied have circumnuclear dust structures on radial scales of $\sim$0.1 to 1 kpc (see also González Delgado et al. 2008). This includes 34 early-type AGN hosts. In a carefully constructed control sample of normal galaxies only a minority (26%) of the early-type galaxies had circumnuclear dust (though all the late-type control galaxies did). Subsequent *Spitzer* observations (Martini et al. 2013) imply dust masses of order $10^6\,M_\odot$ or associated gas masses of order $10^8\,M_\odot$. In a complementary study, Lauer et al. (2005) used HST images to discover a strong connection between the AGN emission-line activity and the presence, quantity, and structure of central dust in a sample of 77 early-type galaxies. All in all, it seems reasonable to conclude that radiative-mode AGNs reside in galaxies where the central (kiloparsec-scale) supply of cold dense gas is substantial.

4.2.3. The starburst-AGN connection.

We have seen above that the connection between SMBH growth and star formation is clearer when the central kiloparsec-scale region of the galaxy is probed. Such central star formation can sometimes occur in a strong episodic burst, presumably related to the short dynamical times near the nucleus. The existence of a direct connection between the growth of an SMBH and intense star formation in the centers of galaxies has long been a matter of speculation. In its most extreme form a direct starburst-AGN connection was posited: AGNs were simply the evolved descendants of starbursts powered by a collection of supernovae and supernova remnants rather than by an SMBH (Terlevich & Melnick 1985, Terlevich et al. 1992). Many other authors have proposed less iconoclastic models in which the delivery of a fresh supply of cold gas to the center of a galaxy leads to both a strong starburst and the efficient fueling of the SMBH (e.g., Sanders et al. 1988a,b; Hopkins et al. 2006, 2008; Di Matteo et al. 2008).

Investigations of the starburst-AGN connection using SDSS spectra have shown that there is indeed a connection, but one that is more subtle than might have been expected. We have described above how SDSS spectra can be used to identify starbursts and poststarbursts using the combination of the 4,000-Å break and the strength of the high-order Balmer absorption lines. Based on this methodology, Kauffmann et al. (2003a) showed that high-luminosity Type 2 AGNs in the SDSS were more likely to have undergone a starburst within the last 10^9 years compared with low-luminosity AGNs or normal galaxies of similar stellar mass (see also Goto 2006 and Yan et al. 2006). This issue was examined in more detail by Wild et al. (2007). Based on a sample of 34,000 early-type galaxies in the SDSS, Wild et al. found that the poststarburst systems had the highest mean AGN luminosity. However, because these are relatively rare, they represent only about 15% of the total amount of SMBH growth in the contemporary Universe. They found that galaxies with ongoing (but less episodic) central star formation are the sites of the majority of SMBH growth.

In a subsequent paper, Wild et al. (2010) examined the time history of SMBH growth during and after an intense burst of central star formation (involving roughly 10% of the galaxy stellar mass). They found that the growth of the SMBH was delayed by about 200 Myr relative to the start of the starburst (**Figure 18**). These results pertain to the region within a radius of $\sim$1 to
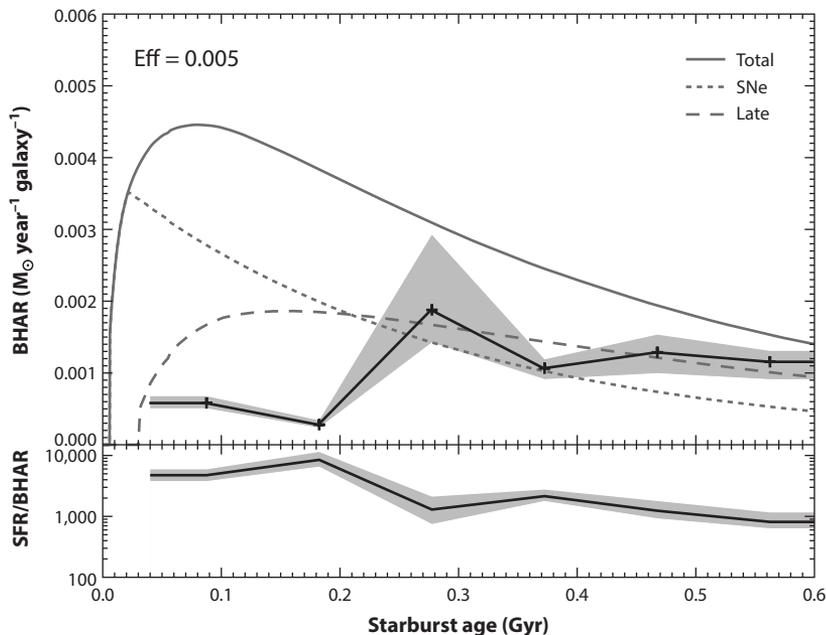
Figure 18

(*Top*) The mean black hole accretion rate (BHAR) averaged over all galaxies in a sample of starburst and poststarburst galaxies (*black line*). The gray-shaded area shows the typical 10th and 90th percentile range on the total BHAR estimated from bootstrap resampling of the data. The model prediction for the average gas mass-loss rate from the stars formed during the starburst (*solid gray line*) assumes an accretion efficiency onto the black hole of 0.5 percent of the ejecta from intermediate- and low-mass stars between the age of 250 and 600 Myr. Stars return mass to the ISM through supernova explosions and fast winds from massive stars (*dotted line*) and planetary nebula ejections and stellar winds from lower-mass stars (*dashed line*). (*Bottom*) The ratio of star-formation rate (SFR) (from Hα) to BHAR, with mean value and errors calculated as for the top panel. The BHAR lags the SFR and becomes significant only after several hundred million years. Reprinted from Wild et al. (2010) with permission.

2 kpc. Qualitatively similar results from the SDSS were found by Schawinski et al. (2007) for galaxies selected morphologically to be ellipticals. On much smaller scales (10–100 pc) and for a much smaller sample, Davies et al. (2007) also find evidence for a delay of order 100 Myr between a starburst and powerful AGN activity. We discuss the implications of these results in Section 6.1 below.

4.3. The Hosts of Jet-Mode AGNs

The results in Section 4.1 above show that the host galaxies of the BHs that dominate the production of jet mechanical energy are nearly disjoint from the host galaxies where BHs are actively growing. These jets are traced by their radio emission. Detailed investigations of the structure and stellar content of the radio-selected AGN population in the SDSS were first undertaken by Best et al. (2005b). They confirmed the widely held view that nearly all such AGNs are hosted by massive elliptical galaxies with old stellar populations: The radio source hosts are highly bulge-dominated (their BH mass versus stellar-mass relation lies on the established BH mass versus bulge mass relation), with 4,000-Å break strengths clustered around 2.0, concentration indices typically between 2.9 and 3.4, and effective stellar surface mass densities around $10^9 M_\odot$ kpc^{-2}. This is entirely consistent with the results summarized in Section 4.1.

More interestingly, Best et al. (2005b) were able to quantify the prevalence of radio-AGN activity as a function of stellar mass and BH mass with much greater statistical robustness than previous studies. They found that the fraction of galaxies selected via radio emission scaled as $M_*^{2.5}$ and as $M_{BH}^{1.6}$, with these results being broadly independent of the radio luminosity limit. This is strikingly different from the mass dependence of the prevalence of emission-line AGN activity (see **Figure 14**). Best et al. (2005b) did not separate their sample into radiative-mode and jet-mode sources, but their sample was dominated by the latter, and it is these sources that drive the strong mass dependence. Janssen et al. (2012) considered the mass dependences of the two populations separately. They showed that the prevalence of radiative-mode radio sources has a much shallower dependence on mass, scaling as $M_*^{1.5}$, albeit that this remains steeper than that found for radio-quiet radiative-mode AGNs selected by their optical emission lines.

For jet-mode sources, Best et al. found no evidence for any strong relationship between the [O III] and radio luminosities; indeed the radio emitting fraction was found to be largely independent whether or not the optical galaxy is classified as an emission-line AGN. This result breaks down at higher radio luminosities, when the radiative-mode radio sources begin to dominate. These have been long known to show a strong correlation between radio- and emission-line luminosities (e.g., Rawlings & Saunders 1991, Xu et al. 1999). Kauffmann et al. (2008) investigated the subset of radio sources within the SDSS that display emission lines, and confirmed this correlation, finding also that it became tighter if Eddington-scaled quantities (i.e., $L_{1.4\,GHz}/M_{BH}$ and $L_{[OIII]}/M_{BH}$) were considered.

Lin et al. (2010) compared the host galaxies of radio sources separated into different radio morphological types. As previously discussed, these two radio morphological classes show a broad overlap with the jet-mode and radiative-mode classes, with most FR1s being jet mode and most FR2s being radiative mode; however, there are substantial differences between the segregation methods, and a significant population of jet-mode (low-excitation) FR2 sources exists. Lin et al. (2010) found that the most significant differences between FR1s and FR2s occurred for the subset of the FR2 population that displayed both strong high-excitation optical emission lines and hot spots close to the end of the radio lobes. They found this FR2 subset to be hosted by lower-mass galaxies, with bluer colors, living in poorer environments and having higher accretion rates than the rest of the radio source population. Similarly Kauffmann et al. (2008) found that their radio-AGNs with emission lines showed lower stellar masses, lower velocity dispersions, lower 4,000-Å break strengths, and stronger Balmer absorption features than those radio-AGNs without emission lines.

Best & Heckman (2012) did an explicit separation of jet-mode and radiative-mode radio sources and confirmed these results. They also constructed matched samples of the two radio source classes to investigate whether observed differences in host-galaxy colors and morphologies were just secondary effects driven by, for example, the different stellar masses of the two samples. They found that the hosts of radiative-mode radio-AGNs have bluer colors, smaller half-light radii, lower concentration indices, and lower 4,000-Å break strengths than the hosts of jet-mode radio-AGNs of the same stellar mass, BH mass, and radio luminosity. These results imply that the radiative-mode radio sources are associated with ongoing star-formation activity, as is also seen in the radio-quiet AGN samples. Further evidence in support of this comes from the work by Sadler et al. (2014), who investigated differences in the mid-IR colors of the two radio source classes using WISE and concluded that star-formation activity was present in the radiative-mode AGNs, but not the jet-mode AGNs (see also Gürkan et al. 2014).

The larger scale lengths and higher concentration indices of the hosts of the jet-mode AGNs can be explained if these sources are preferentially located toward the centers of groups and clusters (as suggested by their clustering and environmental properties; see Section 4.4), where

host galaxies are typically larger and may have more extended (cD-type) light profiles. Mannering et al. (2011) compared the scale lengths of radio-AGNs at both red and blue wavelengths and found that the ratio of the two was higher than that for control galaxy samples, suggesting the possible presence of extended red envelopes (although their control samples were matched only in redshift and magnitude, so this result might be driven by morphology differences between the radio-AGNs and control samples).

Janssen et al. (2012) considered the relationship between AGN classification, radio luminosity, and galaxy color. Red (passive) galaxies show a higher probability of hosting jet-mode radio-AGNs than blue (star-forming) galaxies of the same stellar mass by a factor of a few. Blue galaxies show a higher probability of hosting radiative-mode radio-AGNs at all radio luminosities. For blue galaxies, the likelihood of hosting a radio-AGN of either class is a strong positive function of the SFR. This suggests that the presence of cold, star-forming gas in a galaxy enhances the probability of its central BH becoming a radio-loud AGN. This means that jet-mode AGN activity, especially at high radio luminosities, is not solely related to hot halo gas accretion (see Section 5 below).

4.4. Clustering, Environments, and Halo Masses of AGNs

Since early in the study of Seyfert galaxies, QSOs, and powerful radio sources, attempts have been made to categorize the typical environments in which these sources are found (e.g., Gisler 1978, Longair & Seldner 1979, Yee & Green 1984). Analyses mostly relied on relatively small fields around the AGNs and either considered simple galaxy counts out to some projected radius or divided those counts into annuli to enable a cross-correlation analysis. The majority of analyses indicated that AGNs are found in a wide range of environments, with powerful QSOs and radio sources being often located in group or poor cluster environments, but Seyfert galaxies generally avoiding the densest environments. However, AGN samples were relatively small, and contradictory results were obtained in different studies. Furthermore, AGN activity depends strongly on host-galaxy properties, such as stellar mass (especially for radio-selected AGNs; see previous sections); therefore, to reliably isolate any trends of AGN activity that are explicitly caused by environment, large and homogeneous data sets like that offered by the SDSS are required so that the AGN samples can be compared against control samples carefully matched in other galaxy properties. Even so, there has remained much debate as to the nature of these trends, largely because of the different definitions adopted both for AGN samples (all emission-line AGNs, just Seyfert sources, radio-AGNs, etc.) and for environment (local galaxy density; membership of, or distance from center of, a group or cluster).

Once stellar mass effects are properly accounted for, the incidence of optical emission-line AGNs is generally found to be lower in denser environments and in groups and clusters rather than in the field (Miller et al. 2003, Kauffmann et al. 2004, von der Linden et al. 2007): The fraction of AGNs among galaxies of given stellar mass decreases by a factor of two from the field toward the cluster/group center. This is matched by a decrease in star-formation activity of these galaxies. Hwang et al. (2012) investigate these trends for early and late-type galaxies separately and find that the prevalence of AGN activity in early-type galaxies already begins to decrease at the virial radius of the cluster, whereas in late-type galaxies it only decreases as the cluster center is approached. *Chandra* has revealed significant samples of X-ray-detected AGNs in nearby galaxy clusters (e.g., Martini et al. 2006), the majority of which do not show emission lines and so are not identified as AGNs in optical observations. These may be obscured AGNs or more likely may be jet-mode AGNs. Haines et al. (2012) argue that luminous X-ray AGNs in massive clusters are mostly an infalling population. These results are all generally consistent with a picture in which

there is a gradual decline in emission-line AGN activity as the denser environment decreases the cold gas supply for an AGN.

In contrast to emission-line AGNs, radio-selected AGNs are found to be preferentially located in group and cluster environments (e.g., Best et al. 2005b, Sabater et al. 2013), confirming the results of many previous studies of small radio-loud AGN samples. This is particularly true of the jet-mode subset of the radio-AGN population (Best 2004, Reviglio & Hefland 2006, Sabater et al. 2013), again suggesting a different mechanism for the triggering of AGN activity in these sources than for radiative-mode AGNs. The prevalence of radio-AGN activity among brightest cluster galaxies (BCGs) is especially high (Best et al. 2007, Croft et al. 2007; cf. Burns 1990), whereas that of optical AGNs is lower than in non-BCGs of the same mass (von der Linden et al. 2007).

An alternative view of the environments of AGNs can arise from looking at the two-point correlation function. This describes the excess probability of finding a galaxy at a given distance R from another galaxy due to clustering. In the widely adopted halo-model description of large-scale structure, on small scales (<1 Mpc) the signal in the correlation function is dominated by pairs of galaxies within the same dark matter halo (known as the one-halo term; e.g., Seljak 2000). This therefore measures the prevalence of a particular galaxy type among satellite galaxies in halos. Li et al. (2006) computed the cross-correlation function between Seyfert galaxies and the SDSS spectroscopic main galaxy sample and compared this against the results for a non-AGN control sample that was matched in redshift, stellar mass, BH mass (from velocity dispersion), concentration index, and 4,000-Å break strength. They found that on scales between 100 kpc and 1 Mpc the AGNs showed weaker clustering than the control sample. By comparison with simulations, they argued that this could be understood if AGN activity was dis-favored within satellite galaxies. This interpretation is consistent with the results arising from the study of AGN activity as a function of cluster membership or local galaxy density, discussed above.

On much larger scales (10–20 Mpc) the two-point correlation function measures the correlation between different dark matter halos (the two-halo term), which depends upon the properties of the parent halo for a given galaxy type (see the review by Cooray & Sheth 2002). If the luminosity function and two-point correlation function of a set of objects are known, then (for a given cosmological model) it is possible to estimate the mean mass of the parent dark matter halo (e.g., Sheth et al. 2001). Mandelbaum et al. (2009) used this method to estimate dark matter halo masses for ($z < 0.3$) Seyfert galaxies from the SDSS and confirmed the reliability of their measurements by using an alternative estimate from weak gravitational lensing of background galaxies. They found a mean halo mass of $\sim 10^{12} \, M_\odot$. They compared these results against a control sample of non-AGNs and found that the halo mass versus stellar mass relation was independent of whether or not Seyfert activity was present.

Mandelbaum et al. (2009) also analyzed radio-loud AGNs in the same redshift range. They found for the radio-loud AGNs an average halo mass of 10^{13} solar masses, nearly an order of magnitude higher than that of optically selected AGNs. Much of this increase is because radio-loud AGNs are hosted by more massive galaxies, but Mandelbaum et al. also found that the dark matter haloes of radio-loud AGNs are about twice as massive as those of control galaxies of the same stellar mass. A similar enhancement in the clustering strength of radio-loud AGNs relative to a carefully matched control sample of massive galaxies was found by Donoso et al. (2010) at redshifts $0.4 < z < 0.8$ using the SDSS Luminous Red Galaxy sample. Donoso et al. also showed that the clustering strength of the radio galaxy population is luminosity dependent. At low radio luminosities, where the jet-mode AGNs dominate the radio-AGN samples (these also dominated the Mandelbaum et al. sample), the clustering strength is enhanced relative to radio-loud QSOs. At higher radio luminosities the radio galaxy population is dominated by radiative-mode sources,

and the clustering amplitude is more in line with that of the radio-loud QSOs, as expected from the standard AGN unified model.

The 2dFGRS and SDSS QSO redshift surveys have been used to study the dark matter haloes of powerful AGNs to even higher redshifts (Porciani et al. 2004, Croom et al. 2005, Ross et al. 2009). Intriguingly, the mean mass of haloes hosting QSOs remains roughly constant (at around $2 \times 10^{12}\,M_\odot$) over the entire redshift range $z < 2.5$ and shows only weak dependence on QSO properties like luminosity, color, or BH mass (Croom et al. 2005, Shen et al. 2009). Only at the highest QSO luminosities is the clustering amplitude seen to increase. Shen et al. (2009) find that radio-loud QSOs reside in halos almost an order of magnitude larger than those of radio-quiet QSOs [though note that Donoso et al. (2010) do not find this strong signal among their $z \sim 0.6$ sample]. The result is in line with the local results of Mandelbaum et al.: A large part of this is likely to be driven by the higher typical stellar mass of radio-loud QSO hosts, but radio-AGN activity also seems to be preferentially found in denser environments.

In summary, radiative-mode AGNs are located in dark matter haloes with a mean mass of $10^{12}\,M_\odot$, which is typical for their stellar masses. Once stellar mass biases are accounted for, the prevalence of radiative-mode AGNs is lower in denser environments than in the field, because they are disfavored in satellite galaxies; this mirrors the decrease in star-formation activity in denser environments, with both trends being driven by the reduced cold gas supply. Radiative-mode AGNs that are found in denser environments are more likely to be radio-loud. This partly reflects the trend for radio-loud radiative-mode AGNs to be hosted by more massive galaxies (see **Figure 4**), but may also be enhanced by a boosting of the radio luminosity in dense environments, where confinement of the radio lobes reduces adiabatic losses (e.g., Barthel & Arnaud 1996). In contrast to radiative-mode AGNs, jet-mode AGNs have an increased prevalence in denser environments and, especially, in the central galaxies of groups and clusters. This indicates a different fueling mechanism.

5. BLACK HOLE FUELING

5.1. The Nature of the Accretion Flow

There are three main features that we need to consider when examining the fueling of AGNs: the origin of the fueling gas, the mechanism by which it is transported to the vicinity of the BH (e.g., Hopkins & Quataert 2011), and the nature of the accretion flow onto the BH. With regard to the last of these, the most important determining properties are the BH mass, its spin, and the nature and rate of the inflow. Note that even if the AGN is powered by tapping the BH spin via the Blandford & Znajek (1977) mechanism, accretion is required for this to occur.

Before embarking upon a discussion of the effects of different modes of accretion, it is worth summarizing the lessons that have been learned from studying accretion onto stellar-mass BHs in galactic X-ray binary systems. These are systems consisting of a BH of between roughly $4\,M_\odot$ and $20\,M_\odot$ in a close binary system with a normal star. At least in terms of the BH properties, these represent analogs of accreting SMBHs, scaled down in both luminosity and the accretion timescales. They are not precise equivalents of AGNs because the temperature of the accretion disk around a stellar mass BH is typically two orders of magnitude higher than that around an AGN, which can lead to differences in processes at atomic levels, such as ionization-dependent accretion instabilities. Nevertheless, stellar mass BHs offer the considerable advantage that variations in the accretion flow can be directly tracked; changes in the accretion happen on timescales of less than days. The observed accretion rates vary between the Eddington rate and values several orders of magnitude below this.

X-ray binaries have been shown to display two fundamentally different X-ray spectral states (see the review by Remillard & McClintock 2006 in this journal). In the low-hard state, the source spectrum is characterized by low luminosity and hard (predominantly >10 keV) X-ray emission, and low-power radio jets are ubiquitous. The power of the radio jets is correlated (albeit nonlinearly) with the X-ray luminosity (Gallo et al. 2003). In the high-soft state, sources are dominated by a high-luminosity thermal X-ray component, peaking at lower energies and with the characteristics of a standard geometrically thin, optically thick accretion disk. The primary difference between these two accretion modes is observed to be the accretion rate onto the BH relative to the Eddington rate: The low-hard state is associated with accretion rates below a few percent of the Eddington rate, whereas the high-soft state arises when the accretion rate exceeds that value (Maccarone 2003). X-ray binaries are observed to traverse from one state to another. Within the low-hard state, there are indications that the transition radius between an inner ADAF and an outer thin disk (cf. **Figure 3**) decreases with increasing luminosity (Narayan 2005). As the accretion rate increases, the luminosity increases in all bands until they reach a transition or intermediate phase where they undergo a short-lived but strong radio outburst in which both a thermal accretion disk and powerful and highly relativistic radio jets are seen (e.g., Fender et al. 2004). The radio emission then ceases as the source moves into the high-soft state. A further important property of X-ray binaries is that winds and jets appear to anticorrelate (Miller et al. 2008, Neilsen & Lee 2009, Ponti et al. 2012): Winds occur in the high-soft state when jets are not observed, but they are not observed in the low-hard state in which jets are ubiquitous.

These states of X-ray binary activity each have an analog among the AGN population. The low-hard state X-ray binaries are analogs of the jet-mode radiatively inefficient AGNs. Indeed these AGNs and low/hard X-ray binaries fall on the same fundamental plane of BH accretion: a relationship between the radio luminosity, X-ray luminosity, and black-hole mass of BHs (Merloni et al. 2003, Falcke et al. 2004). The high-soft state X-ray binaries are a direct analog of the radiative-mode AGNs (Seyferts and QSOs). The transition-phase objects have properties that make them a broad analog of the radio-loud radiative-mode AGNs, although in AGNs there is no observational evidence for these sources being a transition phase that pre-empts radio-quiet radiative-mode activity.

The critical accretion rate for the switch between X-ray binary states (a few percent of the Eddington rate) also appears to be broadly comparable in AGNs. As shown in Section 4.2 (**Figure 12a**) the emission-line AGNs (predominantly Seyferts) in gas-rich (star-forming) galaxies in the SDSS show a log-normal distribution of Eddington rates peaking at a few percent of Eddington. This result is also confirmed at higher redshifts with QSOs seen to have lower limits to their accretion rates at around 1% of Eddington (e.g., Kollmeier et al. 2006, Trump et al. 2009). Radiative-mode (Seyfert/QSO-like) radio-AGNs show a similar Eddington ratio distribution (Best & Heckman 2012; see Section 3.2 and **Figure 12b**). In contrast to this, the jet-mode radio-AGNs have accretion rates distributed below a few percent of Eddington (Best & Heckman 2012; see Section 3.2). If powered by the Blandford & Znajek mechanism then these accretion rates would be lower still. This last result is also supported at higher redshift, because BL Lac objects (believed to be beamed versions of the jet-mode sources) are also found to have luminosities below about 1% of Eddington, whereas Russell et al. (2013b) find a transition from jet-mode to radiative-mode AGNs at a similar Eddington ratio among BCGs (see also Churazov et al. 2005, Merloni & Heinz 2007).

As in the case of X-ray binaries, the spectra of the AGN subclass of LINERs (jet-mode AGNs) are best explained if the inner ADAF is supplemented by a truncated thin disk at larger radii, with the transition between the two being dependent upon the Eddington-scaled accretion rate (Yuan & Narayan 2004, Ho 2005). Sadler et al. (2014) found a weak signature of mid-IR AGN emission at the highest radio luminosities in jet-mode radio-AGNs, supporting this idea.

All of these results are in line with theoretical predictions of ADAF, which predict a change in the nature of the inner accretion flow below a critical fraction of the Eddington rate [e.g., see the review by Narayan (2002) or by Yuan & Narayan (2014) in this volume]; the precise value of that fraction depends strongly upon the viscosity of the accretion disk (e.g., Mahadevan 1997, Qiao & Liu 2009). This is consistent with the picture we have advocated in this review: The high-Eddington-rate (radiative-mode) AGNs and the low-Eddington-rate (jet-mode) sources are two fundamentally distinct populations. We include the small population of radio-loud radiative-mode AGNs together with the (radio-quiet) rest of the radiative-mode population: The results in the above sections have shown that their host-galaxy properties and Eddington-scaled accretion rates are broadly similar, albeit that the radio-loud QSOs are predominantly located at the upper end of the range of stellar and BH masses seen in the radio-quiet population (see **Figure 4**).

5.2. The Fueling of Radiative-Mode AGNs

5.2.1. Mergers and interactions. The idea that AGNs are largely triggered through the process of galaxy mergers or strong tidal interactions has long been a key component of most theoretical models (e.g., Kauffmann & Haehnelt 2000; Hopkins et al. 2006, 2008). Nevertheless, it has proven difficult to establish this idea observationally, with many claims and counter-claims in the literature. As we explain below, this is a clear case in which arriving at the correct answer requires superb control of the systematics, and this is made possible by a very large and homogeneous data set like that provided by the SDSS. We consider two types of observational tests for a link between interactions/merger and AGN fueling. The first is to measure the incidence of close companion galaxies and the second is to determine the morphological structure of the host galaxy.

The amplitude of the cross-correlation function on scales less than ∼100 kpc probes interacting pairs of galaxies where tidal forces begin to influence the internal structure of the pair. In two companion papers, Li et al. (2008a,b) used the amplitude of the cross-correlation function on scales of tens of kiloparsecs as a probe of the effects of galaxy interactions on star formation and AGN activity in galaxies. They first showed that on scales less than 100 kpc the amplitude of the cross-correlation function exhibits a strong dependence on the sSFR of the galaxy, reflecting the well-known result that galaxy interactions and mergers trigger starbursts in galaxies (Larson & Tinsley 1978). As the separation between the two galaxies in the pair decreased, their sSFR also increased relative to the mean value for field galaxies of the same mass. In a follow-up paper, Li et al. (2008b) applied the same techniques to AGNs in the survey, showing that interactions do not lead to enhancement of nuclear activity over and above that expected as a result of the boost in the central SFRs. In other words, the relation between central star formation and AGN activity in interacting galaxies is no different from that observed for noninteracting galaxies.

Mergers can be identified quantitatively through measures of the global asymmetry (lopsidedness) of the light distribution of the galaxy (e.g., Conselice et al. 2000). An analysis of the SDSS population of normal and AGN host galaxies by Wild et al. (2007) showed that the majority of BH growth in the contemporary Universe occurs in galaxies with relatively quiescent recent star-formation histories that have not experienced recent mergers or strong interactions. In subsequent work, Reichard et al. (2009) followed up on the Li et al. (2008a,b) analysis by showing that AGN activity is not enhanced in lopsided galaxies, compared with symmetric galaxies of the same central SFR. They found that even among AGNs radiating near the Eddington limit, only a small minority exhibited the highly lopsided morphologies of a major merger.

There are many papers reaching the seemingly contrary conclusions that AGNs are triggered by galaxy interactions and/or mergers. Recent examples are by Koss et al. (2010, 2011, 2012), Alonso et al. (2007), Ellison et al. (2011), Hwang et al. (2012), Liu et al. (2012), and Sabater et al.
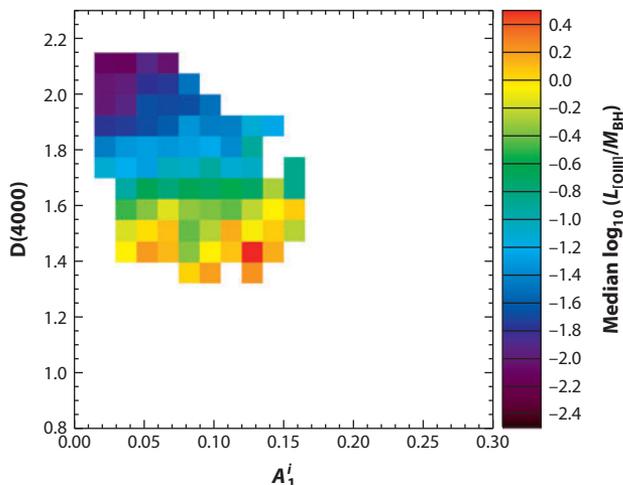
Figure 19

The relationship between $L_{\rm [OIII]}/M_{\rm BH}$, D(4000), and galaxy lopsidedness (A_1^i). The color coding of these two-dimensional histograms indicates the median $L_{\rm [OIII]}/M_{\rm BH}$. The primary correlation is between stellar age and $L_{\rm [OIII]}/M_{\rm BH}$, as is apparent from the horizontal nature of the color contours. There is no independent correlation between $L_{\rm [OIII]}/M_{\rm BH}$ and lopsidedness in these data. Reprinted from Reichard et al. (2009) with permission.

(2013). We stress that these results are actually not at odds with the results above. As Reichard et al. (2009) showed explicitly, the hosts of strong AGNs are in fact more lopsided on average than normal galaxies with the same stellar mass, radius, and concentration. However, they showed that this link is a secondary unphysical one induced by much stronger correlations between lopsidedness and central star formation and between central star formation and the presence of a strong AGN (**Figure 19**). They interpreted this as implying that the fueling of the SMBH is enhanced by the presence of circumnuclear star formation (and its associated cold gas), but this SMBH fueling process does not depend upon the way in which this central star formation arises.

In summary, contrary to the assumption of many theoretical models, most of the AGN activity in the contemporary Universe appears to occur without the need for major mergers or strong tidal interactions. All that is required is an abundant supply of cold, dense gas in the central regions of the galaxy (regardless of its origin).

5.2.2. Fueling via secular evolution. The inward radial transport of gas in a disk galaxy requires torque on the gas that allows angular momentum to be transferred from the gas to the stars or dark matter. Although this can be accomplished in a sudden and spectacular way in a major merger or strong tidal interaction, a slower but significant inflow can be driven by nonaxisymmetric perturbations in the underlying mass distribution that arise through internal dynamical processes in the disk. Examples of such nonaxisymmetric perturbations are bars, oval distortions, and even spiral arms (e.g., Kormendy & Kennicutt 2004, Athanassoula 2008, Sellwood 2014).

Kormendy & Kennicutt (2004) argued that the consequence of this secular evolution for the inner regions of disk galaxies is the creation of a pseudobulge (perhaps more descriptively called a disky bulge by Athanassoula 2005, 2008). These are defined observationally as central regions of enhanced surface brightness relative to an inward extrapolation of the radial surface-brightness profile of the galaxy disk. Unlike classical bulges, they are dynamically cold structures as revealed by the presence of spiral arms, rings, and bars. Unlike typical classical bulges, they are the sites of

significant ongoing star formation (e.g., Gadotti 2009). They have exponentially declining radial surface-brightness profiles whose functional form is more similar to a classic exponential Freeman disk than the $r^{1/4}$ de Vaucouleurs law for elliptical galaxies. The boundary between classical and pseudobulges is typically set at a value for the Sérsic index of $n \sim 2$ for the bulge component (e.g., Kormendy & Kennicutt 2004, Athanassoula 2008, Gadotti 2009, Fisher & Drory 2011).

If the growth of SMBHs in the contemporary Universe is largely fueled by secular processes that transport gas inward, we would therefore expect rapidly growing SMBHs to be found primarily in pseudobulges. We have summarized above the general link between the presence of a young central stellar population (one of the defining characteristics of a pseudobulge) and the rapid growth of the SMBH. Moreover, Kormendy & Ho (2013) show in their figure 17 that the transition from classical bulges to pseudobulges occurs below a bulge velocity dispersion of $\sigma \sim 150$ km s^{-1} and below an SMBH mass $M_{BH} \sim$ few $\times 10^7$ M$_\odot$ (cf. **Figure 9**; and see also Fisher & Drory 2011). This is just the regime where the SDSS shows the bulk of SMBH growth to be occurring today (Heckman et al. 2004, Kauffmann & Heckman 2009).

Is there other more direct evidence that growing SBMHs are preferentially found in pseudobulges? Intriguingly, the compilation of SMBHs by Kormendy & Ho (2013) shows that Seyfert nuclei are present in only 1 of the 45 cases classified as an elliptical galaxy (the powerful radio source Cygnus A) and in only 1 of the 20 cases classified as classical bulges (NGC 4258), but in 11 of the 22 cases classified as pseudobulges. The preference of Seyfert nuclei for pseudobulges is confirmed by the HST imaging survey of nearby active galaxies by Malkan et al. (1998). Simple visual inspection of these images shows that spiral arms, rings, dust lanes, and bars are present in the majority of the AGN hosts on radial scales on the order of a kiloparsec or less from the nucleus (see **Figure 20**). Malkan et al. assigned an inner-Hubble type for each galaxy on the basis of these images, and only 20 of the 107 (19%) of the Type 2 Seyferts had inner Hubble types of E or S0 as expected for a classical bulge. Jiang et al. (2011) reached similar conclusions for an SDSS sample of Type 1 AGNs associated with BHs with estimated masses below 10^6 M$_\odot$.

If AGNs are typically fueled via secular processes, one might naturally expect that they would be preferentially found in barred galaxies (because bars are one of the major mechanisms for driving radial gas flows; e.g., Shlosman et al. 1990). As in the case of establishing a link between interactions and AGNs, there have been many studies over the years that have reached contradictory conclusions on this matter. The most recent studies based on the SDSS do not show evidence for a link once a proper control sample has been identified (Lee et al. 2012, Cisternas et al. 2013 and references therein). Finally we note that there are rare cases of AGNs in galaxies without any detectable bulge at all (Filippenko et al. 1993, Satyapal et al. 2009, Simmons et al. 2013). The fueling mechanism for these systems is mysterious.

5.3. Fueling of Jet-Mode AGNs

The idea that SMBHs can be fed through the accretion of gas shed by evolved stars in the central region of the galaxy is an old one (e.g., Bailey 1980, David et al. 1987, Norman & Scoville 1988, Ciotti & Ostriker 1997). As discussed in Section 4.2, Kauffmann & Heckman (2009) found evidence for two distinct regimes of BH growth in nearby galaxies. We highlight here the regime in which the Eddington ratio distribution is a steep power law. This regime dominates for the more massive BHs living in the older bulges and typically for those accreting at the low Eddington rates associated with jet-mode AGNs (see **Figure 12**). For this population, Kauffmann & Heckman found that at fixed 4,000-Å break strength (broadly, fixed mean stellar age), the time-averaged accretion rate on to the BH scales in proportion with the stellar mass of the galaxy bulge, and the overall rate is higher in galaxies with younger mean stellar ages. They argued that this is consistent with the BH being fueled from the recycled hot gas arising from stellar mass loss.
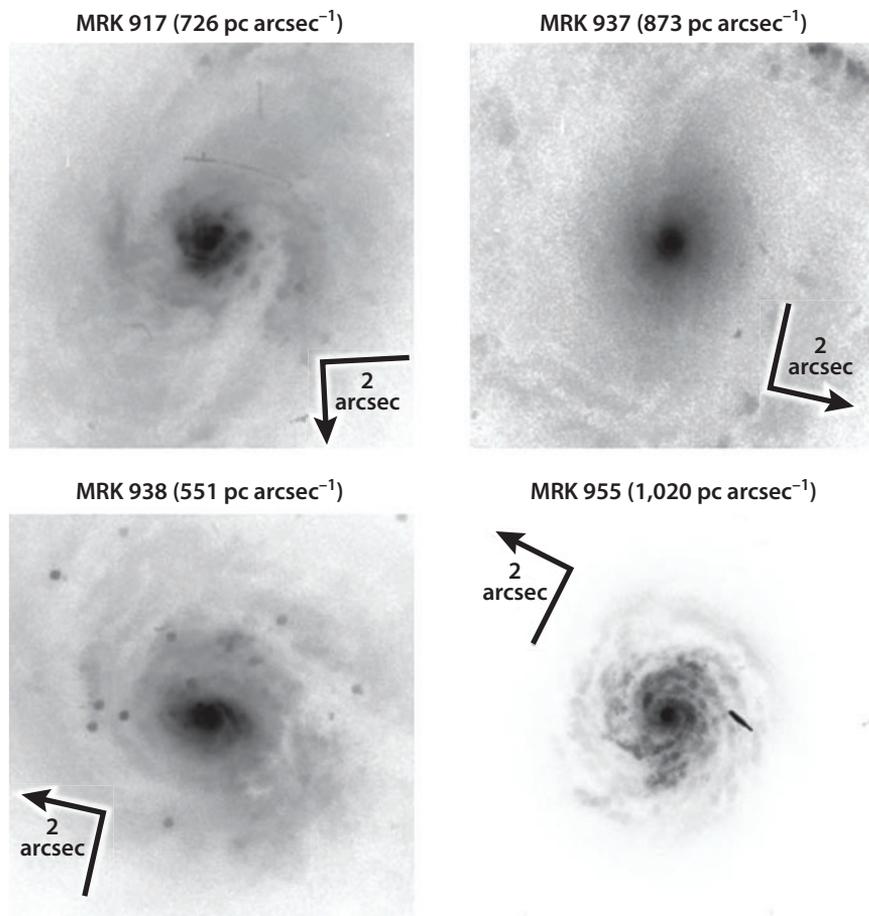
MRK 917 (726 pc arcsec⁻¹)   **MRK 937 (873 pc arcsec⁻¹)**

MRK 938 (551 pc arcsec⁻¹)   **MRK 955 (1,020 pc arcsec⁻¹)**

Figure 20

Hubble Space Telescope optical images of the central regions of four typical Type 2 Seyfert galaxies from Malkan et al. (1998). The arrowhead points north and the bar points east, and the angular scale is indicated. Note that the linear scale (parsecs per arcsecond) quoted in each case assumed $H_0 = 50$ km s^{-1} Mpc^{-1}. In all these examples the central few-kiloparsec-scale region shows the spiral arms and dust lanes typical of pseudobulges.

In fact, hot gas has been widely argued to be the fueling source of the jet-mode radio-AGNs (e.g., Hardcastle et al. 2007). These radio-AGNs are found predominantly in massive galaxies, often at the centers of groups and clusters, with associated hot gaseous X-ray-emitting haloes. These hot gas halos offer not only a potential source of fueling gas for the radio-AGN, but also a confining medium for the radio source to expand against and a depository for the bulk kinetic energy emitted in the radio jet: This allows for the possibility of the radio-AGN feedback cycle that is broadly supported by both observations and galaxy formation models [as we discuss in Section 6; see also the reviews by Cattaneo et al. (2009) and Fabian (2012)].

The rate at which hot gas accretes on a BH was first calculated by Bondi (1952) for a spherically symmetrical geometry with negligible angular momentum or magnetic fields. The Bondi accretion rate from a gas cloud of uniform density (ρ) and pressure is $\dot{M}_B = 4\pi\lambda(GM_{BH})^2\rho/c_s^3$, where λ is an order-unity scaling factor and c_s is the sound speed. In reality, the gas density around a BH is far

from uniform, but the Bondi formula remains approximately correct if ρ and c_s are calculated at the Bondi radius (the radius within which the gravitational potential energy of the BH dominates over the thermal energy of the surrounding gas). Allen et al. (2006) showed that for a sample of 9 nearby systems, a strong correlation exists between the calculated Bondi accretion rate and the jet mechanical energy estimated from the cavities inflated in the surrounding gas. Both the slope and normalization of the relation were found to be close to unity, indicating that simple Bondi accretion of hot gas could be powering these objects.

More recently, however, Russell et al. (2013b) have found a much weaker correlation between Bondi accretion rates and jet powers. Furthermore, for the most luminous radio sources, Bondi accretion rate estimates fall more than two orders of magnitude short of providing the required jet powers (e.g., Cao & Rawlings 2004, McNamara et al. 2011). To produce such powerful sources with direct Bondi accretion would require the BH masses to be far higher than currently estimated (requiring BH masses significantly above 10^{10} M$_\odot$). Such large BH masses would, however, help to explain how the nuclei of these powerful objects can be radiatively inefficient (i.e., below ~1% Eddington; see Hlavacek-Larrondo & Fabian 2011).

A more plausible alternative to direct Bondi accretion of hot gas is that the gas cools out of the hot phase prior to accretion. The most powerful jet-mode radio sources are invariably located in dense galaxy groups or clusters, frequently with strong cooling flows. Hydrodynamic simulations (most recently by Gaspari et al. 2013) that include gas cooling, turbulence, and feedback from AGN heating reveal that when the hot gas is cooling, accretion on to the BH occurs predominantly in a cold and chaotic manner. Cold clouds and filaments form out of the cooling gas in the simulations, decouple from the hot gas, and enter a quasi free-fall regime. Multiple cloud-cloud collisions reduce the angular momentum of the cold gas and lead to stochastic accretion at rates that can be two orders of magnitude higher than the Bondi rate. This is sufficient to produce the observed jet powers of even the most luminous jet-mode sources. Hillel & Soker (2013) suggest that accretion of cooled gas may also dominate over direct Bondi accretion in less extreme systems as well: They argue that even the stellar winds of stars in orbit near the central SMBH would violate the zero-pressure assumption of the Bondi formulism and that the cooling shocked gas from such winds would probably accrete in cold clumps.

Observationally, cool clouds and filaments are almost universally observed in galaxies, groups, and clusters with cooling times significantly below the Hubble time, but not in systems with higher gas entropy (e.g., Hu et al. 1985, Cavagnolo et al. 2008). As extensively reviewed by Fabian (2012), the cooled material is predominantly cold molecular gas, which can extend tens of kiloparsecs around the BCG. This is in good agreement with numerical simulations. The observed masses of cooled molecular gas are comfortably high enough to provide sufficient accretion energy to fuel the inflated cavities (e.g., McNamara et al. 2011); in many objects they are two or more orders of magnitude higher, indicating that the bulk of the cooled molecular gas does not feed the BH but rather fuels star-formation activity, which can also be seen in these systems (e.g., Rafferty et al. 2006, O'Dea et al. 2008).

McNamara et al. (2011) show that the mass of cooled molecular gas does not correlate well with the radio jet power. This implies that either the efficiency with which the cooled gas gets funneled down to the BH must vary greatly (which is at least plausible, given that only a small fraction of the gas reaches the BH) or that another factor as well as the accretion rate is important in determining the jet power. An obvious hidden factor is BH spin. Blandford & Znajek (1977) showed that when material accretes onto rapidly rotating BHs threaded by high-power magnetic fields, the spin energy of the BH can additionally be extracted. Even if the Blandford-Znajek mechanism does not operate, the jet power can still be a strong function of the BH spin, because frame-dragging from the BH's rotation can contribute to the twisting of the magnetic field lines,

amplifying any outflow generated by the Blandford-Payne model (Blandford & Payne 1982; see also Punsly & Coroniti 1990, Meier 1999).

BH spin has been widely cited as a possible explanation for the wide range of radio-loudness observed in the QSO population (the so-called spin paradigm by Wilson & Colbert 1995). According to current models, rapidly spinning BHs are required to produce sufficient jet power to account for the most radio luminous sources (e.g., Meier 2001, Nemmen et al. 2007). Using these models, it is possible to reproduce both the QSO radio loudness distribution and the SDSS-derived local radio luminosity functions of both jet-mode and radiative-mode radio sources (Martínez-Sansigre & Rawlings 2011). This requires a bimodal distribution of BH spins, with BHs either close to maximally spinning or with very low spin parameters. Nevertheless, despite the success of these models, the role of BH spin in powering radio jets remains unproven. Even at the scale of X-ray binaries, there is ongoing debate in the literature as to whether the power of the radio jet produced depends upon the spin of the BH (e.g., Russell et al. 2013a, Steiner et al. 2013).

In conclusion, evidence is strong that a majority of low Eddington fraction AGNs are fueled directly or indirectly from hot gas. The accretion flows are radiatively inefficient, and a significant fraction of the energetic output occurs through jet outflows, the strength of which may be enhanced by rapidly spinning BHs. For many galaxies, the fueling hot gas arises from recycled material from stellar mass loss. In more massive systems (the most massive ellipticals and galaxies at the centers of groups and clusters), extended hot gas halos provide a more abundant gas source, and large-scale cooling flows can greatly enhance the accretion rate. In such systems the extended hot gas halo also provides a working surface for a jet and a medium to confine the expanding radio lobes, minimizing adiabatic losses and leading to luminous radio emission. The hot halo also acts as a repository for the radio jet energy, offering the ideal conditions for a radio-AGN feedback cycle (see Section 6).

6. FEEDBACK PROCESSES

As recently reviewed by Cattaneo et al. (2009) and in this journal by Fabian (2012), feedback from AGNs is currently invoked in both semianalytic models and numerical simulations to successfully reproduce the observed properties of massive galaxies (e.g., Di Matteo et al. 2005, Springel et al. 2005, Bower et al. 2006, Croton et al. 2006, Hopkins et al. 2006, Ciotti et al. 2010). Although AGN feedback is generally assumed to be negative (inhibiting star formation and/or BH growth), it could also be positive in nature (e.g., Ishibashi & Fabian 2012, Zinn et al. 2013, Silk 2013). Feedback from AGNs is generally invoked in two flavors, which relate to the two fundamental modes of AGN activity. The first is a mode of powerful AGN-driven winds that are postulated to occur in galaxies with actively growing BHs and are argued to be responsible for the termination of star formation and the migration of the galaxy from the blue star-forming main sequence to the red sequence. It may also be responsible for setting up the correlation between BH mass and bulge properties (see the review by Kormendy & Ho 2013). We discuss this in Section 6.1. Complementary to this is the requirement to keep the galaxies as red and dead once they have arrived at the red sequence by preventing further gas cooling. Recurrent low-luminosity radio-AGN activity is often posited to be responsible for this kinetic mode of feedback, which is often referred to as maintenance-mode or radio-mode feedback. We examine this in Section 6.2.

6.1. Feedback and Radiative-Mode AGNs

We have reviewed above the evidence that the growth of SMBHs is related to the formation of massive stars in the central (few-kiloparsec-scale) region of the host galaxy. Thus, we first

summarize the evidence for feedback associated with short-lived massive stars and then the evidence for feedback from the BH itself.

6.1.1. Feedback from massive stars. Could the feedback provided by massive stars formed in the central region of the host galaxy affect the fueling of the BH or the evolution of the host galaxy? To set the scale, note that for a normal Kroupa/Chabrier stellar initial mass function, massive stars return about 1.4×10^{49} ergs in kinetic energy per solar mass of star formation (based on Starburst 99; Leitherer et al. 1999). This amount of kinetic energy per unit mass is equivalent to a characteristic velocity of about 1,200 km s^{-1} (far larger than the galaxy escape velocity). Provided that this energy can be efficiently coupled to the surrounding gas, it could indeed result in significant feedback.

There is certainly compelling evidence that this can occur. The most dramatic effect is the production of galactic winds that can be traced in emission and absorption in both the local (e.g., Heckman et al. 1990) and high-redshift (e.g., Steidel et al. 2010, Shapley 2011) Universe. These outflows are driven by the energy and/or momentum supplied by massive stars through their stellar winds, their supernova ejecta, and their radiation (e.g., Chevalier & Clegg 1985, Murray et al. 2011). Although there are detailed multiwaveband studies of relatively small samples of local galactic winds (see the review by Veilleux et al. 2005), the largest census of galactic winds in the local Universe was undertaken by Chen et al. (2010) using SDSS galaxy spectra to measure the interstellar absorption feature produced by neutral Na atoms that trace the outflow. Their work provided statistically robust evidence that local galactic winds are wide-angle bipolar flows along the galaxy minor axis and are associated with galaxies having high SFRs per unit area (cf. **Figure 21**).

Investigations of starburst-driven outflows in the local Universe have only been able to directly detect the flows out to radii of order 10 kpc (e.g., Grimes et al. 2005). However, recent work using absorption-line spectra of background QSOs shows that the wind affects the properties of the surrounding gaseous halo of a starburst galaxy all the way out to the galaxy's virial radius (Borthakur et al. 2013). This is consistent with similar observations of Lyman-break galaxies at $z \sim 3$ (Steidel et al. 2010). Although global feedback from massive stars clearly exists, the evidence that it limits the growth of BHs is only indirect so far. We have described above the result from Wild et al. (2010) that showed that in a large SDSS-derived sample of starburst and poststarburst galaxies, the growth of the SMBHs was delayed by about 200 Myr relative to the onset of the starburst. Wild et al. showed that the turn-on in BH fueling in these galaxies occurred at the time at which the primary source of mass loss from stars in the galaxy's central region switched from supernovae (with ejecta velocities far above the local escape velocity) to intermediate-mass AGB stars (with ejecta velocities far below the local escape velocity). On this basis they speculated that supernova feedback was preventing or inhibiting the accretion of gas by the BH (**Figure 18**). This idea had been previously suggested both theoretically (Norman & Scoville 1988) and on the basis of detailed studies of small samples of local AGNs (Davies et al. 2007).

It is also possible that feedback from massive stars is responsible for the saturation effect found by Kauffmann & Heckman (2009): Once the specific sSFR in the bulge exceeds a value of $\sim 10^{-10}$ years^{-1}, the distribution of the Eddington ratio for the BH assumes a universal log-normal form that does not change at still higher SFRs. Although higher SFRs are associated with a larger gas supply, they are also associated with higher levels of feedback. Kauffmann & Heckman (2009) presented an alternative interpretation: The saturation effect could be understood if the BH regulated its own growth at a fixed average rate of a few percent of the Eddington limit when its fuel supply was plentiful. In a subsequent paper, Hopkins & Hernquist (2009) compared their observational results with their models for self-regulated BH growth, in which feedback produces
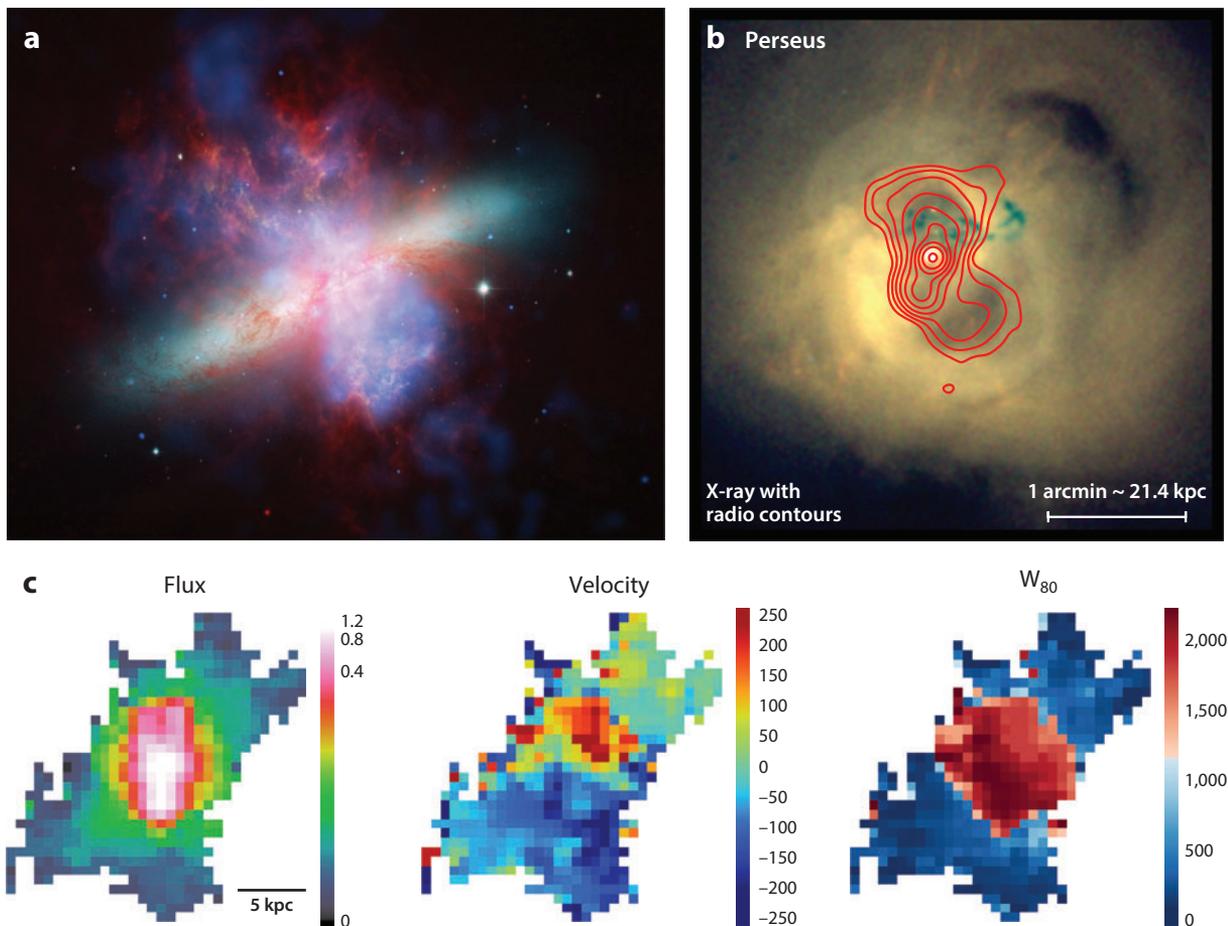
Figure 21

Illustrative examples of feedback effects at work. (*a*) The "Great Observatories" composite image of the starburst-driven galactic wind in M82: Visible light is shown in yellow-green, IR emission in red, Hα emission in orange, and X-ray emission in blue (credit: NASA/JPL-Caltech/STScI/CXC/UofA/). (*b*) The jet-mode feedback in the Perseus cluster (data from Fabian et al. 2006). The color scaling shows the X-ray emission, colored such that hard X-rays are in blue and soft X-rays are in red. The contours indicate the radio emission, which can be seen to have evacuated cavities in the X-ray gas. (*c*) AGN-driven feedback from a high-luminosity radiative-mode AGN (reproduced from Liu et al. 2013b with permission). They show, respectively, the surface brightness (in units of 10^{-14} erg s^{-1} cm^{-2} arcsec^{-2}), relative velocity (in kilometers per second), and velocity width (W_{80} is the velocity width in kilometers per second containing 80% of the emitted line flux) of the [OIII] emission line in the Type 2 QSO SDSS J0319-0019.

a self-regulating phase after the AGN reaches some peak luminosity/BH mass and begins to expel gas and shut down accretion, and found good agreement at the bright end. On that note, we now describe the direct observational evidence for black hole–driven feedback in radio-quiet local AGNs.

6.1.2. Feedback from the black holes in radiative-mode AGNs. As reviewed by Fabian (2012) there is ample direct evidence that radio-quiet AGNs drive outflows. This is primarily based on the frequent presence of blue-shifted absorption lines in the optical, UV, and soft X-ray spectra of Type 1 AGNs (see Crenshaw et al. 2003 and references therein). These trace highly ionized gas

with outflow velocities ranging from several hundred to several thousand kilometers per second in low-luminosity AGNs (Type 1 Seyfert nuclei) to tens of thousands of kilometers per second in powerful QSOs (the broad absorption line systems).

The uncertainty in the feedback effect of these flows arises owing to the difficulty in measuring their basic physical properties. Simple arguments imply that the mass (energy) outflow rate should be proportional to the product of the outflow's total column density times its size times its solid angle times its velocity (cubed). The strong absorption lines measured in the AGN-driven outflows are almost certainly saturated, making it difficult to determine even the ionic column density (let alone a total gas column density). Moreover, the sizes of these outflows have been largely unconstrained. The lack of the detection of such high-velocity outflows in the spectra of typical Type 2 Seyferts (e.g., Krug et al. 2010) is evidence either that the flows in Seyferts do not extend beyond the central few tens of parsecs or that their column densities drop below detectable values on these larger radial scales. It is therefore not surprising that the spectroscopic data in the SDSS on a vast number of local Type 2 AGNs has not uncovered any direct evidence that they are driving large-scale outflows that cannot be attributed to the feedback from central star formation described in Section 6.1.1 above.

Another line of evidence for outflows in typical radio-quiet AGNs comes from mapping the physical and dynamical state of the ionized gas seen in the NLR. This has been reviewed by Veilleux et al. (2005) in this journal, and we refer the reader there for details. In a number of local Seyfert galaxies the ionized gas on a scale of about a kiloparsec from the AGN is clearly being impacted by the collimated outflows (radio jets), which are commonly present even in radio-quiet Seyferts (e.g., Wilson & Heckman 1985; Rosario et al. 2010a,b). It is difficult to accurately estimate the total outflow rates in these cases, but the kinetic energy flux appears to be a small fraction of the AGN bolometric luminosity in typical local Seyfert galaxies (see Veilleux et al. 2005 and references therein).

Although direct evidence for black hole–driven feedback in typical local AGNs is lacking, recently there have been several exciting discoveries that imply that the most luminous AGNs can indeed drive highly energetic outflows that could have a significant impact on both the fueling of the BH and the evolution of the host galaxy. These are AGNs with bolometric luminosities well above the knee in the local AGN luminosity function ($L_* \sim 10^{45}$ erg s$^{-1} \sim 10^{11.5}$ L$_\odot$). As such they are rare, and only rather small samples have been studied so far.

The first such discovery is the prevalence of outflows of molecular gas in ultraluminous infrared galaxies (ULIRGs) with AGN bolometric luminosities above about 3×10^{45} erg s^{-1}. This evidence is of two types. First, the PACS instrument on the *Herschel Space Observatory* has been used to observe the far-IR emission and absorption features due to the OH molecule. Initial results were presented by Fischer et al. (2010) and Sturm et al. (2011). Most recently, Veilleux et al. (2013) and Spoon et al. (2013) summarized observations of an expanded sample of ULIRGs and QSOs at $z < 0.3$. For each object, the fractions of the bolometric luminosity due to a starburst and AGN were determined following the analysis by Veilleux et al. (2009). The OH feature is detected in absorption in most objects, with the majority of these showing evidence for molecular outflows in the form of blue-shifted OH absorption lines. The equivalent widths of the OH absorption features (tracing the column density) do not depend upon the AGN luminosity or the ratio of the AGN/starburst luminosities. The outflow velocities do not depend upon the starburst luminosity, but they do increase with both increasing AGN luminosity and AGN/starburst luminosity ratio. Characterizing the outflow speed by the midpoint in the line profiles yields outflow speeds of order 100 km s^{-1} in the starburst-dominated systems and about 400 km s^{-1} in the AGN-dominated cases, but the most rapidly outflowing gas can reach speeds of order 10^3 km s^{-1}. As noted above, deriving an outflow rate requires determination of a size for the flow. Sturm et al. (2011) have used

a radiative transfer code (González-Alfonso et al. 2014) applied to the observed far-IR spectrum to estimate the size scales and, hence, the outflow rates in five ULIRGs. For an assumed OH/H_2 ratio, the implied outflow rates range from 10^2 to $10^3 \, M_\odot \, year^{-1}$ (comparable with, or larger than, the SFR).

Complementing these probes are measurements of molecular gas in emission in the millimeterwave regime. The molecular outflow in the prototypical AGN-dominated ULIRG Mrk 231 has been mapped in CO (Feruglio et al. 2010, Cicone et al. 2012) and in HCO+, HCN, and HNC (Aalto et al. 2012) using the Plateau de Bure millimeter wave interferometer. The flow is spatially resolved with outflow speeds of up to 800 km s^{-1} detectable over a kiloparsec-scale region and an estimated outflow rate of about 700 $M_\odot$ year^{-1}, in broad agreement with the estimates based on the OH absorption line seen with *Herschel*. Complementary information on this outflow is provided by the spatially-resolved kinematics of neutral atomic gas traced by the NaI absorption line (Rupke & Veilleux 2011). Similar results using CO emission as a tracer have now been found for a small sample of other AGN-dominated ULIRGs (Cicone et al. 2014). They find that the kinetic energy in the molecular outflow is a few percent of the AGN bolometric luminosity and that the momentum flux is about 20 times larger than L_{bol}/c. The primary uncertainty affecting these estimates is the conversion factor used to convert the CO luminosity into an H_2 mass.

These outflow rates are impressive, but the flows can only be traced out to modest radii (kiloparsec scale). Recently, the effects of AGN outflows on the global properties of the host galaxy have been discovered in samples of Type 2 QSOs—obscured AGNs with bolometric luminosities in excess of 10^{46} erg s^{-1} (Zakamska et al. 2004). Greene et al. (2011) reported on the analysis of long-slit optical spectroscopy probing the kinetics of the ionized gas surrounding 15 Type 2 QSOs at $z \sim 0.1$ to 0.45. They found broad emission lines of [OIII] 5007 (full width at 20% of the maximum line intensity of $\sim$500 to 1,500 km s^{-1}) that extended across the entire extent of the galaxy (radii of order 10 kpc). More recently Liu et al. (2013a,b) used the Gemini integral field unit to fully map out the 2-D distributions of the [OIII] and Hβ emission lines around a sample of 11 radio-quiet Type 2 QSOs at $z \sim 0.3$ to 0.65 with typical bolometric luminosities of 10^{47} erg s^{-1}. They obtain similar results to Greene et al. (2011), but their complete spatial coverage enables them to better characterize the structure and kinematics (e.g., **Figure 21**). They find that a simple model of a spherically symmetric outflow at a velocity of 500 to 1,000 km s^{-1} reproduces the data. The estimated outflow rates are uncertain because the density (and hence the mass) of the emitting material is not directly measured. It appears that the entire ISM of the galaxy could be expelled over a timescale of only a few tens of millions of years, implying a kinetic energy flow of order 2% of the bolometric luminosity (similar to the estimates in the molecular outflows described above).

In summary, there is now some persuasive evidence that the most powerful radiative-mode AGNs in the contemporary Universe can drive outflows capable of severely impacting their host galaxies. Evidence for global outflows in typical low-redshift radiative-mode AGNs is lacking.

6.2. Feedback from Radio Sources

As discussed in Section 5.3, radio-AGNs can be fueled from their surrounding hot gaseous haloes, either directly through the Bondi process or via gas that has cooled out of the hot phase in a cooling flow. The bulk of the energy generated from the accretion is channeled into the powerful radio jets, which drive their way outward. The radio jets are confined by the hot halo gas and produce expanding radio lobes filled with relativistic plasma, inflating bubbles or cavities in the hot gas. The bulk of the jet energy is deposited locally, through the mechanical work required to inflate these cavities. Because the repository of the AGN energy is the same gas as that which fuels the AGN, this offers the necessary conditions for a self-regulating AGN feedback cycle.

The most extreme examples of radio-AGN feedback occur in the massive galaxies at the centers of groups and clusters (see **Figure 21**). In these systems the radiative cooling time of the surrounding gas can be substantially shorter than the Hubble time. In the absence of a heating source, a cooling flow would be expected to develop, whereby the temperature in the central regions of the cluster drops and gas flows inward at rates of hundreds or even thousands of solar masses per year (see the review by Fabian 1994). In reality, however, observations show that the gas temperatures in the cluster cores are at most a factor of 3 below the value at large radii, and the amount of cooling gas is only about 10% of the cooling flow prediction (e.g., Peterson et al. 2001, 2003; David et al. 2001; Tamura et al. 2001).

A heating source must be balancing the radiative cooling losses to prevent the gas from cooling further, and this reduces the SFRs in the central galaxy by an order of magnitude (though not to zero—these galaxies can still have SFRs of tens of solar masses per year; e.g., O'Dea et al. 2008). The heating source is almost certainly the jet outflows from the central BH: The prevalence of radio-AGN activity is high (>70%) in central cluster galaxies (Burns 1990), and results from the SDSS show that it is enhanced relative to other galaxies of the same mass (Best et al. 2007). Bubbles and cavities in the X-ray gas are also seen in a high percentage of clusters, reaching nearly 100% in those clusters with cooling times below 3 Gyr (Dunn & Fabian 2006, Fabian 2012). As discussed in Section 2.3.2, the mechanical energy flow rates of the radio jets are calculable either from the observed synchrotron emission or from the pV work required to inflate the radio lobes. Analysis of these cooling clusters indicates that the energy input from the radio jets is in rough balance with the energy losses from radiative cooling within the cooling radius (see the review by McNamara & Nulsen 2007).

For feedback processes to be efficient, it is not only the total available energy that is important but also how and where that energy is deposited. Radio jets are highly anisotropic structures, but gas cooling and inflow need to be switched off in all directions. It is the expanding radio bubbles, rather than direct jet interactions, that must provide the bulk of the energy transfer to the ambient medium. This process is observed in the form of weak shocks or sound waves surrounding some radio bubbles; the most striking example is the Perseus cluster, in which several concentric ripples in X-ray pressure are seen (Fabian et al. 2003, 2006). These ripples have been associated with repeated episodes of bubble-blowing activity from the central AGN. The energy in the sound waves or weak shocks is gradually dissipated over length scales of ~100 kpc (depending upon the gas viscosity). This gentle feedback process is able to transfer the radio jet energy into its environment in a largely isotropic manner without disturbing the intracluster medium to such an extent that the observed temperature and metal abundance gradients would be destroyed by mixing.

The radio-AGN activity appears to be switched on nearly all of the time in cooling flow clusters and must be able to adapt quickly to changes in its environment in order to maintain the close heating-cooling balance. This quick adaption is not possible for standard Bondi accretion, because the infall time of the hot gas from kiloparsec scales down to the BH is more than a billion years (Soker 2006). However, cold clump accretion occurs on a much faster timescale, especially in a viscous accretion flow, and therefore allows the BH to react quickly to changes in the state of its environment (Pizzolato & Soker 2010, Gaspari et al. 2013). This allows for efficient self-regulation of the feedback process.

Although BCGs offer the most striking examples of radio-AGN feedback, which can be individually studied in detail, these massive cooling-flow clusters are relatively rare. The data from large sky surveys have been invaluable in extending analysis to less extreme systems and providing a direct statistical comparison of radio-AGN feedback in systems of different scales. Best et al. (2006) investigated the role of radio-AGN feedback in elliptical galaxies using data from the SDSS. On the assumption that all massive galaxies would go through recurrent short-lived

radio-AGN outbursts, they considered the observed prevalence of powerful ($P_{1.4\,\mathrm{GHz}} > 10^{23}$ W Hz^{-1}) radio-loud AGNs as a function of BH mass and interpreted this as a measure of the duty cycle of powerful radio-AGN activity for galaxies of that BH mass. They combined this with the BH mass–dependent radio luminosity function to estimate, probabilistically, the fraction of its time that a BH of given mass would spend producing a radio source of a given radio luminosity. Using the radio luminosity–to–jet kinetic power conversion (Section 2.3.2) then allowed a calculation of the average rate of jet kinetic energy production of the BH. Note that most of the heating is produced by radio sources of $P_{1.4\,\mathrm{GHz}} \sim 10^{24}-10^{25}$ W Hz^{-1}. The heating contribution from periods of very low radio luminosity, where in this simple picture the radio AGN is considered to be off, can be neglected. Best et al. derived the heating rate for galaxies of different BH mass and compared these results with the X-ray luminosities (i.e., cooling rates) of the hot haloes around the galaxies. They found that for elliptical galaxies of all masses, the radio-AGN heating rate provided a good balance to the gas cooling rate. AGN heating is therefore able to counter-balance cooling and thus explain the old, red, and dead nature of the ellipticals.

The Best et al. (2006) analysis actually underestimated the jet-energy production rate, as they adopted only pV instead of $4pV$ for the cavity energies. Also, for gas cooling rates, they scaled from the total X-ray luminosity rather than considering only the luminosity within the cooling radius (which is the only region where cooling needs to be compensated to avoid catastrophic cooling collapse). Therefore, the radio-AGNs provide, in a time-averaged sense, significantly more energy than is required to suppress cooling on galaxy scales. This was shown more clearly by Best et al. (2007), who compared the time-averaged AGN heating rate against the rate of radiative cooling within the cooling radius for systems of different masses. They suggested that the average heating-to-cooling ratio decreased by two orders of magnitude when going from massive ellipticals/small groups to the most massive clusters. Updated observational determination of the BH mass–dependent radio luminosity function and the radio luminosity–to–jet power conversion have decreased this scale dependence, but it remains well in excess of an order of magnitude. Thus, if the radio-AGN heating rate is at the level that balances cooling in the most massive clusters (or at least the cool-core subset of these), then in smaller systems an order of magnitude more jet mechanical energy is produced than required.

Similar indications have been found by Nulsen et al. (2007; see also Fabian 2012, his figure 5), who found that the pV energy stored in cavities seen in lower-mass systems can be an order of magnitude above that required to balance cooling losses. This result is easily understood, because in individual galaxies or small groups a large fraction of the jet kinetic energy may get deposited on much larger scales than the cooling radius: The jets themselves can extend beyond the cooling flow region, and even if they don't then the bubbles they produce will still rise buoyantly to beyond the cooling radius, whereas the weak shocks produced by the expanding cavities dissipate their energy on similarly large (hundred-kiloparsec) scales (e.g., Fabian et al. 2005).

In lower mass systems the duty cycle of radio source activity is also low; the AGN is turned off for most of the time. The heating-cooling balance is a pseudoequilibrium process whereby in the brief periods in which the radio source does turn on, the instantaneous energetic output is far above that required to balance cooling. This leads to overheating of the gas, seen for example as a temperature difference observed between galaxy groups and low-mass clusters with and without radio-AGNs (Croston et al. 2005, Magliocchetti & Brüggen 2007; see also Shen et al. 2008). After the radio-AGN outburst, the system experiences a period during which accretion rates are suppressed by the turbulent motions and heating that was induced, leading to effectively an off state for the BH. This behavior is seen in hydrodynamic simulations (e.g., Gaspari et al. 2013) and is also suggested both by the episodic history of star formation found by Chen et al. (2013b)

in massive galaxies ($M_* > 10^{11}\,M_\odot$) and by the apparent anticorrelation they find between a recent burst of star formation and the current presence of a radio source. This off period lasts longer in less massive systems because the lower binding energy and gas sound speed lead to a longer recovery time before gas cooling and accretion recommence. The BH therefore acts as a cosmic thermostat, adjusting quickly to its surroundings and switching on powerful radio-AGN activity whenever the gas temperature drops sufficiently to allow significant cooling to occur. Rare intermittent activity (duty cycle 0.001–0.01) suffices to control gas cooling in typical massive ellipticals (of stellar mass $\sim 10^{11}\,M_\odot$), with the system oscillating around an equilibrium state. In contrast, near-constant activity (duty cycle ~ 1) is required to control gas cooling in the most massive cooling flow clusters.

7. THE SITUATION AT HIGH REDSHIFT

The focus of this review has been the contemporary Universe as probed through large surveys (most notably, the SDSS). It is then natural to ask whether the results we have reviewed apply only to the present day or whether a qualitatively similar picture also applies at higher redshift.

7.1. The Representative AGN Population

To begin, let us use the cosmic evolution of the bolometric AGN luminosity function to frame the issues. Although it is customary to refer to the redshift range of 2 to 3 as the QSO era, this is actually rather misleading. It is true that the comoving number density of the most powerful AGNs ($L_{\rm bol} > 10^{14}\,L_\odot$) peaked during this epoch. These are associated with the formation of the most massive SMBHs ($>10^{9.5}\,M_\odot$), and as such comprise only a minor fraction of the BH mass in the local fossil record (Shankar et al. 2009). A much better way to think about the growth of the BH population is to use the data plotted in **Figure 1** to calculate the history of the cumulative growth of the relic mass in SMBHs over time. This leads to the striking result that the growth of BHs is actually a protracted process: 25%, 50%, and 75% of the present-day relic mass was formed by cosmic ages of about 3.3 Gyr ($z \sim 2$), 5 Gyr ($z \sim 1.3$), and 7 Gyr ($z \sim 0.75$), respectively. The history of the mass build-up in galaxies via star formation is very similar (e.g., Shankar et al. 2009). So in a big picture sense, the physics that connected (connects) the growth of galaxies and BHs must have been in place over a significant fraction of the history of the Universe, and the bulk of this coevolution took place at moderate redshifts.

To focus our discussion, we consider the population of AGNs and their host galaxies over the redshift range of 0.5 to 2.5 (during which time about 75% of the current BH mass was created by accretion). The shape of the bolometric luminosity function at $z \sim 2$ (Hopkins et al. 2007b, Shankar et al. 2009) implies that most of the BH growth then occurred for objects near L_*. More quantitatively, half the BH growth occurred for AGNs with bolometric luminosities between $L_{\rm bol} \sim 10^{12.5}$ and $10^{13.3}\,L_\odot$ (or hard X-ray luminosities of 2×10^{44} to 8×10^{44} erg s^{-1}). At $z \sim 0.5$, the same calculation implies that half the BH growth occurred in AGNs with bolometric (hard X-ray) luminosities between $10^{11.2}$ and $10^{12.3}\,L_\odot$ (3×10^{43} to 2×10^{44} erg s^{-1}). We use these fiducial values for redshift and luminosity to define what we henceforth call representative AGNs, by which we mean the objects most responsible for the creation through accretion of the mass locked up in BHs in the present fossil record.

7.2. The Host Galaxies of Radiative-Mode AGNs

Most of the information about AGN host galaxies at high z comes from either deep surveys of fields that probe comoving volumes too small to sample the representative AGN population or observations of individual AGNs of exceptionally high luminosity. It is only over the past few

years that we have learned quite a bit about the properties of the host galaxies of the representative AGNs. For the most part these surveys have selected the AGNs and quantified their properties based on (rest-frame) hard X-ray data. One potentially important caveat is that it is possible that the host galaxies of X-ray-selected AGNs systematically differ from the host galaxies of AGNs selected in the IR or optical (Hickox et al. 2009, Koss et al. 2011, Juneau et al. 2013).

The most detailed investigation of the dependence of AGN properties on the mass of the host galaxy was undertaken by Aird et al. (2012) for a population of X-ray-detected objects over the range $z = 0.2$ to 1.0. They find that the distribution of AGN X-ray luminosity normalized by the stellar mass of the host galaxy (M_*) is essentially independent of M_* over mass bins with centers from $M_* = 10^{9.75}$ to $10^{11.75}\,M_\odot$. Within the uncertainties, this is largely consistent with the [OIII]-based SDSS results at $z \sim 0.1$ we have plotted in **Figure 16**, except that our plot shows a strong drop in normalized luminosity at high galaxy mass. As we noted, the normalized sum of L_{rad} plus L_{mech} is roughly independent of M_* out to the highest masses. In fact, Chen et al. (2013b) found strong evolution in the emission-line AGNs associated with very massive galaxies ($M_* > 10^{11.4}\,M_\odot$) between $z \sim 0.1$ and 0.6. They found that the equivalent width of the [OIII] emission line (a rough proxy for L_{rad}/M_*) increased by an order of magnitude and that the emission lines changed from LINER-like (jet mode) at low z to Seyfert-like (radiative mode) at higher z. This is at least qualitatively consistent with the difference between the results by Aird et al. (2012) and what is seen in the contemporary Universe.

Aird et al. (2012) also conclude that their sample of AGNs shows a universal distribution in Eddington ratio that is independent of galaxy or BH mass. This would be inconsistent with the picture of the downsizing of the population of BHs because the implied timescales for BH mass–doubling through accretion would be independent of BH or galaxy mass. However, their result is based on their assumption of a uniform ratio of BH–to–total galaxy stellar mass ($M_{BH}/M_* = 0.002$) as a function of mass. As we showed explicitly in **Figure 9b**, in the SDSS sample at $z \sim 0.1$ the ratio of BH-to-stellar mass increases by a factor of about 1.5 dex (from 0.0001 to 0.003) over the range in stellar mass bins studied by Aird et al. (centered from $\log M_* = 9.75$ to 11.75). If the relationship between BH and galaxy mass is similar at $z \sim 0.1$ and 0.6, the Aird et al. results would then be entirely consistent with the BH down-sizing picture. This is supported by the conclusions of Kelly & Shen (2013) based on their analysis of the SDSS QSO population.

Mainieri et al. (2011) studied the host galaxies of a sample of 142 X-ray-selected Type 2 AGNs from the *XMM-Newton* COSMOS field. The typical redshifts are in the range of 0.8 to 2, and X-ray luminosities are 10^{44} to 10^{45} erg s^{-1}. They find few detected AGNs in host galaxies with stellar masses less than $10^{10}\,M_\odot$, and they find typical stellar masses of $\sim 10^{10.5}$ to $10^{11.3}\,M_\odot$ (similar to local Seyfert galaxies). A stacked spectrum in the rest-frame optical shows values of the 4,000-Å break and high-order Balmer absorption lines corresponding to a very young star-forming population. The masses (and the SFRs derived from *Herschel* far-IR photometry) imply that the sSFRs are similar to those of normal galaxies on the star-forming main sequence at the same redshifts (see **Figure 22**). Most host galaxies appear to be early-type galaxies (with a significant bulge component), and only a minority show either a prominent disk or a disturbed morphology indicative of a major merger.

Schawinski et al. (2012) investigated the host-galaxy properties of a population of IR-selected heavily obscured AGNs at $z \sim 2$ with typical bolometric luminosities of $\sim 10^{12.5}\,L_\odot$. Their HST imaging reveals that most have a significant disk component and only a small fraction appear to be major mergers. At lower redshifts ($z \sim 0.7$), Cisternas et al. (2011) analyzed HST images of the hosts of AGNs with X-ray luminosities of 10^{43} to 10^{44} erg s^{-1}. They found that at least 85% of the host galaxies have normal undisturbed morphologies (similar to their control sample of non-AGN galaxies).
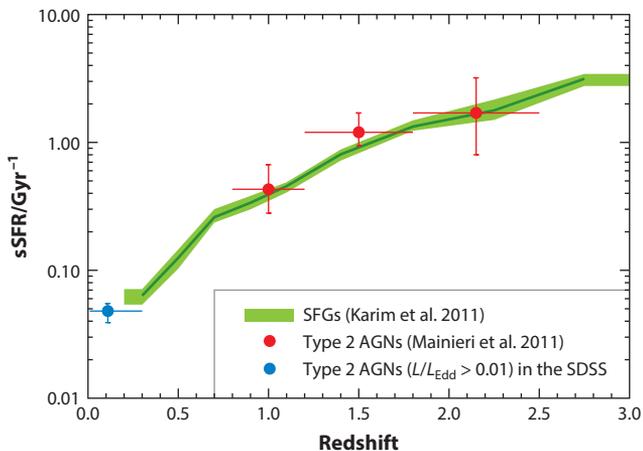
Figure 22

The specific star-formation rate (sSFR = SFR/M_*) of radiative-mode AGN hosts compared with normal star-forming galaxies (SFGs) as a function of redshift. The green-shaded region shows the evolution of the sSFR of galaxies along the star-forming main sequence derived by Karim et al. (2011). The red points show the sSFR of the host galaxies of X-ray-selected Type 2 AGNs from the *XMM-Newton* COSMOS field derived by Mainieri et al. (2011). The blue point indicates the average sSFR of emission-line-selected Type 2 AGNs with $L/L_{Edd} > 0.01$ (i.e., broadly radiative mode) from the Sloan Digital Sky Survey (SDSS). At all redshifts, the sSFRs of radiative-mode AGN hosts are consistent with those of galaxies on the star-forming main sequence.

Santini et al. (2012) investigated samples of X-ray-selected AGNs from the GOODS N and S field and the COSMOS field over the range $z \sim 0.5$ to 2.5. Only the COSMOS field has sufficient volume to probe the population of representative AGNs. Based on *Herschel* far-IR photometry, the SFRs and sSFRs of the AGN hosts in this field are enhanced by a factor of about three relative to the full population of normal galaxies at the same redshift. However, the SFRs in the AGN hosts are consistent with those of the star-forming population of normal galaxies (i.e., the AGNs avoid the quiescent galaxy population). At $z \sim 0.7$, Bournaud et al. (2012) found a high incidence rate of Seyfert-like AGNs in a sample of star-forming galaxies with clumpy disks. They argue that the fueling of AGNs at high z is primarily through inflows triggered by violent disk instabilities rather than major mergers (Elmegreen et al. 2008b, Bournaud et al. 2011).

Rosario et al. (2013) have examined the relationship between SFR (from the far-IR luminosity) and AGN hard X-ray luminosity over the range from $z \sim 0$ to 2.5. They find that at $z < 0.8$ there is a correlation between the AGN luminosity and SFR for AGNs with bolometric luminosities above $\sim 10^{10.5}$ $L_\odot$. At higher redshifts the SFR no longer correlates with AGN luminosity, but rises with increasing redshift (from ~ 10 $M_\odot$ per year at $z \sim 1$ to ~ 50 $M_\odot$ per year at $z \sim 2$). Again, these SFRs are consistent with the properties of typical massive star-forming galaxies at these epochs. Harrison et al. (2012a) reach similar conclusions. These results regarding the complex connection between AGNs and star formation may be related to findings of Kauffmann & Heckman (2009) at low z. As summarized above, they found a threshold value for the sSFR for effective BH growth. Once this threshold is exceeded, BH growth is switched on, but the rate of growth does not increase if the SFR rises further.

To summarize, the hosts of the representative population of radiative-mode AGNs out to $z \sim 2$ are mostly structurally normal galaxies with SFRs corresponding to those of the typical star-forming population of galaxies at that epoch. These results are consistent with most other

investigations of the less powerful AGN population over the same range in redshift (e.g., Pierce et al. 2007; Gabor et al. 2009; Hickox et al. 2009; Silverman et al. 2009, 2011; Schawinski et al. 2011; Kocevski et al. 2012; Mullaney et al. 2012a,b; Aird et al. 2012, 2013; Bohm et al. 2013; Chen et al. 2013a; Juneau et al. 2013; Rosario et al. 2013; Villforth et al. 2014). These results are also consistent with the more detailed picture we have presented for radiative-mode AGNs in the contemporary Universe.

7.3. Evolution of the Radio-Loud AGN Population

The cosmic evolution of the radio luminosity function has been studied for many years, since early work on understanding radio source counts indicated that high luminosity sources undergo substantially stronger cosmic evolution than low luminosity sources (Longair 1966). Seminal work by Dunlop & Peacock (1990) clearly established that the space density of both flat-spectrum (i.e., beamed) and steep-spectrum powerful radio sources is 2–3 orders of magnitude higher by $z \sim 2$ than in the contemporary Universe. Beyond this redshift the space density peaks or declines slowly. In contrast, the low luminosity radio sources show only a factor of <2 increase in space density out to $z \sim 0.5$ (e.g., Sadler et al. 2007, Donoso et al. 2009). Rigby et al. (2011) characterized this differential evolution, showing that the redshift at which the radio source space density peaks is strongly luminosity dependent with low luminosity sources showing a peak space density at $z < 1$.

As discussed earlier, the radio-AGN population comprises both jet-mode (radiatively inefficient) AGNs and radiative-mode (radio-loud QSO/Seyfert-like) AGNs. Best & Heckman (2012) looked at the cosmic evolution of these two populations separately within the narrow redshift range probed by the SDSS and concluded that they showed different cosmic evolution. This has been confirmed by P.N. Best, L.M. Ker, C. Simpson, E.E. Rigby & J. Sabater (in preparation), who show that out to $z \sim 0.7$ the radiative-mode population shows a factor ~ 8 increase in space density at all radio luminosities. The jet-mode sources, however, show only a small increase in space density out to $z = 0.5$, followed by a decline thereafter. These results are easily understood in terms of our earlier discussions on the fueling of these AGNs. The radiative-mode radio-AGNs evolve in broadly the same manner as the upper-mass end of the radiative-mode radio-quiet population, increasing with redshift as the availability of an abundant supply of cold gas increases. If the jet-mode AGNs are largely associated with cooling hot-gas haloes, then their evolution should be closer to that of massive galaxies and, thus, slowly declining toward higher redshifts.

These results indicate that the luminosity-dependent cosmic evolution of the radio luminosity function as a whole is largely driven by the different cosmic evolution of these two AGN populations. As a result of this differential evolution, the dominant radio-AGN population also changes with redshift. Locally, except at the highest radio luminosities, the jet-mode population dominates the radio-AGN number counts. By $z > 1$, however, the QSO/Seyfert-like sources begin to dominate at all (currently observable) luminosities. It is for this reason that the properties of radio-loud and radio-quiet AGNs appear much more comparable in the early Universe than in the contemporary Universe.

Early work to extend the study of the host galaxies of the jet-mode AGNs to higher redshifts paints a picture consistent with that in the contemporary Universe. Tasse et al. (2008) and Donoso et al. (2009) both investigated the relationship between galaxy stellar mass and radio-AGN prevalence at $z \sim 0.5$. If consideration is restricted to only the jet-mode AGNs, then a steep power-law dependence similar to that for the contemporary Universe (Section 4.3) is found. Simpson et al. (2013) recently extended that analysis to $z \sim 1$, confirming the same results. Tasse et al. (2008) also showed that the jet-mode population was typically found in galaxy overdensities (groups or clusters). These results indicate that the feedback balance between radiative cooling

and radio-AGN heating, seen in the contemporary Universe, was already in place in some environments when the Universe was half of its current age.

7.4. AGN Feedback at High z

Feedback from AGNs in the form of ionizing radiation clearly plays a fundamental role in ionizing and heating the intergalactic medium over much of the history of the Universe. Here, we briefly summarize the evidence regarding the existence and physical properties of bulk outflows of mass and kinetic energy driven by AGNs. This evidence is based on detailed investigations of small samples of AGNs.

In a series of papers, Arav and collaborators (Arav et al. 2008, Korista et al. 2008, Moe et al. 2009, Bautista et al. 2010, Dunn et al. 2010, Aoki et al. 2011, Edmonds et al. 2011, Arav et al. 2013, Borguet et al. 2013) have been able to determine the main physical properties of outflows in high-z QSOs as traced by UV absorption lines. The QSOs have bolometric luminosities of $\sim 10^{13.3}$ to $10^{14.7}$ L$_\odot$ and $z \sim 0.6$ to 3 (they are considerably more luminous than the representative AGN population). Of the eight outflows they have analyzed, four are extremely energetic with kinetic energy fluxes of 10^{45} to 10^{46} erg s^{-1}, representing ~ 1 to 5% of L_{bol}. The typical outflows speeds are about 3,000 to 8,000 km s^{-1}, and the inferred size scales of the outflows range from several hundred parsecs to several kiloparsecs. Similar work by this group on less luminous AGNs at lower redshift has so far found only very weak outflows with kinetic energy fluxes $\ll L_{bol}$ (Edmonds et al. 2011, Borguet et al. 2012).

Alexander et al. (2010) and Harrison et al. (2012b) have analyzed spatially resolved maps of the kinematics of the ionized gas surrounding nine radio-quiet AGNs at $z \sim 1.4$ to 3.4. The objects were selected from a parent sample of submillimeter galaxies on the basis of unusually strong and broad [OIII] 5007 emission lines. Evidence for galactic-scale outflows was found in the five AGNs with bolometric luminosities of about 10^{13} L$_\odot$ (roughly L_* at these redshifts), but not in the less luminous cases. The strong rest-frame far-IR emission in these objects implies that they have much higher SFRs than typical AGNs at these redshifts ($\sim 10^3$ M$_\odot$ year^{-1} compared with ~ 30 to 100 M$_\odot$ year^{-1}, respectively). Thus, it is not entirely clear whether the outflows are driven by the AGN or the starburst in these objects.

Using similar techniques, galaxy-scale outflows of ionized gas have been mapped around a small sample of extremely radio-loud QSO-like AGNs at $z \sim 2$ (Nesvadba et al. 2006, 2008). These outflows appear to be driven by the mechanical energy carried by the powerful radio jets in these systems. At the highest redshifts, Maiolino et al. (2012) have mapped an outflow from an exceptionally luminous ($L_{bol} \sim 10^{14}$ L$_\odot$) QSO at $z \sim 6.4$ using the [CII] far-IR emission line. They estimate an outflow rate of several thousand solar masses per year at a velocity of order 10^3 km s^{-1}. We conclude that direct evidence for AGN feedback at high z is limited so far to objects of exceptionally high luminosity or other unusual characteristics. Little is known about whether the representative population of high-z AGNs produces powerful global outflows. Again, this is all consistent with the results derived in the contemporary Universe.

8. SUMMARY AND IMPLICATIONS

Let us begin this final section by briefly summarizing what we regard as the most robust conclusions about the demographics of the populations of AGNs and their host galaxies in the contemporary Universe. We then consider the degree to which these results may be extended to higher redshift and conclude with some speculation about the implications these conclusions may have for our understanding of the formation and evolution of galaxies.

8.1. Some Robust Conclusions

In the contemporary Universe there are two distinct families of AGNs. We have designated them radiative-mode and jet-mode AGNs. The radiative-mode population of AGNs is characterized by the production of significant amounts of radiation with typical bolometric luminosities of 1 to 100% of the Eddington limit. Historically these have called Seyfert galaxies or QSOs depending upon their luminosity. The AGN properties can be explained within the theoretical context of a radiatively efficient geometrically thin accretion disk. In the contemporary Universe these AGNs characteristically have BH masses of 10^6 to $10^8 \, M_\odot$ and reside in host galaxies with typical stellar masses 10^{10} to a few $\times 10^{11} \, M_\odot$ and high stellar surface mass densities ($\mu_* > 10^{8.5} \, M_\odot$ kpc^{-2}). Although these densities are characteristic of early-type disk galaxies, the AGN hosts (unlike most such galaxies) have significant amounts of ongoing star formation in the central few kiloparsecs. When examined at high spatial resolution these inner regions can usually be classified as pseudobulges. Major mergers or strong tidal interactions are not the dominant fueling mechanism for the central star formation and the AGN. Internal secular processes for the radial transport of gas are evidently more important. This summary pertains to the typical AGNs that are the sites of the majority of the growth of SMBHs today. Things may differ for the rare objects with the highest luminosities.

The radiative-mode AGNs are associated with populations of both lower-mass BHs and lower-mass (pseudo)bulges that have volume-averaged mass-doubling times (via accretion and star formation, respectively) of roughly the Hubble time. The volume-averaged ratio of star formation–to–BH growth in these central regions is of order a thousand (similar to the ratio of stellar mass and BH mass in current classical bulges and elliptical galaxies). These are evidently living systems that have not yet reached their evolutionary end point. Although there is indirect evidence that feedback is limiting the growth of the BH, there is little direct evidence of AGN-generated feedback for typical objects. In contrast, there is recent evidence that this may occur in the rare low-z AGNs having the highest luminosity ($L_{bol} \sim 10^{12-14} \, L_\odot$). The association of AGNs with central star formation implies that feedback from massive stars should be present, but its effect on the fueling of the AGN has not been well-quantified.

The second, jet-mode, AGN class is characterized by the production of collimated energetic outflows (jets), but it has little detected emitted radiation (characteristic luminosity below about 1% of the Eddington limit). Historically these have been called (low-excitation) radio galaxies. The more luminous LINERs are also likely to be members of this population. The AGN properties can be explained within the theoretical context of a radiatively inefficient accretion flow. The probability of a galaxy or BH producing a jet of a given radio luminosity is a steep function of mass: Typical radio galaxies are structurally normal massive ellipticals ($M_* \sim 10^{11}$ to $10^{12} \, M_\odot$) with BH masses greater than $10^8 \, M_\odot$. There is no evidence for substantial recent star formation in typical radio galaxies (although there can be for radio-AGNs in the BCGs of extreme cooling flow clusters). There is mostly indirect evidence that the AGN is fueled by the accretion of hot gas seen in X-ray observations. Feedback produced as the jets interact with this hot gas can be directly observed. Although it is energetically possible for this feedback to prevent the gas from cooling rapidly, the details remain uncertain. These AGNs are associated with the populations of both higher mass BHs and spheroids that have mass-doubling times that are orders of magnitude longer than the Hubble time. These are effectively dead systems in which the bulk of the star formation and BH growth occurred at high redshift.

In examining the situation at higher redshift, we have emphasized the importance of focusing on the representative population of AGNs that is responsible for the creation of the majority of the mass in relic SMBHs today. These are AGNs in the redshift range $z \sim 0.5$ to 2.5 and

having luminosities near the knee in the luminosity function. These representative AGNs appear to be hosted by moderately massive galaxies ($M_* > 10^{10} \, M_\odot$) with SFRs that are typical of the star-forming galaxies at that epoch (they are located on the star-forming main sequence). They are typically found in structurally normal galaxies rather than in highly disturbed systems (major mergers). The population of radio-loud AGNs remains prevalent among massive galaxies. Evidence for feedback in the form of powerful AGN-driven outflows is limited so far to objects of either exceptional luminosity or other unusual properties (very high radio luminosity or SFR).

All of this sounds similar to the situation in the contemporary Universe. The main differences are quantitative rather than qualitative: (*a*) The characteristic luminosities of the actively growing BHs are larger than the present day (by a factor of about 3 at $z \sim 0.5$ and ~ 30 at $z \sim 2$), and the characteristic masses of these BHs are also correspondingly larger, by factors that are model-dependent (e.g., Shankar et al. 2013); and (*b*) the sSFRs of host galaxies on the main sequence are higher than the current value by factors of ~ 3 at $z = 0.5$ and ~ 20 at $z = 2$ (e.g., Elbaz et al. 2011). Thus, to zeroth order, the situation at higher z seems like a scaled-up version of the contemporary Universe.

There is also (what we regard as) persuasive indirect evidence that the physical processes that link the formation and evolution of galaxies and BHs at high z are still at play today. As we noted in the introduction, the ratio of the rate of build-up of galaxies through star formation to the rate of the build-up of BHs via accretion has been broadly independent of cosmic time over at least the last ~ 10 Gyrs with a value of $\sim 1,500$ (Shankar et al. 2009, 2013; Hopkins & Beacom 2006). This is hard to understand unless the underlying physics has remained basically the same over this time (see Heckman et al. 2004 and Mullaney et al. 2012b for further discussion of this argument). Indeed, as **Figure 23** shows, this ratio applies not just to the total rates but over all values for the mass of the SMBH.
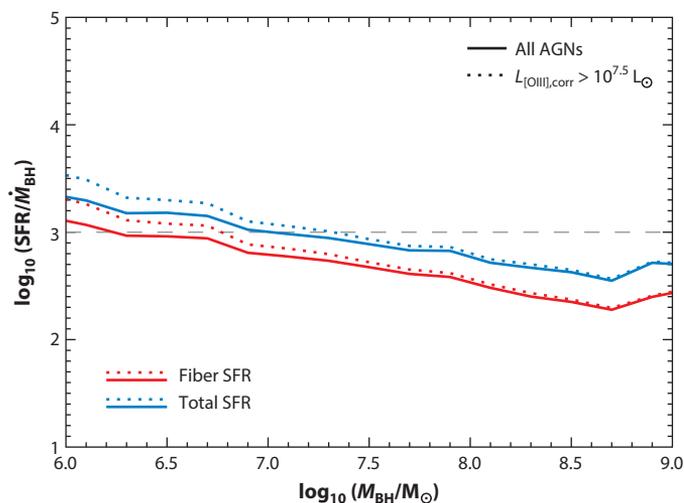

Figure 23

Ratio of the total star-formation rate (SFR) per unit volume in galaxies to the total accretion rate per unit volume onto black holes as traced by Type 2 AGNs plotted as a function of the black hole mass (see Heckman et al. 2004). The sample studied consists of all galaxies from the Sloan Digital Sky Survey main galaxy sample with stellar surface mass density above the characteristic value $\mu_* = 10^{8.5} \, M_\odot \, \mathrm{kpc}^{-2}$. Red lines show the result if the SFR is calculated within the fiber aperture for each galaxy and the blue lines show the result using estimates of the total SFR. Dotted lines show results restricted to the AGNs with (reddening-corrected and star-formation-corrected) $L_{\mathrm{[OIII]}} > 10^{7.5} \, L_\odot$. The horizontal dashed line shows the fiducial value of stellar to black hole mass in bulges and elliptical galaxies.

8.2. Implications and Some Speculation

Our current understanding of the formation and evolution of galaxies is that the build-up of the stellar content of galaxies via star formation is driven primarily by the accretion of gas from the cosmic web. At least since $z = 2$ or 3, the bulk of the star formation occurs in galaxies lying along a strongly evolving star-forming main sequence (a tight relationship between SFR and stellar mass). Although major mergers of gas-rich systems do occur and lead to strong bursts of star formation, they are responsible for only a minority (of order 10%) of the total cosmic star formation. This picture is predicted by numerical simulations and is consistent with observations of the evolving population of star-forming galaxies (e.g., Dekel et al. 2009, Bouche et al. 2010, Elbaz et al. 2011, Wuyts et al. 2011b, Whitaker et al. 2012, Lilly et al. 2013).

Empirically, the accretion-driven mass growth of the population of SMBHs is related to the growth (via star formation) of the inner region of the host galaxy. Evidently, both rates track the rate at which gas is accreted by the galaxy (with relative efficiencies that differ by about three orders of magnitude). Mergers are not the dominant mechanism by which gas flows to these inner regions and, hence, are not the dominant mechanism for growing the population of SMBHs. The gas flows responsible for this may instead be driven by rather slow secular processes in the contemporary Universe (e.g., Kormendy & Kennicutt 2004, Athanassoula 2008) or more violent and rapid instabilities in clumpy gas-rich disks at high z (e.g., Genzel et al. 2014, Bournaud et al. 2010, Elmegreen et al. 2008a, Dekel et al. 2009). This picture would imply that the representative population of actively growing SMBHs (AGNs) would live at the centers of disk-like structures (rather than ellipticals or classical bulges).

This simple picture leaves out one critical fact: We know from observations that the effect of this coevolution over cosmic time must ultimately place the relic (dead) BHs in dynamically hot structures (ellipticals and classical bulges) that contain little cold gas and, correspondingly, little star formation. In the classical picture for the coevolution of galaxies and BHs this is explained economically by positing that the SMBH grew in the aftermath of a major merger that created an elliptical/classical bulge and that feedback from the rapidly growing BH blew away the remaining gas (e.g., Hopkins et al. 2006, 2008, Di Matteo et al. 2008). How can this be explained in the more sedate scenario we are advocating? Let us try a two-part answer.

First, though low-mass bulges can be built through secular processes and disk instabilities (e.g., Athanassoula 2008, Bournaud et al. 2011, Hopkins et al. 2012), major mergers are the only way to build the population of massive classical bulges and elliptical galaxies. In this case, the sedate scenario would imply that these major mergers only modestly augment the masses of gas accreted by the BH and of gas turned into stars. The M_{BH} versus σ relationship would have to be essentially prebuilt before a major merger takes place (consistent with the recent simulations by Anglés-Alcázar et al. 2013). A major merger mostly rearranges the stars in the pre-existing disks (and their black-hole-containing pseudobulges) into a classical bulge or elliptical galaxy and a more massive (merged) BH. Subsequent dry merging between classical bulges or ellipticals can further populate the upper end of the M_{BH} versus σ relation (e.g., Kormendy & Ho 2013).

The second part of the answer requires an explanation for the dry-up of the reservoir of cold gas and the subsequent quenching of star formation. In current models, this shutdown in star formation in a typical massive galaxy is connected to the transition from an accretion mode in which gas reaches the galaxy in a cold form (gas temperature much less than the virial temperature) to a mode where the accreted gas is heated to roughly the virial temperature upon arrival and then slowly cools (via radiation) and is gradually accreted. This transition is predicted to occur when the galaxy halo mass grows via mergers and exceeds some critical value. Dekel et al. (2009) argue that this critical mass corresponds to the observed transition between the high-mass mostly

quiescent galaxy population and the lower-mass galaxy population that defines the star-forming main sequence (see also Bouche et al. 2010, Lilly et al. 2013, Mutch et al. 2013). Although current models still need to incorporate AGN feedback to quench star formation, it is possible that this is a result of the difficulty in incorporating the relevant physical processes with the necessary fidelity in current state-of-the-art numerical simulations. In this case, late feedback from AGNs might only be required to be strong enough to suppress the late cooling flows of hot gas and keep the quiescent galaxy suitably red and dead. This may be accomplished by the low-luminosity radio-AGNs, through the self-regulating feedback loop we have described in Section 6.2 above (the so-called maintenance mode of AGN feedback).

As we have emphasized, this sedate model is designed to match the detailed picture we have of the contemporary Universe and the emerging picture we have of the representative population of AGNs and their host galaxies at higher redshift. What about the more extreme cases? More specifically, one might ask about the physical mechanism(s) responsible for imposing a characteristic AGN luminosity at a given epoch [$L_*(z)$] above which the number density of AGNs steeply falls. In part this must reflect the knee in the BHMF. However, there is also evidence that the most powerful AGNs (at both high z and low z) are different from their less luminous kin. There are indications that the fraction of AGN host galaxies that are major mergers increases at the highest AGN luminosities (e.g., Liu et al. 2009, Mainieri et al. 2011, Treister et al. 2012). This is at least qualitatively consistent with the models presented by Hopkins & Hernquist (2009), Draper & Ballantyne (2012), Shankar et al. (2012), and Hopkins et al. (2013), which partition the amount of BH growth associated with mergers and secular processes. We have also seen that the most luminous AGNs at low and high redshift can drive powerful outflows that could affect the fueling of the BH and even the bulk properties of the gas in the host galaxy and its halo. It is tempting to speculate that the knee of the AGN luminosity function marks the transition from a sedate model of fueling by accretion and subsequent internal processes with weak/no AGN feedback to a dramatic model of fueling by mergers with strong AGN feedback.

In this review, we have stressed the importance of large surveys of the contemporary Universe in revealing the way in which galaxies and their SMBHs coevolve(d). We fully expect that the next generation of large ground- and space-based surveys will extend this type of robust and sophisticated understanding to the era when the bulk of the mass in galaxies and BHs was assembled.

DISCLOSURE STATEMENT

ACKNOWLEDGMENTS

LITERATURE CITED

Aalto S, Garcia-Burillo S, Muller S, et al. 2012. *Astron. Astrophys.* 537:A44
Aird J, Coil A, Moustakas J, et al. 2012. *Ap. J.* 749:90
Aird J, Coil A, Moustakas J, et al. 2013. *Ap. J.* 775:41

Alexander EM, Swinbank AM, Smail I, McDermid R, Nesvadba NPH. 2010. *MNRAS* 402:2211–20

Allen SW, Dunn RJH, Fabian AC, Taylor GB, Reynolds CS. 2006. *MNRAS* 372:21–30

Alonso MS, Lambas DG, Tissera P, Coldwell G. 2007. *MNRAS* 375:1017–24

Anderson SF, Voges W, Margon B, et al. 2003. *Astron. J.* 126:2209–29

Anglés-Alcázar D, Özel F, Davé R. 2013. *Ap. J.* 770:5

Antonucci R. 1993. *Annu. Rev. Astron. Astrophys.* 31:473–521

Antonucci R. 2012. *Astron. Astrophys. Trans.* 27:557–602

Aoki K, Oyabu S, Dunn JP, et al. 2011. *Publ. Astron. Soc. Jpn.* 63:457–67

Arav N, Borguet B, Chamberlain C, Edmonds D, Danforth C. 2013. *Ap. J.* Submitted. arXiv:1305.2181

Arav N, Moe M, Constantini E, et al. 2008. *Ap. J.* 681:954–64

Athanassoula E. 2005. *MNRAS* 358:1477–88

Athanassoula E. 2008. *MNRAS* 390:L69–72

Baade W, Minkowski R. 1954. *Ap. J.* 119:206–14

Bailey ME. 1980. *MNRAS* 191:195–206

Baldry IK, Glazebrook K, Brinkmann J, et al. 2004. *Ap. J.* 600:681–94

Baldwin JA, Phillips MM, Terlevich R. 1981. *Publ. Astron. Soc. Pac.* 93:5–19

Balick B, Heckman TM. 1982. *Annu. Rev. Astron. Astrophys.* 20:431–68

Balogh ML, Morris SL, Yee HKC, Carlberg R, Ellingson E. 1999. *MNRAS* 307:463–79

Barthel PD, Arnaud KA. 1996. *MNRAS* 283:L45

Baumgartner WH, Tueller J, Markwardt CB, et al. 2013. *Ap. J. Suppl.* 207:19

Bautista MA, Dunn JP, Arav N, et al. 2010. *Ap. J.* 713:25–31

Becker RH, White RL, Helfand DJ. 1995. *Ap. J.* 450:559–77

Bell AR. 1978. *MNRAS* 182:443–55

Bell EF, de Jong RS. 2001. *Ap. J.* 550:212–29

Bell EF, McIntosh DH, Katz N, Weinberg MD. 2003. *Ap. J. Lett.* 585:L117–20

Bentz MC, Denney KD, Grier CJ, et al. 2013. *Ap. J.* 767:149

Best PN. 2009. *Astron. Nachr.* 330:184–89

Best PN. 2004. *MNRAS* 351:70–82

Best PN, Heckman TM. 2012. *MNRAS* 421:1569–82

Best PN, Kaiser CR, Heckman TM, Kauffmann G. 2006. *MNRAS* 368:L67–71

Best PN, Kauffmann G, Heckman TM, Ivezić Ž. 2005a. *MNRAS* 362:9–24

Best PN, Kauffmann G, Heckman TM, et al. 2005b. *MNRAS* 362:25–40

Best PN, von der Linden A, Kauffmann G, Heckman TM, Kaiser CR. 2007. *MNRAS* 379:894–908

Bîrzan L, McNamara BR, Nulsen PEJ, Carilli CL, Wise MW. 2008. *Ap. J.* 686:859–90

Bîrzan L, Rafferty DA, McNamara BR, Wise MW, Nulsen PEJ. 2004. *Ap. J.* 607:800–9

Blandford RD, Payne DG. 1982. *MNRAS* 199:883–903

Blandford RD, Znajek RL. 1977. *MNRAS* 179:433–56

Blanton MR, Hogg DW, Bahcall NA, et al. 2003. *Ap. J.* 594:186–207

Blundell KM, Rawlings S. 2000. *Astron. J.* 119:1111–22

Bock DC-J, Large MI, Sadler EM. 1999. *Astron. J.* 117:1578–93

Bohm A, Wisotzki L, Bell EF, et al. 2013. *Astron. Astrophys.* 549:A46

Böhringer H, Voges W, Fabian AC, Edge AC, Neumann DM. 1993. *MNRAS* 264:L25–28

Bondi H. 1952. *MNRAS* 112:195–204

Borguet B, Arav N, Edmonds D, Chamberlain C, Benn C. 2013. *Ap. J.* 762:49

Borguet B, Edmonds D, Arav N, Dunn J, Kriss GA. 2012. *Ap. J.* 751:107

Borthakur S, Heckman T, Strickland D, Wild V, Schiminovich D. 2013. *Ap. J.* 768:18

Bouche N, Dekel A, Genzel R, et al. 2010. *Ap. J.* 718:1001–18

Bournaud F, Dekel A, Teyssier R, et al. 2011. *Ap. J. Lett.* 741:L33

Bournaud F, Elmegreen BG, Teyssier R, Block DL, Puerari I. 2010. *MNRAS* 408:1088–99

Bournaud F, Juneau S, Le Floc'h E, et al. 2012. *Ap. J.* 757:81

Bower RG, Benson AJ, Malbon R, et al. 2006. *MNRAS* 370:645–55

Brandt WN, Hasinger G. 2005. *Annu. Rev. Astron. Astrophys.* 43:827–59

Brinchmann J, Charlot S, White S, et al. 2004. *MNRAS* 351:1151–79

Brown TM, Ferguson HC, Stanford SA, Deharveng JM. 1998. *Ap. J.* 504:113–38

Brown TM, Smith E, Ferguson H, et al. 2008. *Ap. J.* 682:319–35

Bruzual AG. 1983. *Ap. J.* 273:105–27

Bruzual G, Charlot S. 2003. *MNRAS* 344:1000–28

Buchanan C, Gallimore JF, O'Dea CP, et al. 2006. *Astron. J.* 132:401–19

Burbidge EM, Burbidge GR, Prendergast KH. 1959. *Ap. J.* 130:26–45

Burns JO. 1990. *Astron. J.* 99:14–30

Cao X. 2010. *Ap. J.* 725:388–93

Cao X, Rawlings S. 2004. *MNRAS* 349:1419–27

Capetti A, Baldi RD. 2011. *Astron. Astrophys.* 529:A126

Cattaneo A, Best PN. 2009. *MNRAS* 395:518–23

Cattaneo A, Faber SM, Binney J, et al. 2009. *Nature* 460:213–19

Cavagnolo KW, Donahue M, Voit GM, Sun M. 2008. *Ap. J. Lett.* 683:L107–10

Cavagnolo KW, McNamara BR, Nulsen PEJ, et al. 2010. *Ap. J.* 720:1066–72

Chen CT, Hickox RC, Alberts S, et al. 2013a. *Ap. J.* 773:3

Chen Y-M, Kauffmann G, Heckman TM, et al. 2013b. *MNRAS* 429:2643–54

Chen Y-M, Tremonti CA, Heckman TM, et al. 2010. *Astron. J.* 140:445–61

Chevalier RA, Clegg AW. 1985. *Nature* 317:44–45

Churazov E, Brüggen M, Kaiser CR, Böhringer H, Forman W. 2001. *Ap. J.* 554:261–73

Churazov E, Sazonov S, Sunyaev R, et al. 2005. *MNRAS* 363:L91–95

Cicone C, Feruglio C, Maiolino R, et al. 2012. *Astron. Astrophys.* 543:A99

Cicone C, Maiolino R, Sturm E, et al. 2014. *Astron. Astrophys.* 562:A21

Cid Fernandes R, González Delgado RM, Schmitt H, et al. 2004a. *Ap. J.* 605:105–26

Cid Fernandes R, Gu Q, Melnick J, et al. 2004b. *MNRAS* 355:273–96

Cid Fernandes R, Heckman T, Schmitt H, et al. 2001. *Ap. J.* 558:81–108

Cid Fernandes R, Mateus A, Sodre L, Stasinska G, Gomes JM. 2005. *MNRAS* 358:363–78

Cid Fernandes R, Stasińska G, Mateus A, Vale Asari N. 2011. *MNRAS* 413:1687–99

Ciotti L, Ostriker JP. 1997. *Ap. J. Lett.* 487:L105–8

Ciotti L, Ostriker JP, Proga D. 2010. *Ap. J.* 717:707–23

Cisternas M, Gadotti DA, Knapen JH, et al. 2013. *Ap. J.* 776:50

Cisternas M, Jahnke K, Inskip KJ, et al. 2011. *Ap. J.* 726:57

Colless M, Dalton G, Maddox S, et al. 2001. *MNRAS* 328:1039–63

Condon JJ. 1989. *Ap. J.* 338:13–23

Condon JJ. 1992. *Annu. Rev. Astron. Astrophys.* 30:575–611

Condon JJ, Cotton WD, Greisen EW, et al. 1998. *Astron. J.* 115:1693–716

Conselice CJ, Bershady MA, Jangren A. 2000. *Ap. J.* 529:886–910

Cooray A, Sheth R. 2002. *Phys. Rep.* 372:1–129

Crenshaw DN, Kraemer SB, George IM. 2003. *Annu. Rev. Astron. Astrophys.* 41:117–67

Croft S, de Vries W, Becker RH. 2007. *Ap. J. Lett.* 667:L13–16

Croom SM, Boyle BJ, Shanks T, et al. 2005. *MNRAS* 356:415–38

Croom SM, Richards GT, Shanks T, et al. 2009. *MNRAS* 399:1755–72

Croston JH, Hardcastle MJ, Birkinshaw M. 2005. *MNRAS* 357:279–94

Croton DJ, Springel V, White S, et al. 2006. *MNRAS* 365:11–28

Daly RA, Sprinkle TB, O'Dea CP, Kharb P, Baum SA. 2012. *MNRAS* 423:2498–2502

David LP, Durisen RH, Cohn HN. 1987. *Ap. J.* 316:505–16

David LP, Nulsen PEJ, McNamara BR, et al. 2001. *Ap. J.* 557:546–59

Davies RI, Müller Sánchez F, Genzel R, et al. 2007. *Ap. J.* 671:1388–412

de Vries WH, Becker RH, White RL. 2006. *Astron. J.* 131:666–79

Dekel A, Sari R, Ceverino D. 2009. *Ap. J.* 703:785–801

Diamond-Stanic AM, Rieke GH. 2012. *Ap. J.* 746:168

Diamond-Stanic AM, Rieke GH, Rigby JR. 2009. *Ap. J.* 699:623–31

Di Matteo T, Colberg J, Springel V, Hernquist L, Sijacki D. 2008. *Ap. J.* 636:33–53

Di Matteo T, Springel V, Hernquist L. 2005. *Nature* 433:604–7

Dong R, Greene JE, Ho LC. 2012. *Ap. J.* 761:73

Donley JL, Rieke GH, Perez-Gonzalez PG, Barro G. 2008. *Ap. J.* 687:111–32

Donoso E, Best PN, Kauffmann G. 2009. *MNRAS* 392:617–29

Donoso E, Li C, Kauffmann G, Best PN, Heckman TM. 2010. *MNRAS* 407:1078–89

Donoso E, Yan L, Tsai C, et al. 2012. *Ap. J.* 748:80

Draper AR, Ballantyne DR. 2012. *Ap. J.* 751:72

Dressler A, Gunn JE. 1983. *Ap. J.* 270:7–19

Dunlop JS, Peacock JA. 1990. *MNRAS* 247:19–42

Dunn JP, Bautista M, Arav N, et al. 2010. *Ap. J.* 709:611–31

Dunn RJH, Fabian AC. 2006. *MNRAS* 373:959–71

Dunn RJH, Fabian AC, Taylor GB. 2005. *MNRAS* 364:1343–53

Edmonds D, Borguet B, Arav N, et al. 2011. *Ap. J.* 739:7

Elbaz D, Dickinson M, Hwang HS, et al. 2011. *Astron. Astrophys.* 533:A119

Ellison SL, Patton DR, Mendel JT, Scudder JM. 2011. *MNRAS* 418:2043–53

Elmegreen BG, Bournaud F, Elmegreen DM. 2008a. *Ap. J.* 688:67–77

Elmegreen BG, Bournaud F, Elmegreen DM. 2008b. *Ap. J.* 684:829–34

Fabello S, Kauffmann G, Catinella B, et al. 2011. *MNRAS* 416:1739–44

Fabian AC. 1994. *Annu. Rev. Astron. Astrophys.* 32:277–318

Fabian AC. 2012. *Annu. Rev. Astron. Astrophys.* 50:455–89

Fabian AC, Reynolds CS, Taylor GB, Dunn RJH. 2005. *MNRAS* 363:891–96

Fabian AC, Sanders JS, Allen SW, Crawford CS, Iwasawa K, et al. 2003. *MNRAS* 344:L43–47

Fabian AC, Sanders JS, Taylor GB, Allen SW, Crawford CS, et al. 2006. *MNRAS* 366:417–28

Falcke H, Körding E, Markoff S. 2004. *Astron. Astrophys.* 414:895–903

Fanaroff BL, Riley JM. 1974. *MNRAS* 167:P31

Fardal MA, Katz N, Weinberg DH, Davé R. 2007. *MNRAS* 379:985–1002

Fender RP, Belloni TM, Gallo E. 2004. *MNRAS* 355:1105–18

Ferrarese L, Ford H. 2005. *Space Sci. Rev.* 116:523–624

Ferrarese L, Merritt D. 2000. *Ap. J. Lett.* 539:L9–12

Feruglio C, Maiolino R, Piconcelli E, et al. 2010. *Astron. Astrophys.* 518:L155

Filippenko A, Ho L, Sargent W. 1993. *Ap. J. Lett.* 410:L75–78

Fiore F, Puccetti S, Grazian A, et al. 2012. *Astron. Astrophys.* 537:A16

Fischer J, Sturm E, González-Alfonso E, et al. 2010. *Astron. Astrophys.* 518:L41

Fisher DB, Drory N. 2011. *Ap. J. Lett.* 733:L47

Forman W, Jones C, Churazov E, et al. 2007. *Ap. J.* 665:1057–66

Gabor JM, Impey CD, Jahnke K. 2009. *Ap. J.* 691:705–22

Gadotti DA. 2009. *MNRAS* 393:1531–52

Gallo E, Fender RP, Pooley GG. 2003. *MNRAS* 344:60–72

Gandhi P, Horst H, Smette A, Honig S, Comastri A. 2009. *Astron. Astrophys.* 502:457–72

Gaspari M, Ruszkowski M, Oh SP. 2013. *MNRAS* 432:3401–22

Gebhardt K, Bender R, Bower G, et al. 2000. *Ap. J. Lett.* 539:L13–16

Gelbord JM. 2003. *Probing circumnuclear material in Seyfert galaxies with X-ray spectroscopy*. PhD Thesis, Johns Hopkins Univ.

Gendre MA, Best PN, Wall JV. 2010. *MNRAS* 404:1719–32

Gendre MA, Best PN, Wall JV, Ker LM. 2013. *MNRAS* 430:3086–101

Genzel R, Förster Schreiber NM, Lang P, et al. 2014. *Ap. J.* 785:75

Giacconi R, Gursky H, Paolini F. 1962. *Phys. Rev. Lett.* 9:439–43

Gisler GR. 1978. *MNRAS* 183:633–43

González-Alfonso E, Fischer J, Graciá-Carpio J, et al. 2014. *Astron. Astrophys.* 561:A27

González Delgado RM, Cid Fernandes R, Pérez E, et al. 2004. *Ap. J.* 606:127–43

González Delgado RM, Pérez E, Cid Fernandes R, Schmitt H. 2008. *Astron. J.* 135:747–65

Goto T. 2006. *MNRAS* 369:1765–72

Goulding AD, Alexander DM. 2009. *MNRAS* 398:1165–93

Graham AW, Driver SP, Allen PD, Liske J. 2007. *MNRAS* 387:198–210

Graham AW, Scott N. 2013. *Ap. J.* 764:151

Greene JE, Ho LC. 2007a. *Ap. J.* 670:92–104

Greene JE, Ho LC. 2007b. *Ap. J.* 667:131–48

Greene JE, Zakamska NL, Liu X, et al. 2009. *Ap. J.* 702:441–59

Greene JE, Zakamska N, Ho LC, Barth AJ. 2011. *Ap. J.* 732:9

Grier CJ, Martini P, Watson LC, et al. 2013. *Ap. J.* 773:90

Grimes JP, Heckman T, Stickland D, Ptak A. 2005. *Ap. J.* 628:187–204

Gürkan G, Hardcastle MJ, Jarvis MJ. 2014. *MNRAS* 438:1149–61

Haines CP, Pereira MJ, Sanderson AJR, et al. 2012. *Ap. J.* 754:97

Hainline KN, Hickox R, Greene JE, Myers AD, Zakamska NL. 2013. *Ap. J.* 774:145

Hao L, Strauss MA, Fan X, et al. 2005a. *Astron. J.* 129:1795–808

Hao L, Strauss MA, Tremonti CA, et al. 2005b. *Astron. J.* 129:1783–94

Hardcastle MJ, Evans DA, Croston JH. 2007. *MNRAS* 376:1849–56

Haring N, Rix HW. 2004. *Ap. J. Lett.* 604:L89–92

Harrison CM, Alexander DM, Mullaney JR, et al. 2012a. *Ap. J. Lett.* 760:L15

Harrison CM, Alexander DM, Swinbank AM, et al. 2012b. *MNRAS* 426:1073–96

Hasinger G, Miyaji T, Schmidt M. 2005. *Astron. Astrophys.* 441:417–34

Heckman TM. 1980. *Astron. Astrophys.* 87:152–64

Heckman TM, Armus, L, Miley GK. 1990. *Ap. J. Suppl.* 74:833–68

Heckman TM, Balick B, Sullivan WT III. 1978. *Ap. J.* 224:745–60

Heckman TM, Blitz L, Wilson AS, Armus L, Miley GK. 1989. *Ap. J.* 342:735–58

Heckman TM, Kauffmann G, Brinchmann J, et al. 2004. *Ap. J.* 613:109–18

Heckman TM, Ptak A, Hornschemeier A, Kauffmann G. 2005. *Ap. J.* 634:161–68

Heywood I, Blundell KM, Rawlings S. 2007. *MNRAS* 381:1093–102

Hickox RC, Jones C, Forman W, et al. 2009. *Ap. J.* 696:891–919

Hicks EKS, Davies RI, Maciejewski W, et al. 2013. *Ap. J.* 768:107

Hillel S, Soker N. 2013. *MNRAS* 430:1970–75

Hine RG, Longair MS. 1979. *MNRAS* 188:111–30

Hlavacek-Larrondo J, Fabian AC. 2011. *MNRAS* 413:313–21

Ho LC. 2005. *Ap. Space Sci.* 300:219–25

Ho LC. 2008. *Annu. Rev. Astron. Astrophys.* 46:475–539

Ho LC, Darling J, Greene JE. 2008. *Ap. J.* 681:128–40

Hopkins AM, Beacom JF. 2006. *Ap. J.* 651:142–54

Hopkins PF, Hernquist L. 2009. *Ap. J.* 694:599–609

Hopkins PF, Hernquist L, Cox TJ, et al. 2006. *Ap. J. Suppl.* 163:1–49

Hopkins PF, Hernquist L, Cox TJ, Keres D. 2008. *Ap. J. Suppl.* 175:356–89

Hopkins PF, Hernquist L, Cox TJ, Robertson B, Krause E. 2007a. *Ap. J.* 669:45–66

Hopkins PF, Keres D, Murray N, Quataert E, Hernquist L. 2012. *MNRAS* 427:968–78

Hopkins PF, Kocevski DD, Bundy K. 2013. *Ap. J.* In press. arXiv:1309.6321

Hopkins PF, Quataert E. 2011. *MNRAS* 415:1027–50

Hopkins PF, Richards GT, Hernquist L. 2007b. *Ap. J.* 654:731–53

Hu EM, Cowie LL, Wang Z. 1985. *Ap. J. Suppl.* 59:447–98

Hubble EP. 1925. *Popul. Astron.* 33:252–55

Hwang HS, Park C, Elbaz D, Choi Y-Y. 2012. *Astron. Astrophys.* 538:A15

Ibar E, Cirasuolo M, Ivison RJ, et al. 2008. *MNRAS* 386:953–62

Ishibashi W, Fabian AC. 2012. *MNRAS* 427:2998–3005

Ivezić Ž, Menou K, Knapp GR, et al. 2002. *Astron. J.* 124:2364–400

Janssen RMJ, Röttgering HJA, Best PN, Brinchmann J. 2012. *Astron. Astrophys.* 541:A62

Jiang YF, Greene JE, Ho LC, Xiao T, Barth AJ. 2011. *Ap. J.* 742:68

Juneau S, Dickinson M, Bournaud F, et al. 2013. *Ap. J.* 764:176

Karim A, Schinnerer E, Martínez-Sansigre A, et al. 2011. *Ap. J.* 730:61

Kaspi S, Smith PS, Netzer H, et al. 2000. *Ap. J.* 533:631–49

Kauffmann G, Haehnelt M. 2000. *MNRAS* 311:576–88

Kauffmann G, Heckman TM. 2009. *MNRAS* 397:135–47

Kauffmann G, Heckman TM, Best PN. 2008. *MNRAS* 384:953–71

Kauffmann G, Heckman TM, Budavari T, et al. 2007. *Ap. J. Suppl.* 173:357–76

Kauffmann G, Heckman TM, Tremonti C, et al. 2003a. *MNRAS* 346:1055–77

Kauffmann G, Heckman TM, White SDM, et al. 2003b. *MNRAS* 341:54–69

Kauffmann G, White SDM, Heckman TM, et al. 2004. *MNRAS* 353:713

Kelly BC, Merloni A. 2012. *Adv. Astron.* 2012:7–34

Kelly BC, Shen Y. 2013. *Ap. J.* 764:45

Kerr R. 1963. *Phys. Rev. Lett.* 11:237–38

Kewley LJ, Dopita MA, Sutherland RS, Heisler CA, Trevena J. 2001. *Ap. J.* 556:121–40

Kewley LJ, Groves B, Kauffmann G, Heckman T. 2006. *MNRAS* 372:961–76

Kocevski DD, Faber SM, Mozena M, et al. 2012. *Ap. J.* 744:148

Kollmeier JA, Onken CA, Kochanek CS, et al. 2006. *Ap. J.* 648:128–39

Korista KT, Bautista MA, Arav N, et al. 2008. *Ap. J.* 688:108–15

Kormendy J, Ho LC. 2013. *Annu. Rev. Astron. Astrophys.* 51:511–653

Kormendy J, Kennicutt RC. 2004. *Annu. Rev. Astron. Astrophys.* 42:603–83

Koss M, Mushotzky R, Treister E, et al. 2012. *Ap. J. Lett.* 746:L22

Koss M, Mushotzky R, Veilluex S, et al. 2011. *Ap. J.* 739:57

Koss M, Mushotzky R, Veilleux S, Winter L. 2010. *Ap. J.* 716:L125–30

Krolik J. 1999. *Active Galactic Nuclei.* Princeton, NJ: Princeton Univ. Press

Krug HB, Rupke DSN, Veilleux S. 2010. *Ap. J.* 708:1145–61

Lackner CN, Gunn JE. 2012. *MNRAS* 421:2277–302

Lacy M, Storrie-Lombardi LJ, Sajina A, et al. 2004. *Ap. J. Suppl.* 154:166–69

Lagos CDP, Lacey CG, Baugh CM, Bower R, Benson A. 2011. *MNRAS* 416:1566–84

Laing RA, Jenkins CR, Wall JV, Unger SW. 1994. In *Spectrophotometry of a Complete Sample of 3CR Radio Sources: Implications for Unified Models*, ed. GV Bicknell, MA Dopita, PJ Quinn. *ASP Conf. Ser.* 54:201–8. San Francisco: ASP

LaMassa S, Heckman TM, Ptak A, Urry CM. 2013. *Ap. J. Lett.* 765:L33

LaMassa S, Heckman TM, Ptak A, et al. 2010. *Ap. J.* 720:786–810

LaMassa S, Heckman TM, Ptak A, et al. 2012. *Ap. J.* 758:1

Larson RB. 2010. *Nat. Phys.* 6:96–98

Larson RB, Tinsley BM. 1978. *Ap. J.* 219:46–59

Lauer T, Faber SM, Gebhardt K, et al. 2005. *Astron. J.* 129:2138–85

Lee G-H, Woo J-H, Lee MG, et al. 2012. *Ap. J.* 750:141

Leitherer C, Schaerer D, Goldader J, et al. 1999. *Ap. J. Suppl.* 123:3–40

Li C, Kauffmann G, Heckman TM, White SDM, Jing YP. 2008a. *MNRAS* 385:1903–14

Li C, Kauffmann G, Heckman TM, White SDM, Jing YP. 2008b. *MNRAS* 385:1915–22

Li C, Kauffmann G, Wang L, et al. 2006. *MNRAS* 373:457–68

Lilly SJ, Carollo CM, Pipino A, Renzini A, Peng Y. 2013. *Ap. J.* 772:119

Lin Y-T, Shen Y, Strauss MA, Richards GT, Lunnan R. 2010. *Ap. J.* 723:1119–38

Lintott C, Schawinski K, Bamford S, et al. 2011. *MNRAS* 410:166–78

Liu G, Zakamska NL, Greene JE, Nesvadba NPH, Liu X. 2013a. *MNRAS* 430:2327–45

Liu G, Zakamska NL, Greene JE, Nesvadba NPH, Liu X. 2013b. *MNRAS* 436:2576–97

Liu X, Shen Y, Strauss M. 2012. *Ap. J.* 745:94

Liu X, Zakamska NL, Greene JE, et al. 2009. *Ap. J.* 702:1098–117

Longair MS. 1966. *MNRAS* 133:421–36

Longair MS, Seldner M. 1979. *MNRAS* 189:433–53

Lupton RH, Ivezić Z, Gunn JE, et al. 2002. In *Survey and Other Telescope Technologies and Discoveries*, ed. JA Tyson, S Wolff. *Proc. SPIE Conf. Ser.* 4836:350–56. Bellingham, WA: SPIE

Maccarone TJ. 2003. *Astron. Astrophys.* 409:697–706

Machalski J, Condon JJ. 1999. *Ap. J. Suppl.* 123:41–78

Machalski J, Godlowski W. 2000. *Astron. Astrophys.* 360:463–71

Madau P, Dickinson M. 2014. *Annu. Rev. Astron. Astrophys.* 52:415–86

Magliocchetti M, Brüggen M. 2007. *MNRAS* 379:260–74

Magliocchetti M, Maddox SJ, Lahav O, Wall JV. 1998. *MNRAS* 300:257–68

Mahadevan R. 1997. *Ap. J.* 477:585–601

Mainieri V, Bongiorno, Merloni A, et al. 2011. *Astron. Astrophys.* 535:A80

Maiolino R, Gallerani S, Neri R, et al. 2012. *MNRAS* 425:L66–70

Maiolino R, Ruiz M, Rieke GH, Papadopoulos P. 1997. *Ap. J.* 485:552–69

Malkan M, Gorjian V, Tam R. 1998. *Ap. J. Suppl.* 117:25–88

Mandelbaum R, Li C, Kauffmann G, White SDM. 2009. *MNRAS* 393:377–92

Mannering EJA, Worrall DM, Birkinshaw M. 2011. *MNRAS* 416:2869–81

Marconi A, Hunt LK. 2003. *Ap. J. Lett.* 589:L21–24

Marconi A, Risaliti G, Gilli R, et al. 2004. *MNRAS* 351:169–85

Martin DC, Fanson J, Schiminovich D, et al. 2005. *Ap. J. Lett.* 619:L1–6

Martínez-Sansigre A, Rawlings S. 2011. *MNRAS* 414:1937–64

Martini P, Dicken D, Storchi-Bergmann T. 2013. *Ap. J.* 766:121

Martini P, Kelson DD, Kim E, Mulchaey JS, Athey AA. 2006. *Ap. J.* 644:116–32

Mauch T, Sadler EM. 2007. *MNRAS* 375:931–50

McConnell NJ, Ma CP. 2013. *Ap. J.* 764:184

McLure RJ, Dunlop JS. 2002. *MNRAS* 331:795–804

McMahon RG, White RL, Helfand DJ, Becker RH. 2002. *Ap. J. Suppl.* 143:1–23

McNamara BR, Nulsen PEJ. 2007. *Annu. Rev. Astron. Astrophys.* 45:117–75

McNamara BR, Rohanizadegan M, Nulsen PEJ. 2011. *Ap. J.* 727:39

Meier DL. 1999. *Ap. J.* 522:753–66

Meier DL. 2001. *Ap. J. Lett.* 548:L9–12

Merloni A, Heinz S. 2007. *MNRAS* 381:589–601

Merloni A, Heinz S. 2008. *MNRAS* 388:1011–30

Merloni A, Heinz S, Di Matteo T. 2003. *MNRAS* 345:1057–76

Miley G. 1980. *Annu. Rev. Astron. Astrophys.* 18:165–218

Miley GK, Neugebauer G, Soifer BT. 1985. *Ap. J. Lett.* 293:L11–14

Miller CJ, Nichol RC, Gómez PL, Hopkins AM, Bernardi M. 2003. *Ap. J.* 597:142–56

Miller JM, Raymond J, Reynolds CS, et al. 2008. *Ap. J.* 680:1359–77

Mirabel IF, Wilson AS. 1984. *Ap. J.* 277:92–105

Moe M, Arav N, Bautista MA, Korista KT. 2009. *Ap. J.* 706:525–34

Mullaney JR, Daddi E, Béthermin M, et al. 2012a. *Ap. J. Lett.* 753:L30

Mullaney JR, Pannella M, Daddi E, et al. 2012b. *MNRAS* 419:95–115

Murphy KD, Yaqoob T. 2009. *Ap. J.* 701:635–41

Murray N, Menard B, Thompson TA. 2011. *Ap. J.* 735:66

Mutch SJ, Croton DJ, Poole GB. 2013. *MNRAS* 435:2445–59

Nagar NM, Falcke H, Wilson AS. 2005. *Ap. J.* 435:521–43

Narayan R. 2002. In *Lighthouses of the Universe*, ed. M Gilfanov, R Sunyaev, E Churazov, pp. 405–29. Berlin/Heidelberg: Springer-Verlag

Narayan R. 2005. *Astrophys. Space Sci.* 300:177–88

Narayan R, Yi I. 1994. *Ap. J. Lett.* 428:L13–16

Narayan R, Yi I. 1995. *Ap. J.* 444:710–35

Neilsen J, Lee JC. 2009. *Nature* 458:481–84

Nemmen RS, Bower RG, Babul A, Storchi-Bergmann T. 2007. *MNRAS* 377:1652–62

Nesvadba NPH, Lehnert MD, De Breuck C, Gilbert AM, van Breugel W. 2008. *Astron. Astrophys.* 491:407–24

Nesvadba NPH, Lehnert MD, Eisenhauer F, et al. 2006. *Ap. J.* 650:661–68

Netzer H. 2009. *MNRAS* 399:1907–20

Netzer H. 2013. *The Physics and Evolution of Active Galactic Nuclei*. Cambridge, UK: Cambridge Univ. Press

Netzer H, Mainieri V, Rosati P, Trakhtenbrot B. 2006. *Astron. Astrophys.* 453:525–33

Norman CA, Scoville NZ. 1988. *Ap. J.* 332:124–34

Nulsen PEJ, Jones C, Forman WR, et al. 2007. In *ESO Astrophys. Symp.*, ed. H Böhringer, GW Pratt, A Finoguenov, P Schuecker, pp. 210–15. Berlin/Heidelberg: Springer-Verlag

Nusser A, Silk J, Babul A. 2006. *MNRAS* 373:739–46

O'Dea CP, Baum SA, Privon G, et al. 2008. *Ap. J.* 681:1035–45

O'Dea CP, Daly RA, Kharb P, Freeman KA, Baum SA. 2009. *Astron. Astrophys.* 494:471–88

Osterbrock DE, Ferland G. 2005. *Astrophysics of Gaseous Nebulae and Active Galactic Nuclei*. Mill Valley, CA: Univ. Sci. Books

Padovani P, Miller N, Kellermann KI, et al. 2011. *Ap. J.* 740:20

Panter B, Heavens AF, Jimenez R. 2003. *MNRAS* 343:1145–54

Panter B, Jimenez R, Heavens AF, Charlot S. 2007. *MNRAS* 378:1550–64

Pasquali A, Kauffmann G, Heckman TM. 2005. *MNRAS* 361:1121–30

Peterson BM. 1997. *An Introduction to Active Galactic Nuclei*. Cambridge, UK: Cambridge Univ. Press

Peterson BM. 2013. *Space Sci. Rev.* In press. doi: 10.1007/s11214-013-9987-4

Peterson JR, Bleeker JAM, Ferrigno C, et al. 2001. *Astron. Astrophys.* 365:L104–9

Peterson JR, Kahn SM, Paerels FBS, et al. 2003. *Ap. J.* 590:207–24

Pettini M, Pagel BEJ. 2004. *MNRAS* 348:L59–63

Pierce CM, Lotz JM, Laird ES, et al. 2007. *Ap. J. Lett.* 660:L19–22

Pizzolato F, Soker N. 2010. *MNRAS* 408:961–74

Ponti G, Fender RP, Begelman MC, et al. 2012. *MNRAS* 422:L11–15

Porciani C, Magliocchetti M, Norberg P. 2004. *MNRAS* 355:1010–30

Punsly B, Coroniti FV. 1990. *Ap. J.* 350:518–35

Qiao E, Liu BF. 2009. *Publ. Astron. Soc. Jpn.* 61:403–10

Quataert E. 2001. In *Probing the Physics of Active Galactic Nuclei by Multiwavelength Monitoring*, ed. BM Peterson, RW Pogge, RS Polidan. *ASP Conf. Ser.* 224:71–85. San Francisco: ASP

Rafferty DA, McNamara BR, Nulsen PEJ, Wise MW. 2006. *Ap. J.* 652:216–31

Rawlings S, Saunders R. 1991. *Nature* 349:138–40

Reichard TA, Heckman TM, Rudnick G, et al. 2009. *Ap. J.* 691:1005–20

Remillard RA, McClintock JE. 2006. *Annu. Rev. Astron. Astrophys.* 44:49–92

Rengelink RB, Tang Y, de Bruyn AG, et al. 1997. *Astron. Astrophys. Suppl.* 124:259–80

Reviglio P, Hefland DJ. 2006. *Ap. J.* 650:717–26

Richards G, Fan X, Newberg H, et al. 2002. *Astron. J.* 123:2945–75

Richards G, Lacy M, Storrie-Lombardi LJ, et al. 2006. *Ap. J. Suppl.* 166:470–97

Rigby EE, Best PN, Brookes MH, et al. 2011. *MNRAS* 416:1900–15

Rigby JR, Diamond-Stanic AM, Aniano G. 2009. *Ap. J.* 700:1878–83

Rosario DJ, Santini P, Lutz D, et al. 2012. *Astron. Astrophys.* 545:A45

Rosario DJ, Shields GS, Taylor GB, Salviander S, Smith KL. 2010a. *Ap. J.* 716:131–43

Rosario DJ, Trakhtenbrot B, Lutz D, et al. 2013. *Astron. Astrophys.* 560:A72

Rosario DJ, Whittle M, Nelson CH, Wilson AS. 2010b. *Ap. J. Lett.* 711:L94–98

Rosenfield P, Johnson LC, Girardi L, et al. 2012. *Ap. J.* 755:131

Ross NP, Shen Y, Strauss MA, et al. 2009. *Ap. J.* 697:1634–55

Roy AL, Norris RP, Kesteven MJ, Troup ER, Reynolds JE. 1998. *MNRAS* 301:1019–30

Rupke M, Veilleux S. 2011. *Ap. J. Lett.* 729:L27

Russell DM, Gallo E, Fender RP. 2013a. *MNRAS* 431:405–14

Russell HR, McNamara BR, Edge AC, et al. 2013b. *MNRAS* 430:530–53

Sabater J, Best PN, Argudo-Fernández M. 2013. *MNRAS* 430:638–51

Sadler EM, Cannon RD, Mauch T, et al. 2007. *MNRAS* 381:211–27

Sadler EM, Ekers RD, Mahony E, Mauch T, Murphy T. 2014. *MNRAS* 438:790–824

Sadler EM, Jackson CA, Canoon RD, et al. 2002. *MNRAS* 329:227–45

Sadler EM, Jenkins CR, Kotanyi CG. 1989. *MNRAS* 240:591–635

Sadler EM, McIntyre VJ, Jackson CA, Cannon RD. 1999. *Publ. Astron. Soc. Aust.* 16:247–56

Saintonge A, Kauffmann G, Cramer C, et al. 2011. *MNRAS* 415:32–60

Saintonge A, Tacconi LJ, Fabello S, et al. 2012. *Ap. J.* 758:73

Salim S, Charlot S, Rich RM, et al. 2005. *Ap. J. Lett.* 619:L39–42

Sandage A. 1965. *Ap. J.* 141:1560–80

Sanders DB, Soifer BT, Elias JH, Neugebauer G, Matthews K. 1988a. *Ap. J. Lett.* 328:L35–39

Sanders DB, Soifer BT, Elias JH, et al. 1988b. *Ap. J.* 325:74–91

Santini P, Rosario DJ, Shao L, et al. 2012. *Astron. Astrophys.* 540:A109

Sargent MT, Schinnerer E, Murphy E, et al. 2010. *Ap. J. Suppl.* 186:341–77

Sarzi M, Shields JC, Schawinski K, et al. 2010. *MNRAS* 402:2187–210

Satyapal S, Böker T, McAlpine W, et al. 2009. *Ap. J.* 704:439–52

Satyapal S, Vega D, Dudik RP, Abel NP, Heckman T. 2008. *Ap. J.* 677:926–42

Schawinski K, Simmons BD, Urry CM, Treister E, Glikman E. 2012. *MNRAS* 425:L61–65

Schawinski K, Thomas D, Sarzi M, et al. 2007. *MNRAS* 382:1415–31

Schawinski K, Treister E, Urry CM, et al. 2011. *Ap. J. Lett.* 727:L31

Schawinski K, Urry CM, Virani S, et al. 2010. *Ap. J.* 711:284–302

Scheuer P. 1974. *MNRAS* 166:513–28

Schiminovich D, Wyder T, Martin DC, et al. 2007. *Ap. J. Suppl.* 173:315–41

Schmidt M. 1963. *Nature* 197:1040

Seljak U. 2000. *MNRAS* 318:203–13

Sellwood JA. 2014. *Rev. Mod. Phys.* 86:1–46

Seyfert CK. 1943. *Ap. J.* 97:28–40

Shabala SS, Godfrey LEH. 2013. *Ap. J.* 769:129

Shankar F, Marulli F, Mathur S, Bernardi M, Bournaud F. 2012. *Astron. Astrophys.* 540:A23

Shankar F, Weinberg D, Miralda-Escudé J. 2009. *Ap. J.* 690:20–41

Shankar F, Weinberg D, Miralda-Escudé J. 2013. *MNRAS* 428:421–46

Shao L, Kauffmann G, Cheng L, Wang J, Heckman TM. 2013. *MNRAS* 436:3451–63

Shapley A. 2011. *Annu. Rev. Astron. Astrophys.* 49:525–80

Shen S, Kauffmann G, von der Linden A, White SDM, Best PN. 2008. *MNRAS* 389:1074–86

Shen S, White SDM, Mo HJ, et al. 2006. *MNRAS* 369:1639–53

Shen Y, Strauss MA, Ross NP, et al. 2009. *Ap. J.* 697:1656–73

Sheth RK, Mo HJ, Tormen G. 2001. *MNRAS* 323:1–12

Shimasaku K, Fukugita M, Doi M, et al. 2001. *Astron. J.* 122:1238–50

Shlosman I, Begelman MC, Frank J. 1990. *Nature* 345:679–86

Silk J. 2013. *Ap. J.* 772:112

Silverman JD, Kampczyk P, Jahnke K, et al. 2011. *Ap. J.* 743:2

Silverman JD, Lamareille F, Maier C, et al. 2009. *Ap. J.* 696:396–410

Simmons BD, Lintott C, Schawinski K, et al. 2013. *MNRAS* 429:2199–211

Simoes Lopes R, Ramiro D, Storchi-Bergmann T, de Fatima Saraiva M, Martini P. 2007. *Ap. J.* 655:718–34

Simpson C, Rawlings S, Ivison RJ, et al. 2012. *MNRAS* 421:3060–83

Simpson C, Westoby P, Arumugam V, et al. 2013. *MNRAS* 433:2647–56

Soker N. 2006. *New Astron.* 12:38–46

Soltan A. 1982. *MNRAS* 200:115–22

Spinoglio L, Malkan MA. 1989. *Ap. J.* 342:83–99

Spoon HWW, Farrah D, Lebouteiller V, et al. 2013. *Ap. J.* 775:127

Springel V, Di Matteo T, Hernquist L. 2005. *MNRAS* 361:776–94

Stasinska G, Cid Fernandes R, Mateus A, Sodre L, Asari NV. 2006. *MNRAS* 371:972–82

Stasinska G, Vale Asari N, Cid Fernandes R, et al. 2008. *MNRAS* 391:L29–33

Steidel CC, Erb DK, Shapley AE, et al. 2010. *Ap. J.* 717:289–322

Steiner JF, McClintock JE, Narayan R. 2013. *Ap. J.* 762:104

Stern D, Assef RJ, Benford DJ, et al. 2012. *Ap. J.* 753:30

Stern D, Eisenhardt P, Gorjian V, et al. 2005. *Ap. J.* 631:163–68

Stern J, Laor A. 2012a. *MNRAS* 426:2703–18

Stern J, Laor A. 2012b. *MNRAS* 423:600–31

Strauss MA, Weinberg DH, Lupton RH, et al. 2002. *Astron. J.* 124:1810–24

Sturm E, González-Alfonso E, Veilleux S, et al. 2011. *Ap. J. Lett.* 733:L16

Tamura T, Bleeker JAM, Peterson JR, et al. 2001. *Astron. Astrophys.* 365:L87–92

Tasse C, Best PN, Röttgering HJA, Le Borgne D. 2008. *Astron. Astrophys.* 490:893–904

Terlevich R, Melnick J. 1985. *MNRAS* 213:841–56

Terlevich R, Tenorio-Tagle G, Franco J, Melnick J. 1992. *MNRAS* 255:713–28

Toffolatti L, Franceschini A, Danese L, de Zotti G. 1987. *Astron. Astrophys.* 184:7–15

Treister E, Schawinski K, Urry CM, Simmons BD. 2012. *Ap. J. Lett.* 758:L39

Tremaine S, Gebhardt K, Bender R, et al. 2002. *Ap. J.* 574:740–53

Trump JR, Impey CD, Kelly BC, et al. 2009. *Ap. J.* 700:49–55

Tundo E, Bernardi M, Hyde JB, Sheth RK, Pizella A. 2007. *Ap. J.* 663:53–60

Ueda Y, Hiroi K, Isobe N, et al. 2011. *Publ. Astron. Soc. Jpn.* 63:937–45

Urry CM, Padovani P. 1995. *Publ. Astron. Soc. Pac.* 107:803–45

Veilleux S, Cecil G, Bland-Hawthorn J. 2005. *Annu. Rev. Astron. Astrophys.* 43:769–826

Veilleux S, Meléndez M, Sturm E, et al. 2013. *Ap. J.* 776:27

Veilleux S, Osterbrock DE. 1987. *Ap. J. Suppl.* 63:295–310

Veilleux S, Rupke DSN, Kim D-C, et al. 2009. *Ap. J. Suppl.* 182:628–66

Villforth C, Hamann F, Rosario DJ, et al. 2014. *MNRAS* 439:3342–56

Vitale M, Zuther J, García-Marín M, et al. 2012. *Astron. Astrophys.* 546:A17

Voges W, Aschenbach B, Boller T, et al. 1999. *Astron. Astrophys.* 349:389–405

von der Linden A, Best PN, Kauffmann G, White SDM. 2007. *MNRAS* 379:867–93

Whitaker K, van Dokkum PG, Brammer G, Franx M. 2012. *Ap. J. Lett.* 754:L29

Wild V, Heckman T, Charlot C. 2010. *MNRAS* 405:933–47

Wild V, Kauffmann G, Heckman T, et al. 2007. *MNRAS* 381:543–72

Willott CJ, Rawlings S, Blundell KM, Lacy M. 1999. *MNRAS* 309:1017–33

Wilson AS, Colbert EJM. 1995. *Ap. J.* 438:62–71

Wilson AS, Heckman TM. 1985. In *Astrophysics of Active Galaxies and Quasi-Stellar Objects*, ed. JS Miller, pp. 39–110

Winter L, Lewis KT, Koss M, et al. 2010. *Ap. J.* 710:503–39

Woo J-H, Schulze A, Park D, et al. 2013. *Ap. J.* 772:49

Worthey G, Ottaviani DL. 1997. *Ap. J. Suppl.* 111:377–86

Wright EL, Eisenhardt PPM, Mainser AK, et al. 2010. *Astron. J.* 140:1868–81

Wuyts S, Förster Schreiber NM, Lutz D, et al. 2011a. *Ap. J.* 738:106

Wuyts S, Förster Schreiber NM, van der Wel A, et al. 2011b. *Ap. J.* 742:96

Xu C, Livio M, Baum S. 1999. *Astron. J.* 118:1169–76

Yan R, Blanton MR. 2012. *Ap. J.* 747:61

Yan R, Newman JA, Faber SM, et al. 2006. *Ap. J.* 648:281–98

Yee HKC, Green RF. 1984. *Ap. J.* 280:79–90

Yip CW, Connolly AJ, Szalay AS, et al. 2004. *Astron. J.* 128:585–609

Yu Q, Tremaine S. 2002. *MNRAS* 335:965–76

Yuan F, Narayan R. 2004. *Ap. J.* 612:724–28

Yuan F, Narayan R. 2014. *Annu. Rev. Astron. Astrophys.* 52:529–88

Zakamska N, Strauss MA, Heckman T, Ivezić Z, Krolik J. 2004. *Astron. J.* 128:1002–16

Zinn PC, Middelberg E, Norris RP, Dettmar RJ. 2013. *Ap. J.* 774:66

Contents

Indexes

Errata

An online log of corrections to *Annual Review of Astronomy and Astrophysics* articles may be found at http://www.annualreviews.org/errata/astro